STUDIES ON HIGH TEMPERATURE-TYPE PROTON CONDUCTIVE SOLID ELECTROLYTE BASED ON $SrCeO_3$

1984

HIROYUKI UCHIDA

STUDIES ON HIGH TEMPERATURE-TYPE PROTON CONDUCTIVE SOLID ELECTROLYTE BASED ON $SrCeO_3$

($SrCeO_3$ 系高温型プロトン導電性固体電解質に関する研究)

1984

HIROYUKI UCHIDA

PREFACE

The work in this thesis was performed under the guidance of Professor Dr. Hiroyasu Iwahara at Department of Environmental Chemistry and Technology, Faculty of Engineering, Tottori University.

The object of this study is to investigate the proton conduction in $SrCeO_3$-based sintered oxides and to examine their applications as the solid electrolytes for various electrochemical cells at high temperature.

The author hopes that this work will contribute to the development of the electrochemistry and the solid state ionics.

The author is greatly indebted to Professor Dr. Hiroyasu Iwahara for his kind guidance, valuable suggestions and hearty encouragement throughout this work.

The author wishes to thank Professor Dr. Zenichiro Takehara at Kyoto University for his valuable suggestions for this thesis.

The author is very grateful to Associate Professor Dr. Takao Esaka at Tottori University for his helpful advices and discussion.

Finally, thanks are given to Mr. Nozomu Maeda, Mr. Junji Kondo, Mr. Shinichiro Tanaka and all the other members of Iwahara Laboratory for their help and support.

Hiroyuki Uchida

HIROYUKI UCHIDA

Faculty of Engineering,
Tottori University
Koyamacho, Tottori 680
Japan

CONTENTS

GENERAL INTRODUCTION

The resources of fossile raw materials are strictly limited and their prices are quite increasing. Alternative energy carriers are required for substitution of fossile fuels. On introducing hydrogen as a future energy carrier, important conditions are the production and utilization of hydrogen with high efficiency. Among the various possibilities, electrochemical methods, such as fuel cell generation and water electrolysis for hydrogen production, are of interest because their energy conversion efficiencies are high in principle. Although the operating temperature of conventional water electrolyzer is below 100°C or phosphoric acid fuel cell is operated at about 200°C, the efficiency of such energy conversion process can be much more increased by high temperature operation.

High temperature(800 - 1000°C) steam electrolysis using solid electrolytes have been considered to be an effective method of large scale hydrogen generation[1-7]. Supplying electrical energy and water vapor, hydrogen and oxygen gases are produced. When such a solid electrolyte cell is operated inversely, it generates electric power by consuming the stored hydrogen, that is, it acts as a fuel cell with high conversion efficiency[6-8], as well as in steam electrolysis. Therefore, this solid electrolyte cell device may be regarded as a promising direct energy converter in a future energy system.

As solid electrolytes for such a cell, oxide ion conductive ceramics, such as stabilized zirconias, have been studied by many workers. For example, using yttria or ytterbia stabilized

zirconias as an electrolyte, high temperature steam electrolyzers or fuel cells have been investigated in several national projects in West Germany[3], U.S.A.[7,8] and Japan[9,10].

High temperature-type proton conductive solids are also favorable materials as the electrolytes for such cells. The use of the proton conductive solids instead of oxide ion conductors will have the following advantages; (1) pure hydrogen free from steam is available in the electrolysis, (2) fuel circulation is not necessary in the fuel cell because no water molecules are generated at the fuel electrode.

However, good proton conductors at high temperature are not very well known, although several investigators have studied proton conduction in some oxides or hydroxyapatites in the presence of hydrogen or water vapor at high temperatures[11-19]. Unfortunately, these studies do not provide a direct demonstration of proton conduction, or the proton conductivities are not sufficiently high for practical use.

As described above, high temperature-type solid electrolytes exhibiting high proton conductivity are not only of great importance for steam electrolyzer, fuel cell, new-type gas sensitive material and hydrogen extractor, etc., but also of special interest for the proton conduction phenomenon in solids itself. Therefore, the research for finding good high temperature-type solid protonic conductor and the examination of the performances of such solid electrolyte cells have significant meanings in view of electrochemistry or of energy conversion technology. Furthermore, obtaining the information about the mechanism of the proton conduction in solids at high temperature is one of aids

for the potential development of the solid state ionics.

From the above viewpoint, high temperature-type solid proton conductors have been studied in this work, and it was found that some sintered oxides based on $SrCeO_3$ exhibited appreciably high proton conduction at high temperature.

Then, the electrochemical characteristics of the $SrCeO_3$-based sinters are studied and the applications of these sinters as the solid electrolyte for various gas cells are examined.
In chapter 1, the experimental verification of proton conduction in $SrCeO_3$-based sinters is described. The applications of these proton conductive sinters as the solid electrolytes for the steam electrolyzers and the fuel cells are examined in chapter 2. In chapter 3, the polarization behavior of the gas electrodes on the high temperature-type proton conductive solid electrolyte is studied in the fuel cells and the steam electrolyzers by using current interruption method. The characteristics of the steam concetration cell are examined using a $SrCeO_3$-based proton conductor as the solid electrolyte in chapter 4. In chapter 5, the galvanic cell-type humidity sensors are constructed using $SrCe_{0.95}Yb_{0.05}O_{3-\alpha}$ electrolyte and their performances are tested. In chapter 6, the hydrogen concentration cell is examined using a $SrCeO_3$-based electrolyte, and various gas cells using proton conductor or oxide ion conductor are characterized under hydrogen-water vapor or oxygen-water vapor atmosphere. Chapter 7 is concerned with the relation between proton and hole conduction in $SrCeO_3$-based solid electrolytes under water-containing atmosphere in order to find a clue to clarify the mechanism of proton conduction.

CHAPTER 1 PROTON CONDUCTION IN SINTERED OXIDES BASED ON $SrCeO_3$*

1.1 Introduction

The proton, massive but very small compared with other ions, may have the nature between ions and electrons. There has been a special interest in the proton conduction in solids, because the proton has large polarizability and no electron clouds. Many investigators have been working on the proton conduction in solids at temperatures below 100°C[20-27]. For example, $H_3Mo_{12}PO_{40}\cdot 29H_2O$[21], $H_3W_{12}PO_{40}\cdot 29H_2O$[21], $H_8UO_2(IO_6)_2\cdot 4H_2O$[22], $HUO_2PO_4\cdot 4H_2O$[23,24], $HUO_2AsO_4\cdot 4H_2O$[22,25] and H_3O^+ β''-Al_2O_3[26, 27] exhibit high proton conductivities at ambient temperature.

However, high temperature-type solid proton conductors have not been so widely studied[11]. Stotz and Wagner[12] have discussed the existence of protons in Cu_2O, CuO, NiO and some stabilized zirconias at high temperature in the presence of water vapor. Shores and Rapp[13] have reported the proton conduction in thoria-based sinters. Several investigators have studied the proton transport in glasses[14,15] and some hydroxyapatites[19] at temperatures above several hundred degrees centigrade. Takahashi and Iwahara have reported the proton conduction in some perovskite-type oxides based on $LaYO_3$ or $SrZrO_3$ [18]. Although high temperature-type solid proton conductors with high proton conductivity have been considered to be a prospective material for the solid electrolyte of the steam electrolyzers and fuel cells, the conductivities reported in these

---

* Solid State Ionics, 3/4, 359 (1981)

previous works are not sufficiently high for practical use or a direct demonstration of the proton conduction is not provided clearly.

Recently, it was found that some sintered oxides based on $SrCeO_3$ exhibited appreciably high proton conduction in hydrogen- or water-containing atmospheres at high temperature. Confirmaions of the proton conduction in these oxides are described in this chapter. The possibilities of applications of these sinters as the solid electrolytes for hydrogen fuel cells, steam concentration cells and steam electrolyzers to produce hydrogen are also demonstrated.

1.2 Experimental

The ceramics tested were strontium cerium trioxide and its derivatives $SrCe_{1-x}M_xO_{3-\alpha}$ in which Ce in $SrCeO_3$ was partially substituted by the aliovalent cation M (where α is the number of oxygen deficiencies per perovskite-type oxide unit cell). These were prepared by the solid state reaction of cerium dioxide, strontium carbonate and the oxides or carbonates of various metals. The powders of raw materials were mixed and calcined at 1300-1450°C for 5-10 h in air. The calcined oxides were finely ground and pressure molded hydrostatically(2×10^3 Kg cm^{-2}) into the column (diameter : 13 mm) and sintered at 1350-1450°C for 10 h in air. The sintered oxides were subjected to X-ray diffraction analysis to assure the formation of the prescribed single phase. The sinters thus obtained were sliced in thin discs(thickness : 0.5 mm, diameter : 12 mm) to provide test specimens.

The proton conduction was confirmed primarily by studying the electromotive force(emf) behaviors of the following gas concentration cell at high temperatures using the specimen ceramics as the electrolyte diaphragm.

gas I, Pt | ceramic disc | Pt, gas II (1-1)

The construction of the solid electrolyte gas cell is illustrated in Fig. 1. The electrode compartments were separated by the specimen electrolyte, each face of which was smeared with platinum paste(fine platinum powders suspended in n-butyl acetate without flux) and baked at 1000°C for 1 hour to provide porous electrode materials.

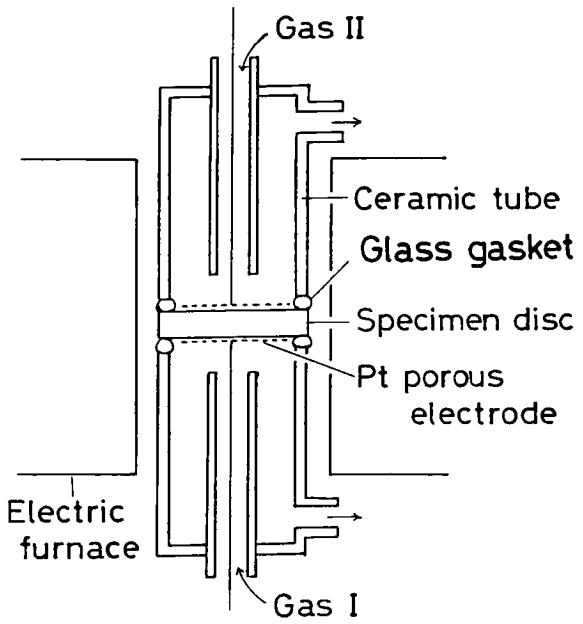

Fig. 1 Schematic illustration of a gas cell

Figure 2 shows a SEM(scanning electron micrograph) picture of the freshly prepared platinum porous electrode on the specimen surface. It can be observed that the electrode is porous and the platinum particles are fine and fairly uniform in size. Each electrode compartment was sealed by glass ring gasket.

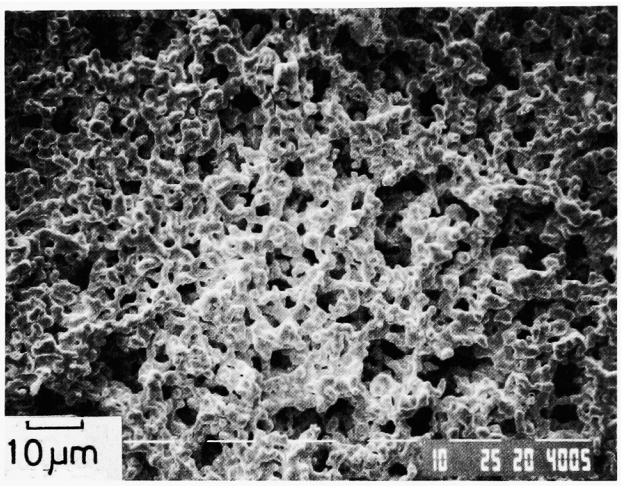

Fig. 2 SEM picture of the freshly prepared Pt electrode on the specimen disc

Air, oxygen or hydrogen at 1 atm was used as gas I or gas II. They were used in wet or dry states. Wet gas was prepared by saturating the water vapor at room temperature and dry gas by passing through P_2O_5 powder.

For the measurement of the conductivity, cylindrical specimens(dia : 4-5 mm) with various thickness(3- 10 mm) were used with porous platinum as the electrode materials. An A.C. impedance bridge was employed and the frequency mainly used was 10 kHz. At the frequency of 10 kHz, the phase angle of the

impedance was close to zero and the relation between the resistance and the thickness of the specimen was linear. Therefore, the conductivities measured at 10 kHz could be regarded as the bulk conductivities of the oxide and not that of the Pt/specimen interface.

In the steam electrolysis, the steam at 1 atm was supplied to the anode compartment and dry argon was passed through the cathode compartment to carry the gas generated during the electrolysis to a detector. The determination of the generated gas was made by gas chromatography using active carbon(30-60 mesh) as adsorbent.

1.3 Results and discussion

1.3.1 Structure and some properties of $SrCeO_3$-based sinters

Undoped $SrCeO_3$ (nominally pure) sinters had a color of light green. When Ce in $SrCeO_3$ was partially substituted by the aliovalent cation, the color became more deep. These sinters could be dissolved in dilute HCl aqueous solution to liberate Cl_2.

Figure 3 shows the X-ray diffraction patterns of $SrCe_{0.95}Yb_{0.05}O_{3-\alpha}$. Undoped $SrCeO_3$ and the other doped sinters gave the almost same patterns. In good agreement with the previous crystallographic studies for $SrCeO_3$[28,29], an orthorhombic single phase was observed in this study. According to Mastromonaco et al[29], a = 8.584(Å), b = 6.001, c = 6.155 and Z = 4. However, in the heavily doped sinters($SrCe_{0.80}Yb_{0.20}O_{3-\alpha}$), the appearance of the second phase (probably $SrYb_2O_3$) was observed.

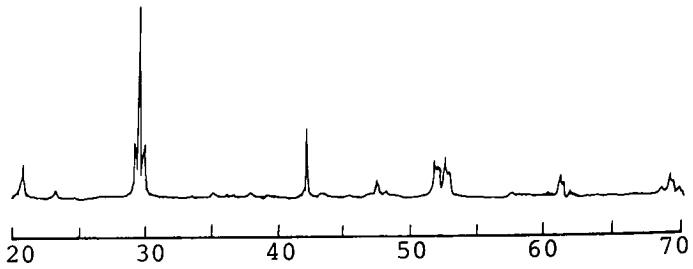

Fig. 3 X-ray diffraction pattens of $SrCe_{0.95}Yb_{0.05}O_{3-\alpha}$

The apparent density of the sintered specimen was roughly estimated from the weight and the size. Although the number of α was not yet determined accurately, the density of the sintered oxides seemed to be more than 90 % of the theoretical one and the porosity may be very small.

1.3.2 Emf of various gas cells

The cells using undoped $SrCeO_3$ (nominally pure) as a diaphragm showed an unstable emf in all cases examined. However, when doped ceramics $SrCe_{1-x}M_xO_{3-\alpha}$ were applied as the electrolyte diaphragm, the cells showed a peculiar emf, which could not be explained by the specimen being either an oxide ion conductor or simple electronic conductor.

The emfs of the various gas cells are tabulated in Table 1 for the cases of $SrCe_{0.95}Yb_{0.05}O_{3-\alpha}$ and $SrCe_{0.95}Mg_{0.05}O_{3-\alpha}$ as typical examples. When dry gases with different oxygen partial pressure, P_{O_2}, (gas I : air, gas II : pure oxygen) were introduced to each electrode compartment, only a very small unstable emf was observed as shown in cell 1 in Table 1, suggesting that the

conduction in the oxides was mainly electronic. However, when each gas of the above cell was moistened, a stable emf of the oxygen concentration cell was observed(cell 2 in Table 1) although the values were low compared to the theoretical values(29.5 mV at 600°C and 35.7 mV at 800°C).

A stable emf was also observed when air with different humidities were supplied to the electrode compartments(cell 3). In this case, the electrode with the higher humidity was the negative. This is a sort of steam concentration cell. A steady stable current could be drawn from this cell. Cell 4 and 5 show that the electrodes with higher humidity are also negative, and that the absolute emf values at 600°C are higher than those of oxygen concentration cells.

Table 1 Emf of various gas cells; gas I, Pt/specimen/Pt, gas II

Cell No.	Cell-type[a] gas I//gas II	emf / mV [b]			
		$SrCe_{0.95}Yb_{0.05}O_{3-\alpha}$		$SrCe_{0.95}Mg_{0.05}O_{3-\alpha}$	
		600°C	800°C	600°C	800°C
1	dry air//dry O_2	0.5	1.0	0.1	-0.3
2	wet air//wet O_2	25.0	14.0	16.0	12.0
3	wet air//dry air	59.0	30.0	39.0	17.0
4	wet air//dry O_2	69.5	30.5	46.8	19.5
5	dry air//wet O_2	-43.5	-13.0	-25.0	-10.5

a) Dry gas: dried with P_2O_5, wet gas: saturated with H_2O at room temperature(21-22°C)

b) Negative sign shows that the electrode of gas II is negative

Table 2 shows the effect of water vapor on the emf of the hydrogen-air fuel cell using $SrCe_{0.95}Sc_{0.05}O_{3-\alpha}$ as the electrolyte. In this case, emfs were very stable and a steady stable current could be drawn out, suggesting the possibility of the application of this oxide as an electrolyte for the hydrogen fuel cell. Higher emfs were observed when the oxygen gas(air) contained a smaller amount of water vapor than did the hydrogen gas. This phenomenon is inverse to the hydrogen-air fuel cell with an oxide ion conductor.

Some other specimens containing Y, In, Zn, Nd, Sm, and Dy as M in $SrCe_{1-x}M_xO_{3-\alpha}$ ($x = 0.05 - 0.10$) were observed to behave in the same manner as described above.

Table 2 Effect of water vapor on the emf of the fuel cell; H_2, Pt / $SrCe_{0.95}Sc_{0.05}O_{3-\alpha}$ / Pt, air

Cell No.	H_2O content/ Torr		emf / mV		
	H_2 electrode	air electrode	700°C	800°C	1000°C
1	15.5	4.6	1119	1057	903
2	4.6	15.5	1108	1047	897
3	15.5	15.5	1108	1047	894
	Theoretical emf of cell 3		1128	1111	1078
	ion transport number in cell 3		0.98	0.94	0.83

1.3.3 Confirmation of proton conduction

The cell behavior described above cannot be explained by oxide ion conduction or normal electronic conduction in the ceramics. However, if the specimen has proton conduction in

the wet atmosphere, these phenomena can be rationally explained as follows.

(1) If the specimen diaphragm in cell 3 is a proton conductor, the difference in partial pressure of water vapor, P_{H_2O}, between two electrodes can be a driving force of the following electrode reactions.

Electrode reaction with higher P_{H_2O}:

$$H_2O \longrightarrow 2\ H^+ + 1/2\ O_2 + 2\ e^- \qquad (1\text{-}2)$$

Electrode reaction with lower P_{H_2O}:

$$2\ H^+ + 1/2\ O_2 + 2e^- \longrightarrow H_2O \qquad (1\text{-}3)$$

For this reason, this cell may give a stable emf, with the electrode of lower P_{H_2O} being the cathode in spite of the negligible pressure difference of oxygen between two electrodes. In Fig. 4, the electrode reactions for this steam concentration cell are illustrated schematically.

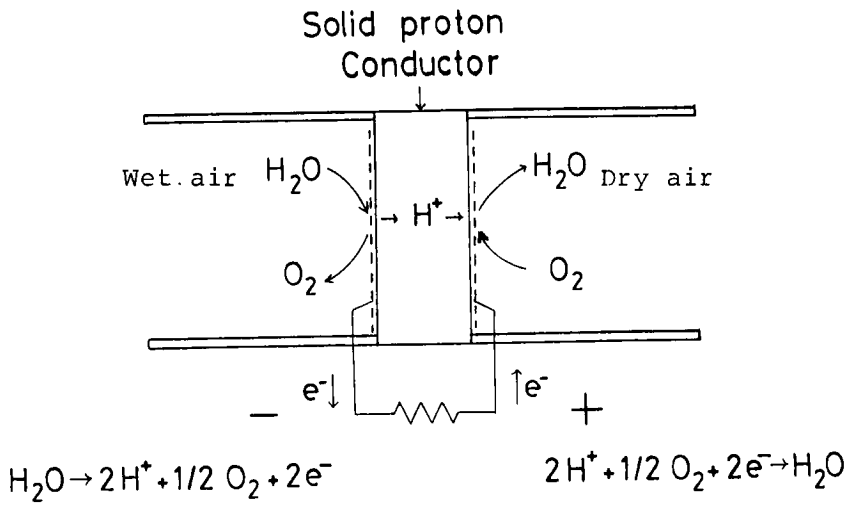

Fig. 4 Concept of steam concentration cell

(2) When two electrode gases have different oxygen partial pressure but equal P_{H_2O} like cell 2 in Table 1, the equilibrium partial pressure of hydrogen at high temperatures differ from each other: the gas having the higher P_{O_2} decreases the hydrogen partial pressure. As a result, if the diaphragm is a proton conductor, the emf of the hydrogen concentration cell appears making the electrode with the higher P_{O_2} the cathode. Thus, the stable emf of cell 2 can be explained assuming that the diaphragm has proton conduction.

(3) Generally, when gas I and gas II in the gas cell include oxygen and water vapor at different partial pressures, the emf E of the steam concentration cell is given as

$$E = \frac{RT}{2F} \ln \frac{P_{H_2O}(I)}{P_{H_2O}(II)} \left(\frac{P_{O_2}(II)}{P_{O_2}(I)} \right)^{1/2} \qquad (1\text{-}4)$$

where P_{H_2O} and P_{O_2} are partial pressure of water and oxygen, respectively, and R, F and T are gas constant, Faraday's constant and absolute temperature, respectively. The emf behaviors of cell 4 and 5 can also be explained qualitatively by Eq.(1-4) provided the diaphragm is a proton conductor.

The proton conduction could also be verified by the emf behavior of a hydrogen-air fuel cell. If the electrolyte of this cell is a proton conductor, the proton has a tendency to migrate across the electrolyte to the air electrode, where it discharges to form water vapor. Therefore, the emf given by

$$E = E^\circ - \frac{RT}{2F} \ln \frac{P_{H_2O}}{P_{H_2} \, P_{O_2}^{1/2}} \qquad (1\text{-}5)$$

must be controlled by the P_{H_2O} at the air electrode; the higher

the P_{H_2O} at the cathode, the lower the emf of the cell, while the change in P_{H_2O} at the hydrogen electrode will not influence the emf. On the other hand, if the electrolyte is an oxide ion conductor, the situation is inverse; the emf must be controlled by the P_{H_2O} at the hydrogen electrode. The results listed in Table 2 coincide with that for the proton conductor. In Table 2, the proton transport numbers, which were determined by the ratio of the measured emf to the theoretical emf of this cell, are also given.

The proton conductivities were not separately determined in the present experiment. However, the conductivities measured in hydrogen atmosphere by A.C. bridge at 10 kHz(Fig. 5) will be close to the proton conductivities, since the proton transport numbers in Table 2 are close to unity.

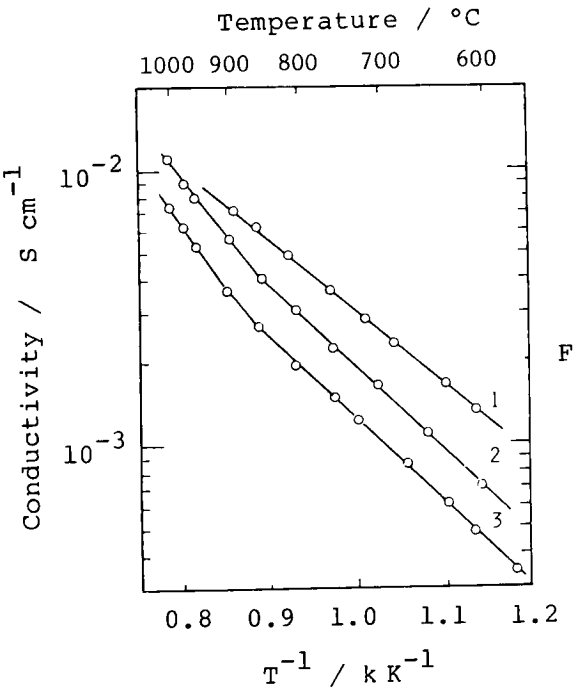

Fig. 5 Conductivities in hydrogen atmosphere.
1: $SrCe_{0.95}Yb_{0.05}O_{3-\alpha}$
2: $SrCe_{0.90}Y_{0.10}O_{3-\alpha}$
3: $SrCe_{0.95}Sc_{0.05}O_{3-\alpha}$

1.3.4 Possible mechanism of proton formation

Figure 6 shows the conductivities of $SrCe_{0.95}Yb_{0.05}O_{3-\alpha}$ measured in various atmospheres. The conductivities increased as the P_{O_2} increased, indicating that the conduction mode is p-type(conduction by electron holes) in dry atmosphere. The electron holes may be formed by charge compensation on substituting the aliovalent cation Yb^{3+} for Ce^{4+} in $SrCeO_3$. The addition of water vapor decreased the conductivity, probably due to the decrease in the hole concentration. The proton conduction appears in this wet condition as described above.

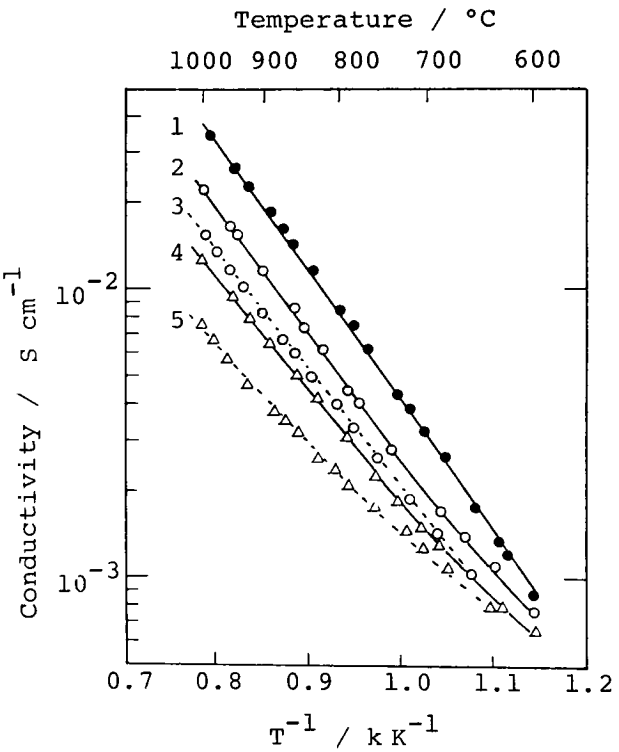

Fig. 6 The conductivities of $SrCe_{0.95}Yb_{0.05}O_{3-\alpha}$ in various gases. 1: in dry O_2, 2: in dry air, 3: in wet air, 4: in dry N_2, 5: in wet N_2

These phenomena suggest that the protons in the oxide may be provided from H_2O at the expense of the electron holes[12,13]. One of the possible mechanisms for proton formation is

$$H_2O + 2\ h^+(\text{oxides}) \longrightarrow 2\ H^+(\text{oxides}) + 1/2\ O_2 \quad (1\text{-}6)\ .$$

The small emfs in Table 1 compared to the theoretical values calculated from Eq.(1-4) may be ascribed to the conduction by electron holes surviving in the oxide. Detailed discussion for the relation between the proton conductivity and the hole conductivity will be presented in chapter 7.

1.3.5 Electrolysis of steam

Using the specimen ceramics as the electrolyte, water vapor could be electrolyzed at high temperature to get hydrogen gas. The steam at 1 atm was supplied to the anode compartment, and dry argon gas was passed through the cathode compartment to carry the generated gas to a detector. On passing the direct current through the cell at 600-1000°C, evolution of hydrogen gas at the cathode was recognized by gas chromatography. This fact is a direct demonstration of protonic conduction in the specimen oxides, since the protons formed at the steam electrode must migrate across the solid electrolyte to discharge at the cathode.

Figure 7 shows the relation between the electrolytic current and the hydrogen evolution rate, which was determined from the hydrogen concentration in argon carrier gas(%) and the gas flow rate. Current efficiencies for hydrogen evolution were 50-95 % in the range of 0.1-0.8 A cm^{-1} depending on the type of specimens and electrode conditions. The current efficiency in the cell

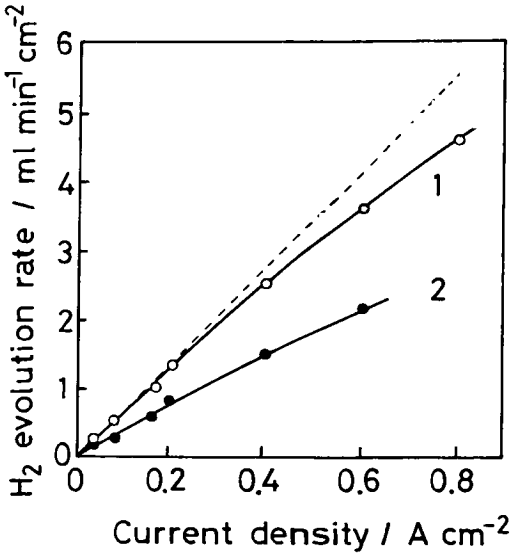

Fig. 7 Hydrogen evolution rate versus current density at 900°C. Electrolyte; 1: $SrCe_{0.90}Sc_{0.10}O_{3-\alpha}$, 2: $SrCe_{0.95}Sc_{0.05}O_{3-\alpha}$ (broken line shows theoretical rate)

with $SrCe_{0.95}Sc_{0.05}O_{3-\alpha}$ electrolyte was lower than that in the $SrCe_{0.90}Sc_{0.10}O_{3-\alpha}$ cell. One of the reasons was that the $SrCe_{0.95}Sc_{0.05}O_{3-\alpha}$ electrolyte was not so dense as $SrCe_{0.90}Sc_{0.10}O_{3-\alpha}$. Another reason was that the doping of Sc with 5 % might be insufficient to exhibit the high proton conduction in the steam electrolyzer

This electrolytic cell can be operated inversely as a hydrogen fuel cell. The performances and characteristics of the fuel cell and the steam electrolyzer will be shown in the next chapter.

1.4 Summary

Some sintered oxides based on $SrCeO_3$ were confirmed to exhibit appreciably high proton conduction in hydrogen-containing atmospheres at high temperatures. $SrCe_{0.95}Yb_{0.05}O_{3-\alpha}$, $SrCe_{0.95}Mg_{0.05}O_{3-\alpha}$, $SrCe_{0.95}Sc_{0.05}O_{3-\alpha}$, $SrCe_{0.90}Sc_{0.10}O_{3-\alpha}$, $SrCe_{0.90}Y_{0.10}O_{3-\alpha}$ etc., belong to this type of oxides. Using these specimens as the solid electrolytes, the verification of the proton conduction was made by studying the emf of various gas cells. These materials could be applied to the solid electrolyte for hydrogen fuel cells, steam concentration cells and steam electrolyzers to produce hydrogen.

CHAPTER 2 HIGH TEMPERATURE FUEL CELLS AND STEAM ELECTROLYZERS USING PROTON CONDUCTIVE SOLID ELECTROLYTES*

2.1 Introduction

High temperature steam electrolysis using solid electrolytes is expected to be an effective method of large scale hydrogen generation. The high temperature electrolyzer has the following advantages in comparison to conventional low temperature-type (< 100°C) device[1-6].

(i) The electrical energy required for the electrolytic decomposition of water ($\Delta G°$) decreases with increasing temperature;

$$H_2O(g) \xrightarrow{\Delta G°} H_2(g) + 1/2\ O_2(g)$$

$$\Delta G°(\ J\ mol^{-1}) = 240203 - 3.93\ T\ ln\ T - 0.00690\ T^2 + 0.00000155\ T^3 - 16.4\ T \qquad [30]$$

(ii) Without applying noble metal catalysts, the electrochemical reactions are accelerated in such a way that current densities can be significantly higher with lower polarization losses than those at ambient temperature.

Consequently, the efficiency of high temperature steam electrolysis is higher than conventional electrolysis due to the above mentioned favorable thermodynamic and kinetic conditions. The amount of heat needed for the steam electrolysis may be easily supplied by internal resistivity losses of the cell itself or by direct heat input from a high temperature heat sources, such as a nuclear reactor(HTR, high temperature gas reactor) or a coal

---

* J. Power Sources, 7, 293 (1982)

gasification plant.

When such a solid electrolyte cell is operated inversely, it generates electric power by consuming the stored hydrogen, that is, it acts as a fuel cell. In the high temperature fuel cells, since the electrochemical reactions proceed smoothly as well as the steam electrolysis, high current and power densities can be achieved without much polarization loss. Due to the high temperature, not only hydrogen but also various fuels(CO and natural gas, etc.) may be used to generate electricity with high efficiency. whereas CO or some hydrocarbons must be eliminated from the fuel for phosphoric acid fuel cell (operating temperature: about 200°C) because the noble metal catalysts are poisoned by them.

Thus, this solid electrolyte cell device may be regarded as a promising direct energy converter between hydrogen and electricity in a future hydrogen energy system. As the solid electrolytes for such a cell, oxide ion conductive ceramics, such as stabilized zirconias, have been studied by many workers.

For the steam electrolyzer, using yttria or ytterbia stabilized zirconia electrolytes, various fundamental problems in the electrode reaction kinetics, the electrode materials and the other elements of the cell have been intensively studied[1-7, 31-37]. The technical realization of this cell process has been also studied in West Germany(project HOT ELLY)[3] or in U.S.A. (General Electrics[1,4,31] and Westinghouse Electrics[7]).

Using calcia, yttria or ytterbia stabilized zirconias and some other oxides as the electrolytes, the high temperature fuel cells have been investigated by many workers[6-10, 38-47].

Examinations of the performances of the fuel cell stacks are in progress under several national projects in U.S.A., Japan and West Germany, etc.

High temperature-type proton conductive solids are also favorable materials as electrolytes for such cells, and the cells have unique advantages as described below. However, few good high temperature-type proton conductors are known, although several investigators have studied proton conduction in some oxides in the presence of hydrogen or water vapor at high temperatures[11]. And high temperature fuel cell and steam electrolyzer using a proton conductor as the electrolytes have not been examined.

Recently, it has been found that some sintered oxides based on $SrCeO_3$ exhibit appreciable proton conduction under a hydrogen-containing atmosphere at high temperature. $SrCe_{0.95}Yb_{0.05}O_{3-\alpha}$, $SrCe_{0.90}Sc_{0.10}O_{3-\alpha}$, $SrCe_{0.90}Y_{0.10}O_{3-\alpha}$, etc. belong to the family of this type conductor.

In this chapter, some attempts to apply these materials as the electrolyte for a fuel cell and a steam electrolyzer are described. And their unique characteristics are also described.

2.2 Operating principles---- Advantages of proton conductive solids as an electrolyte for fuel cells and steam electrolyzers

Figure 8 illustrates the difference between the proton conductor and the oxide ion conductor in the cases of fuel cell and steam electrolyzer. In general, solid electrolytes for such cells perform the dual function of providing both ionic con-

duction and a diaphragm between the anode and the cathode. Porous electrodes are deposited on both faces of the electrolyte

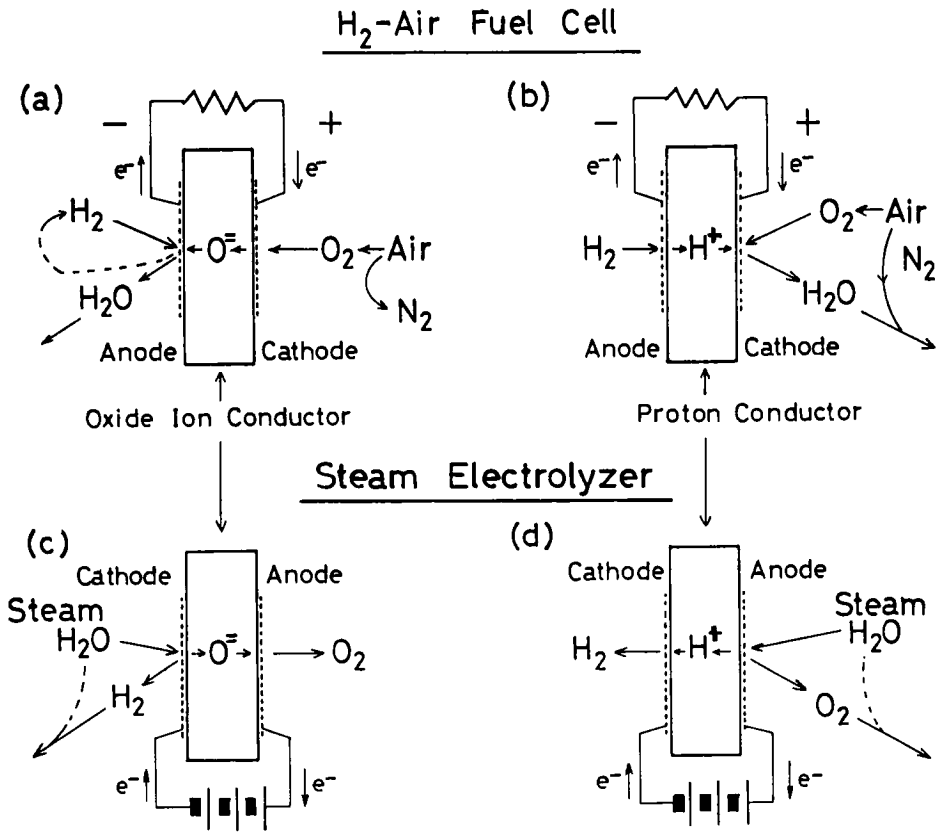

Fig. 8 Schematic illustrations of a high temperature H_2 fuel cell((a), (b)) and a steam electrolyzer ((c), (d)). Electrolyte; oxide ion conductor: (a),(c), proton conductor: (b), (d)

2.2.1 Hydrogen-air fuel cell

In the case of an oxide ion conductor, a hydrogen-air fuel cell generates water molecules at the hydrogen electrode since oxide ions in the electrolyte migrate toward the anode, where they react with hydrogen((a) in Fig.8).

Electrode reactions are given by

Cathode :

$$1/2\ O_2(gas) + 2\ e^-(electrode) \longrightarrow O^=(electrolyte) \qquad (2\text{-}1)$$

Anode :

$$O^=(electrolyte) + H_2(gas) \longrightarrow H_2O(gas) + 2\ e^-(electrode) \qquad (2\text{-}2)$$

As a result, the fuel gas is diluted by water vapor, and the cell performances deteriorate unless the fuel gas is circulated to remove water vapor.

In the case of a proton conductor, on the other hand, hydrogen-air fuel cell gives water molecules at the air electrode since protons migrate from the hydrogen electrode to the air electrode where they react with oxygen gas ((b) in Fig.8). Electrode reactions are

Anode :

$$H_2(gas) \longrightarrow 2\ H^+(electrolyte) + 2e^-(electrode) \qquad (2\text{-}3)$$

Cathode :

$$2\ H^+(electrolyte) + 1/2\ O_2(gas) + 2e^-(electrode) \rightarrow H_2O(gas) \qquad (2\text{-}4).$$

In this case it is unnecessary to recycle the fuel gas because water is not formed at the hydrogen electrode.

Of course, it is necessary to allow air to flow through the cathode compartment in order to avoid an accumulation of water vapor in the air electrode. On the other hand, the necessity for air flow is essential even in the case of an oxide ion conductor cell, because accumulation of nitrogen gas at the air electrode is inevitable due to consumption of oxygen by the cell reaction.

Since the overall reaction for both cases can be written as

$$H_2(gas) + 1/2\ O_2(gas) \longrightarrow H_2O(gas), \qquad (2\text{-}5)$$

the emf of the cell can be written as

$$E = E^\circ - \frac{RT}{2F} \ln \frac{P_{H_2O}}{P_{H_2}\ P_{O_2}^{1/2}} \qquad (2\text{-}6)$$

where P_{H_2O}, P_{H_2} and P_{O_2} are the partial pressure od water, hydrogen and oxygen, respectively. and E° is determined from the change of free energy in reaction(2-5) at the given temperature. However, it should be noted that the meaning of P_{H_2O} is different between the two cells; P_{H_2O} is important in the cathode compartment in the case of a proton conductor, and in the anode compartment in the case of oxide ion conductor.

2.2.2 Steam electrolyzer

In the steam electrolyzer using an oxide ion conductor((c) in Fig. 8), steam is supplied to the cathode compartment of the cell, and oxygen is electrochemically extracted from H_2O in the form of oxide ions which are forced to migrate toward the anode by the electric field applied to the electrolyte. Oxide ions discharge to produce oxygen at the anode.

These reactions are

Cathode :

$$H_2O(gas) + 2\ e^-(electrode) \longrightarrow H_2(gas) + O^=(electrolyte) \qquad (2\text{-}7)$$

Anode :

$$O^=(electrolyte) \longrightarrow 1/2\ O_2(gas) + 2\ e^-(electrode) \qquad (2\text{-}8).$$

In this electrolysis, hydrogen gas obtained at the cathode is accompanied by unreacted water vapor.

Conversely when a proton conductor is used as the electrolyte for such a cell, the steam must be introduced into the anode compartment and hydrogen is electrochemically extracted from H_2O in the form of protons, which are forced to migrate towards the cathode by the electric field((d) in Fig. 8). Protons discharge to generate hydrogen at the cathode.

Anode :

$$H_2O(gas) \longrightarrow 2\ H^+(electrolyte) + 1/2\ O_2(gas) + 2\ e^-(electrode) \quad (2\text{-}9)$$

Cathode :

$$2\ H^+(electrolyte) + 2\ e^-(electrode) \longrightarrow H_2(gas) \quad (2\text{-}10)$$

Therefore, pure hydrogen without water vapor can be taken from the cathode compartment.

Consequently, the use of proton conductive solids instead of oxide ion conductors will have the following advantages; (1) pure hydrogen free from steam is available in the electrolysis, (2) fuel circulation is not necessary in the fuel cell because water molecules are not generated at the fuel electrode.

2.3 Experimental

Specimens used in this experiment were $SrCe_{1-x}M_xO_{3-\alpha}$ (M = Sc, Yb, x = 0.05 or 0.10). These were prepared in the same manner as that described in chapter 1.

The construction of the solid electrolyte gas cell was similar to Fig. 1 in chapter 1, however, a reference electrode was used in this study in order to measure the polarization of individual electrode. In Fig. 9, an example of test hydrogen fuel cell is illustrated. As the reference electrode, a platinum wire was wound to the lateral of the electrolyte disc.

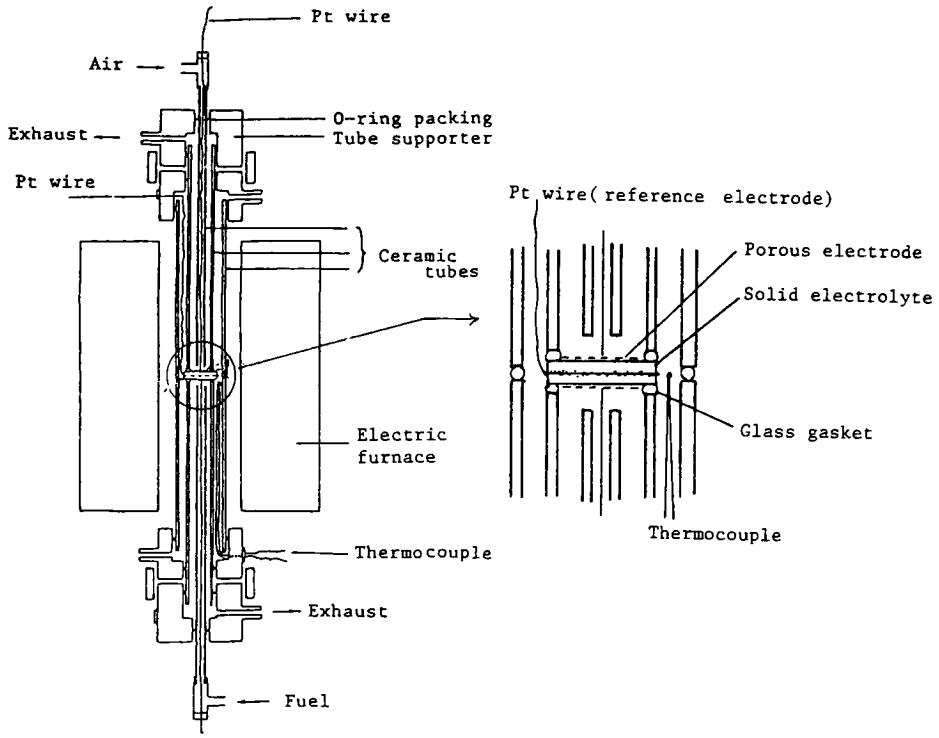

Fig. 9 Construction of test fuel cell

This reference electrode may act as a hydrogen electrode, the potential of which depends on the partial pressure of hydrogen produced by the thermal dissociation equilibrium between water vapor and oxygen in the atmosphere in the electric furnace. Therefore, this exhibited a different potential value depending on the experimental conditions(cell temperature, P_{H_2O} in air, etc.)

Figure 10 illustrates the steam electrolyzer. Water vapor at 1 atm was supplied to the anode compartment, and argon gas, dried over P_2O_5, was passed through the cathode compartment to carry the evolved hydrogen to a detector. The exiting argon gas from the cathode compartment was introduced to an oxygen meter which was an oxygen gas concentration cell using YSZ(yttria stabilized zirconia) with platinum porous electrodes. Since the

oxygen partial pressure under the equilibrium between hydrogen and water vapor could be known from the emf of the oxygen meter kept at 800°C, the content of hydrogen in argon could be monitored by using water-saturator at a known temperature. After the emf of the oxygen meter became a stable value, the hydrogen content was analyzed quantitatively by a conventional gas chromatograph (Shimazu, Model GC-3BT, carrier gas: argon, column packing: active carbon 30-60 mesh or molecular sieves 5A 30-60 mesh, which has larger sensitivity for hydrogen than active carbon). The hydrogen content in argon measured was from 0.3 to 8 % in this experiment.

In order to correct for the ohmic losses in the cells, the current interruption method was employed. A current pulse (pulse width : 0.1 ms, repeat time : 2 ms) was applied to the cells from a current pulse generator(Hokuto Denko, Model HC-110). Then the transient behavior of the electrode potential was measured by a conventional electrometer(Hokuto Denko, Model HE-101) and monitored by an oscilloscope(Hitachi, Model VC-801L).

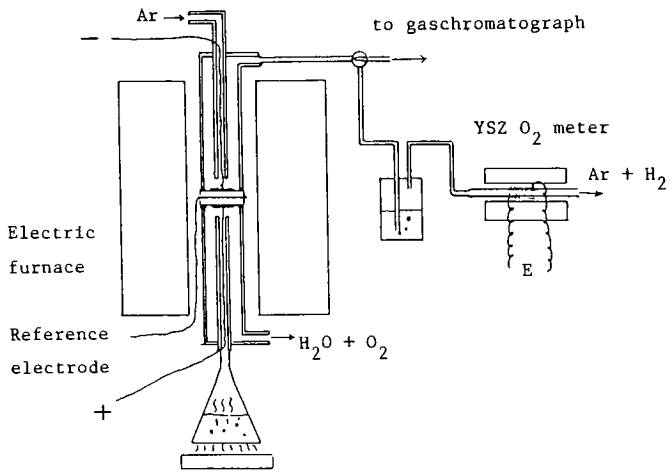

Fig. 10 Construction of the steam electrolyzer

2.4 Results and discussion

2.4.1 Hydrogen-air fuel cells

A hydrogen-air fuel cell was constructed using the sintered specimen as the electrolyte diaphragm and porous platinum as the electrode materials.

Typical cell performances are shown in Fig. 11. A steady and stable current could be drawn from the cell, indicating that the ceramic diaphragm could be employed as the solid electrolyte of a hydrogen-air fuel cell. Above 800°C, the relation between terminal voltage and current output was linear. During discharge at a constant current density, the terminal voltage was very stable and little deterioration in cell performances was observed after 8 hours(Fig. 12).

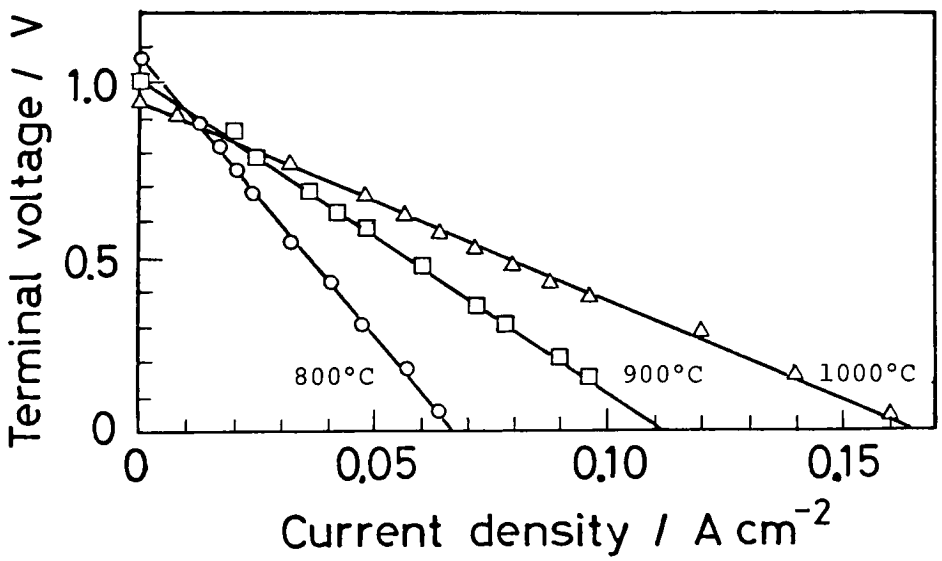

Fig. 11 Performance of the fuel cell ;
H_2, Pt | $SrCe_{0.95}Yb_{0.05}O_{3-\alpha}$ | Pt, Air

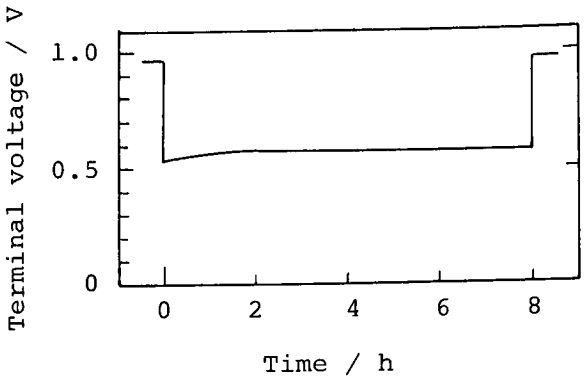

Fig. 12 Continuous discharge test of the fuel cell same as in Fig. 11. Temp : 900°C, i = 0.05 A cm^{-2}

When this cell was short-circuited for a few hours, detectable water vapor, which condensed at the air exhaust pipe, was observed. In order to know the evolution rate of water vapor at the cathode, the humidity of exhaust air from the cathode was measured by an automatic dew point meter(Michell Instruments Ltd.). Figure 13 shows typical example of the humidity change on discharging the fuel cell. The evolution rate of water vapor was estimated from the humidity change thus measured and the flow rate of the air. As shown in Fig. 14, the evolution rate coincides with the theoretical rate calculated from Faraday's law. This indicates that water molecules, the product of the cell reaction, are formed at the air electrode and that movile ions in the electrolyte are protons and not oxide ions.
As shown in Table 3, the cell emf decreased when the cathode gas was moistened but was unaffected when the anode gas was moistened. This is further evidence that these ceramics have proton conduction.

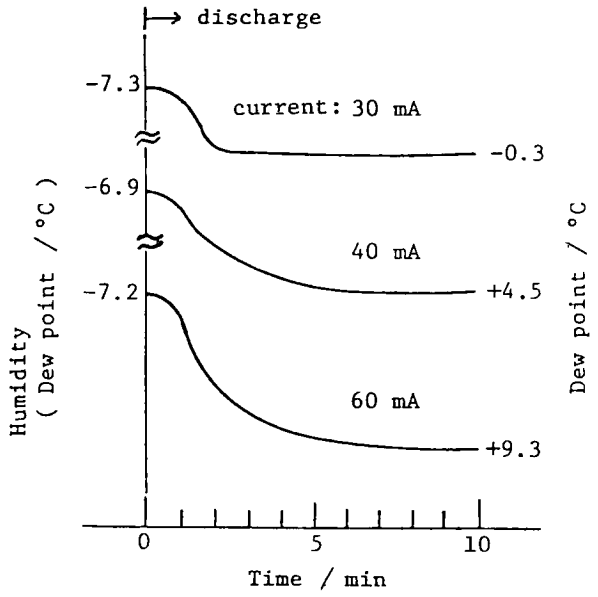

Fig. 13 Humidity change of the cathode air on discharging the fuel cell(900 °C).

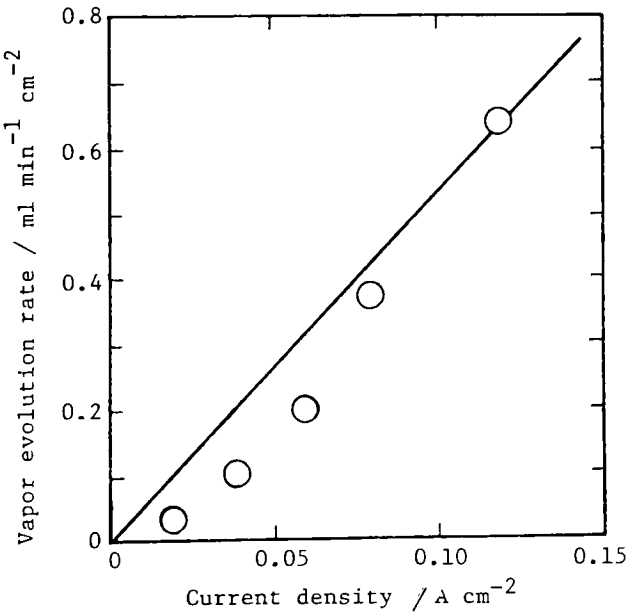

Fig. 14 Evolution rate of water vapor at the cathode on discharging the fuel cell(900°C). (Solid line shows the theoretical rate)

Table 3 Effect of water vapor on the emf of the fuel cell at 800°C. H_2, Pt / specimen electrolyte / Pt, air

Cell type		Electrolyte	
Anode gas	Cathode gas	$SrCe_{0.95}Sc_{0.05}O_{3-\alpha}$	$SrCe_{0.95}Yb_{0.05}O_{3-\alpha}$
wet H_2	dry air	1057	1098
dry H_2	wet air	1047	1073
wet H_2	wet air	1047	1072

wet gas - saturated with H_2O at room temperature (16-17 Torr)

dry gas - dried with P_2O_5 for the case of $SrCe_{0.95}Yb_{0.05}O_{3-\alpha}$ and saturated with H_2O at 0°C (4.6 Torr) for the case of $SrCe_{0.95}Sc_{0.05}O_{3-\alpha}$

Figure 15 shows the polarization characteristics of the hydrogen and air electrodes. Since the potential of the reference electrode changed with the cell temperature, the potentials of the anode and the cathode were shifted to negative with increasing the cell temperature. The potential of hydrogen electrode corrected for ohmic loss exhibits an almost constant value against the reference electrode within the range of current output examined. At 1000°C, little polarization was observed and the cell performance depends mainly on the resistance of the electrolyte. At 800°C, polarization of the air electrode was apparent at high current densities. Such polarization may be caused by : (1) the adsorption or accumulation of generated water molecules in the electrode reaction zone, (2) diffusion limitation of oxygen from the air to the electrode reaction zone through the pores of electrode materials. When oxygen gas was used instead of air, a decrease in the cathodic polarization was observed. Therfore, the diffusion limit of oxygen may be dominant for the

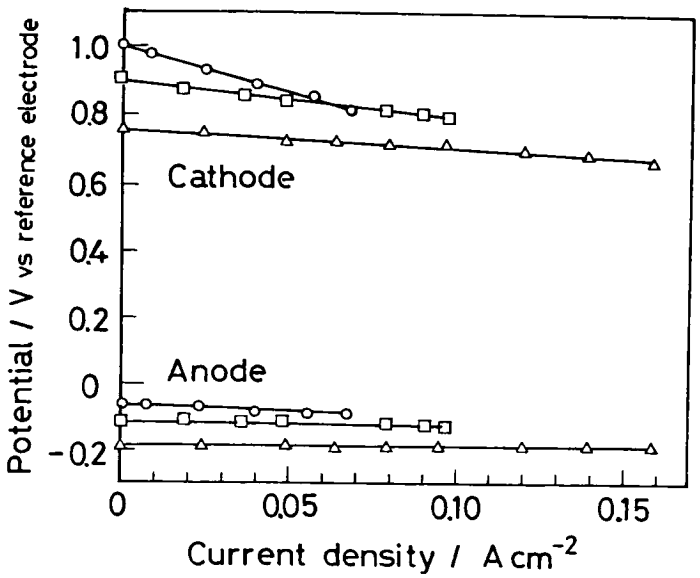

Fig. 15 Polarization of the fuel cell(iR free)
Symbols as in Fig. 11

polarization of the air electrode. Detailed studies of the polarization of the air electrode will be described in the next chapter.

2.4.2 Steam electrolyzers

Steam electrolysis was carried out at 700 - 900°C, as described in the experimental section, using $SrCe_{0.90}Sc_{0.10}O_{3-\alpha}$ sinters as the solid electrolyte. The evolution of hydrogen gas at the cathode on passing direct current through the cell was confirmed by gas chromatography. The evolution of oxygen gas was also detected at the anode at half the hydrogen evolution rate. When the anode gas(1 atm water vapor) was substituted by argon gas dried with P_2O_5, no hydrogen gas was detected in the cathode gas. This fact supports the existence of the proton conduction

in the specimen electrolyte, since the protons formed from the H_2O molecules at the anode(see Eq.(2-9)) must migrate across the electrolyte to discharge at the cathode(Eq.(2-10)).

Figure 16 shows the dependence of the hydrogen evolution rate V(ml $min^{-1}cm^{-2}$) on the electrolytic current density. The evolution rate was determined from the concentration of hydrogen gas, C(%), in the argon carrier gas and its flow rate u(ml min^{-1}),

$$V = \frac{u\ C}{(100-C)\ S} \qquad (2\text{-}11)$$

where S is the projected electrode area(cm^2). The theoretical evolution rate, V_{theo}, was calculated according to Faraday's law and is shown in Fig. 16 by a broken line.

The current efficiencies for hydrogen evolution were about 0.9 in the range of 0.1 - 0.8 A cm^{-2}. Up to 0.2 A cm^{-2}, the current

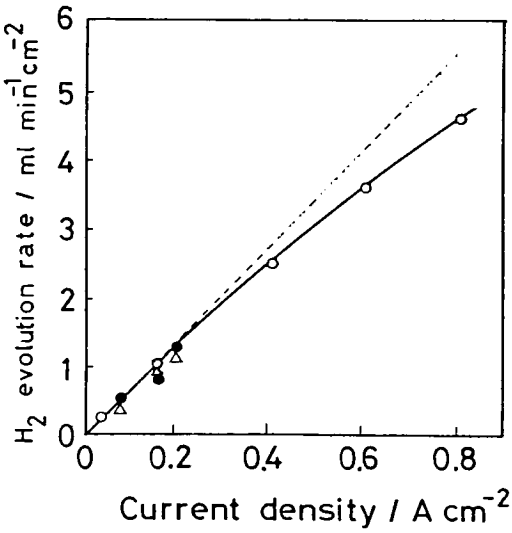

Fig. 16 Hydrogen evolution rate vs. current density at 700°C(△), 800°C(●) and 900°C(○). Electrolyte: $SrCe_{0.90}Sc_{0.10}O_{3-\alpha}$ (broken lines shows theoretical rate)

efficiency seemed to be independent of the operating temperature. In the high current density region, the current efficiency decreased to some extent. It may be ascribed to the hole conduction caused by the accumulation of oxygen evolved at the anode.

Figure 17 shows the relation between the electrolytic current and the applied voltage with and without the correction for ohmic loss at 900°C. A rather high voltage was necessary to electrolyze the water vapor due to insufficient conductivity of the specimen electrolyte. However, the polarization except the ohmic loss was rather low as indicated by curve (a) in Fig. 17.

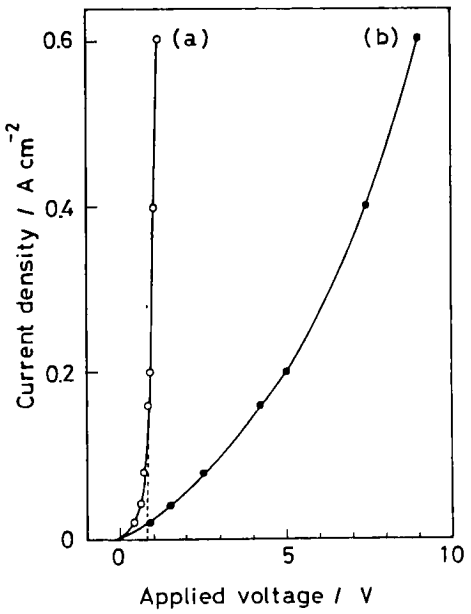

Fig. 17 Polarization curve of the steam electrolyzer at 900°C with (a), and without (b), correction for ohmic loss. Electrolyte: $SrCe_{0.90}Sc_{0.10}O_{3-\alpha}$

The theoretical decomposition voltage for water vapor is given by Eq.(2-6), in similar manner to the emf of the hydrogen fuel cell. Using the thermodynamic data[30], E° was calculated as 0.94 V at 900°C. In order to calculate the second term of

Eq.(2-6), the pressures of each gas(P_{H_2} and P_{O_2}) evolving at the electrode during the electrolysis must be known. The values at an electrolytic current density of 0.4 A cm^{-2} were estimated to be P_{H_2} = 0.044 atm, P_{O_2} = 0.022 atm and P_{H_2O} = 0.978 atm, taking the flow rate of both electrode gases to be 30 ml min^{-1}. Substituting these values into Eq.(2-6), the decomposition voltage of water vapor was calculated to be 0.7 V at 900°C.

The experimental decomposition voltage obtained by extrapolating the curve (a) in Fig. 17 back to zero current was 0.8 V, which was somewhat higher than that estimated from Eq.(2-6). However, the experimental value may be rather in good agreement with the theoretical one if one consider the errors caused by estimation of partial pressures and by extrapolation of the curve.

The actual applied voltage excluding ohmic loss was 0.95 V at 0.2 A cm^{-2}, 1.0 V at 0.4 A cm^{-2} and 1.2 V at 0.6 A cm^{-2}. This indicates that the resistance due to the polarization is fairly small compared with that of conventional water electrolysis. Although the conductivities of these proton conductors are not sufficiently high(e.g. 5 x 10^{-3} S cm^{-1} at 900°C for $SrCe_{0.90}Sc_{0.10}O_{3-\alpha}$), they may be prospective materials if they can be used as thin films to reduce ohmic loss.
For example, if the thickness of the electrolyte can be reduced to 10 μm, the required applied voltage is 1.08 V at 0.4 A cm^{-2} and 1.32 V at 0.6 A cm^{-2}

2.5 Summary

High temperature hydrogen-air fuel cells and steam electrolyzers could be constructed by using the high temperature-type

proton conductive solid electrolyte based on $SrCeO_3$.
The cells have, in principle, the following unique advantages;
(1) fuel circulation is not necessary in the fuel cell because water molecules are not generated at the fuel electrode.
(2) pure hydrogen, free from steam, is obtained from the electrolyzer.

In these cells, the polarization, excluding ohmic loss, were relatively low compared with cells using aqueous electrolytes.

Although the conductivities of these proton conductors are not sufficiently high, they may be prospective materials if they can be used as thin films to reduce ohmic loss.
Such a solid electrolyte cell may be used as a reciprocal direct energy converter between hydrogen and electricity with high conversion efficiency in a future hydrogen energy system.

CHAPTER 3 POLARIZATION CHARACTERISTICS OF GAS ELECTRODES ON HIGH TEMPERATURE-TYPE PROTON CONDUCTIVE SOLID ELECTROLYTE*

3.1 Introduction

Recently, many investigators have studied solid oxide electrolytes for use in high temperature fuel cells and steam electrolyzers. The overpotential behavior of such devices is of interest from both theoretical and practical viewpoints. It has been observed by various electrochemical methods like a complex impedance method and a current interruption method that the polarization losses at the anode in the fuel cells or at the cathode in the steam electrolyzers are significant in the case of oxide ion conductor cells. Since the electrochemically active sites might be located in the three phase region(gas-electrode-electrolyte), more interesting informations may be obtained by use of proton conductor other than oxide ion conductor.

Using the high temperature-type proton conductive solid electrolyte based on $SrCeO_3$, the hydrogen-air fuel cell and the steam electrolyzer could be constructed. Although both cells could be operated stably at 800-1000°C, the polarization characteristics of gas electrodes on these solid electrolytes were not exactly clear.

In this chapter, the polarization behaviors of the gas electrodes on the high temperature-type proton conductive solid electrolyte are studied in the fuel cell and the steam

---

* J. Appl. Electrochem., in publication
Solid State Ionics, 9/10, 1021 (1983)
Denki Kagaku, 51, 187 (1983)

electrolyzer. Using the current interruption method, it was found that the cathodic polarizations are significant in both cells with platinum electrodes.

3.2 Experimental

The experimental procedures were the same as described in the previous chapters. However, in order to obtain more dense sinters, the sintering was carried out at about 1500°C for 10 h in air.

3.3 Results and discussion

3.3.1 Polarization of platinum electrodes in hydrogen fuel cell

Figure 18 shows the performance of a hydrogen-air fuel cell in which porous platinum was used as the electrode material. The cell could be operated stably as well as the previous cell and the performances were better than these shown in chapter 2, since the quality of the ceramic disc was

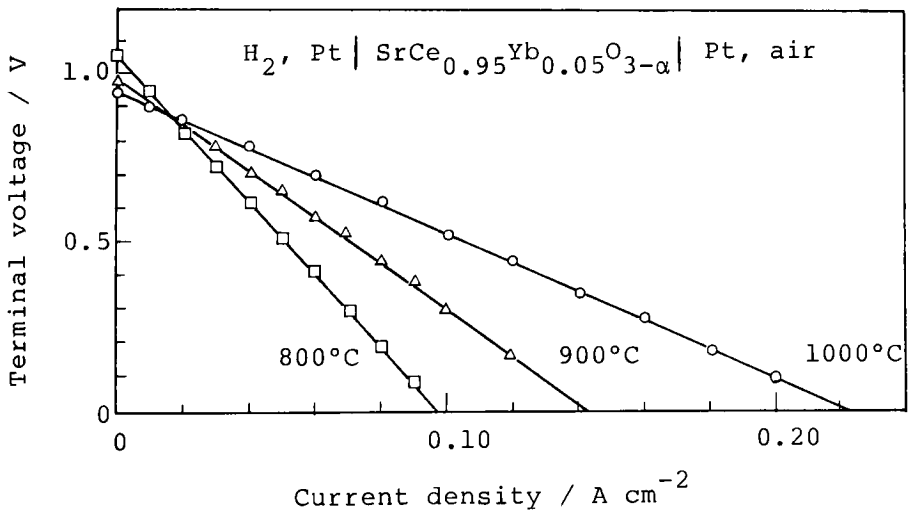

Fig. 18 Performances of the fuel cell

improved with respect to its density and the conductivity. The more dense sinters had the higher conductivity. Another reason for the improvement of the cell performances was that the method of preparing the electrodes was somewhat improved.

Figure 19 shows the typical transient behavior of the electrode potential on interrupting the discharge current. The instantaneous voltage drop after the current interruption is taken as the iR drop. Since this iR drop is large compared to the residual voltage drop, the major limitation of this cell can be regarded as the resistance of the solid electrolyte as observed in the previous chapter. In this cell, the polarization of the anode was negligibly small in the whole temperature range examined. However, the polarization of the cathode could not be neglected below 900°C.

Changing the partial pressure of oxygen(P_{O_2}), the polarization curves at the cathode were measured by the interruption method and the results are shown in Fig. 20. The relation between the overpotential and the current density is linear and the gradient of the line is steep at lower P_{O_2} and lower temperature. The polarization resistance, R_p, was calculated from the gradient of the line in Fig. 20 and plotted against the P_{O_2} in Fig. 21. The relation between log R_p and log P_{O_2} is linear in the P_{O_2} range examined and the gradient is about $-1/4$ ($R_p \propto P_{O_2}^{-1/4}$) Figure 22 shows the plot of log R_p against $1/T$ for the platinum cathode. The activation energy is about 96 kJ mol^{-1} (0.99 eV) being independent of the P_{O_2}

The anodic and cathodic polarization phenomena have been studied at some noble metal electrodes on solid oxide elec-

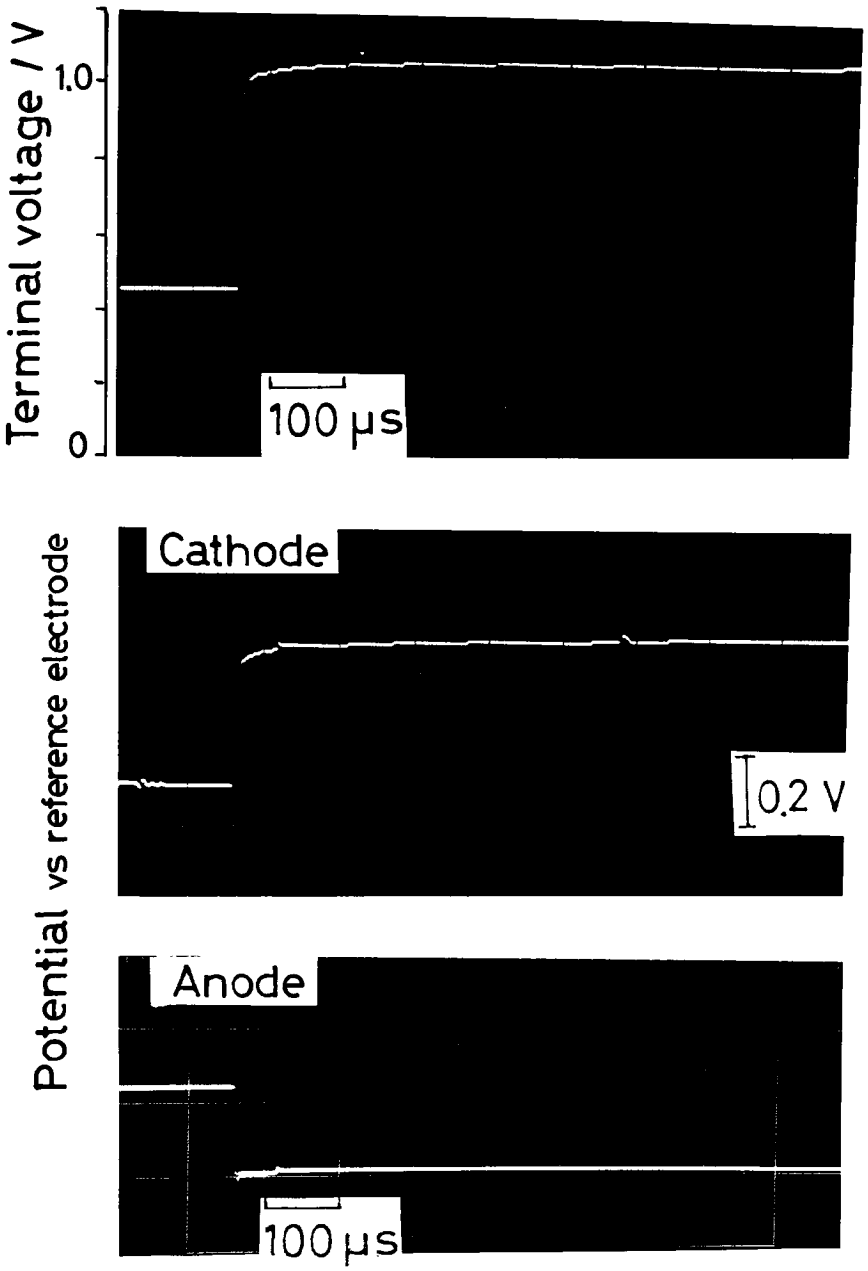

Fig. 19 Typical transient behavior of the electrode potential on current interruption.

H_2, Pt | $SrCe_{0.95}Yb_{0.05}O_{3-\alpha}$ | Pt, Air

Temperature: 900°C, Current density: 0.05 A cm^{-2}

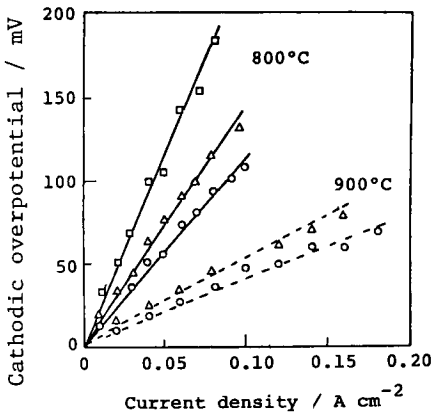

Fig. 20 Polarization characteristics of the Pt cathode in H_2-fuel cell. P_{O_2} (atm) in the cathode gas; ○:1.0, △:0.21, □:1.71 x 10^{-2}

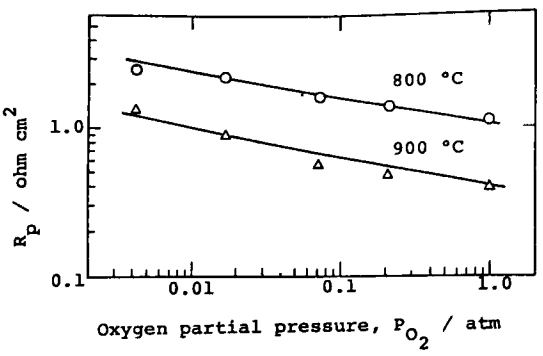

Fig. 21 Plot of R_p against P_{O_2} at the cathode.

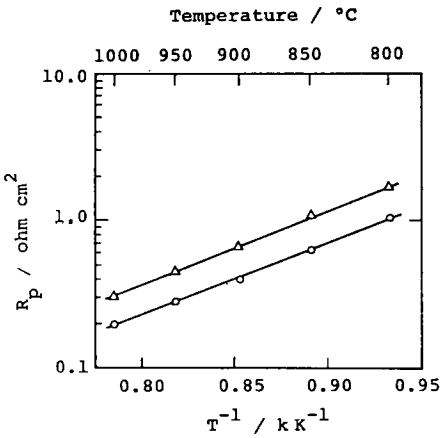

Fig. 22 Arrhenius plots of R_p. P_{O_2} (atm) in the cathode gas; ○:1.0, △:8.36 x 10^{-2}

trolytes[33-38,41-44,47-58] Depending on the electrode material, the preparation method of the electrodes and their morphology, various different results have been reported. In the fuel cell operation mode, the anodic overpotential seems to be significant, whereas the polarization loss at the cathode (air electrode) is not so large in general. However, when the gas with relatively low P_{O_2} is used, the cathodic over-

potential becomes significant due to the diffusion limitation of oxygen molecules or oxygen atoms.

Sasaki et al[55] have reported the electrode process of stabilized zirconia cell ($O_2 + 4e^- \rightleftarrows 2O^=$) by a complex impedance method. In their studies, the resistance of the electrode reaction (R_r) was found to be proportional to $P_{O_2}^{-1/4}$ for platinum electrodes and it was indicated that the rate-determining step (rds) would be i) the dissociation of oxygen molecules into atoms, ii) the surface diffusion of adsorbed oxygen atoms(O(ad)) or iii) the charge transfer step($O(ad) + 2e^- \rightarrow O^=$).

Wang and Nowick[49-51,53] have studied the electrode polarization on doped ceria. For the fine platinum paste electrodes, they showed that the electrode polarization was controlled by a charge transfer[49]. In their experiment, the exchange current density I_0 was proportional to $P_{O_2}^{1/4}$ above 600°C and the activation energy from I_0 vs 1/T was 0.99 eV(96 kJ mol^{-1}). They found that oxygen for the charge transfer process was supplied from adsorbed oxygen atoms on the platinum electrode surface which obey the Langmuir isotherm. However, except when the electrode particles were extremely small, the diffusion of oxygen atoms along the electrode was rds($I_0 \propto P_{O_2}^{3/8}$)[53]. Similar conclusion as Wang and Nowick[53] has been reported by Verkerk and Burggraaf[57], although the dependence of the resistance of the electrode reaction(R_r) upon P_{O_2} was somewhat different.

The cathodic overpotential was observed at the platinum electrode on a proton conductive solid electrolyte based on $SrCeO_3$. Similar to the case of the oxide ion conductor cell, in the fuel cell using the proton conductor, oxygen atoms must

diffuse into the electrochemically active site, where protons which have migrated across the electrolyte would react with oxygen atoms and electrons($2H^+ + 1/2\,O_2 + 2e^- \longrightarrow H_2O$). Schematic illustrations of the electrode reactions and possible elementary steps are shown in Fig. 23 and Table 4.

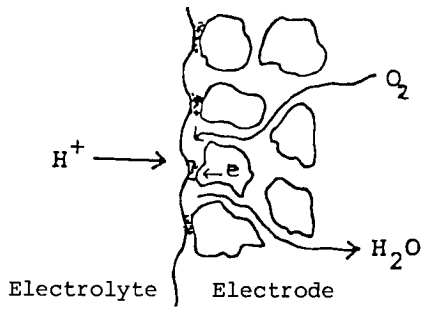

Fig. 23 Schematic illustration of the cathode reaction in the H_2-fuel cell using proton conductor

Table 4 Elementary reaction steps at the cathode and value of n in $R_p \propto P_{O_2}^{-n}$

reaction step	n in $R_p \propto P_{O_2}^{-n}$
(1) $O_2(g) \longrightarrow O_2(ad)$	1
(2) $O_2(ad) \longrightarrow 2\,O(ad)$	1 - 0
(3) Surface diffusion of O(ad)	1/2- 0
(4) $O(ad)+2H^+ + 2e^- \longrightarrow H_2O(ad)$	1/2- 0
(5) $H_2O(ad) \longrightarrow H_2O(g)$	0
Overall: $2H^+ + 1/2\,O_2(g) + 2e^- \longrightarrow H_2O(g)$	

The value of n in the form of $R_p \propto P_{O_2}^{-n}$, characteristics of each rds, is also given in Table 4[55] If step 1 is rds, R_p should be proportional to P_{O_2} (n = 1) From the experimental results obtained above, n is not unity. So, this diffusion process of oxygen molecules among the electrode particles is considered not to be rds. When step 2 is rds and the adsorption of oxygen obeys the Langmuir isotherm, n should take values from 1 to 0. Similarly, n should take values from 1/2 to 0 when step 3 or 4 is rds. On the other hand, when the diffusion of water vapor produced (step 5) is rds, R_p should not depend

upon P_{O_2} (n = 0). For step 2-4, n can be estimated rigorously if the surface coverage of oxygen atoms, θ_{ads} , is known. Several investigators have been discussed the meaning of n (in I_0 vs $P_{O_2}^{\ n}$ or R_r vs $P_{O_2}^{\ -n}$) [49,53,57,58] assuming $1 - \theta_{ads} \approx 1$. According to their reports, n was 1/4 when the charge transfer ($O(ad) + 2e^- \longrightarrow O^=$) was rds, whereas n was 3/8 or 1/2 when the surface diffusion of O(ad) (step 3 in Table 4) was rds. However, in the proton conductor fuel cell, water vapor formed at the cathode must be taken into consideration, and since θ_{ads} for the platinum electrode in the presence of water vapor is still unclear, the expression as in Table 4 is adopted.

In this study. n was found to be 1/4. Then, either one of the steps from 2 to 4 may be rds. Verkerk showed that, if step 3 is rds, the activation energy E_a of R_p is given by $E_a = \Delta H_d - n\Delta H_{ads}$ where ΔH_d and ΔH_{ads} are the activation energy for surface diffusion and the heat of adsorption, respectively[57]. Lewis and Gomer[59] found a surface diffusion enthalpy of 1.48 eV for oxygen atoms on platinum at T > 500 K. From this value and the activation energy E_a = 0.99 eV. ΔH_{ads} is caluculated to be 1.96 eV, which is close to the value in the literature[57,58]. For the charge transfer step (step 4), the situation should be different from that in the oxide ion conductor cell. In spite of using different kinds of solid electrolytes (proton and oxide ion), n is 1/4 (or around 1/4) in both cases. This suggests that the rds for the platinum electrode may be the surface diffusion of adsorbed oxygen atoms toward the electrochemically active site on the solid electrolyte.

3.3.2 Nickel anode and oxide cathode for the fuel cell

In place of expensive platinum, an attempt was made to adopt different kinds of electrode materials for the fuel cell. In order to examine nickel as an anode material, nickel formate suspended in n-butyl acetate was smeared on the surface of the specimen disc and baked at 900°C for an hour in air to adhere it as nickel oxide. When hydrogen is supplied to the anode compartment, nickel oxide is reduced to porous metallic nickel and served as an electrode material.

The performances of this cell are shown in Fig. 24. Nickel electrode thus prepared behaved as a good anode material and showed negligible anodic polarization at the current densities examined(< 0.2 A cm^{-2}), although the contact resistance must be improved. Cobalt was also tried as an anode material, but the cell performance was unsatisfactory because of its large polarization and high contact resistance.

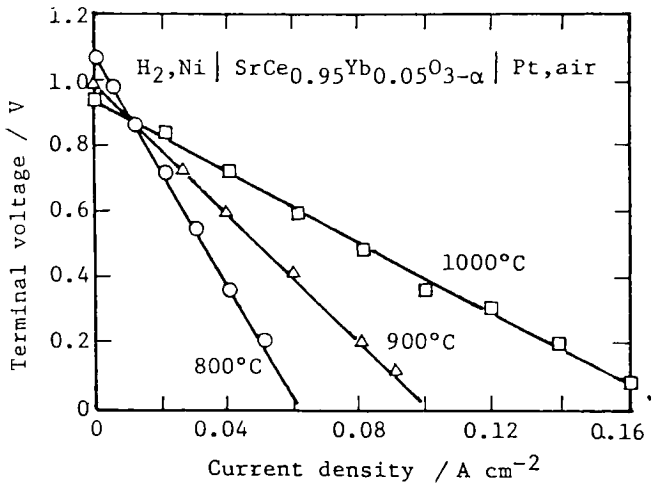

Fig. 24 Performance of the fuel cell with nickel anode

Many oxide electrodes have been studied in the case of the oxide ion conductor fuel cell[6-9,40,60]. Several semiconducting oxides were examined as the cathode for the proton conductor fuel cell. Some perovskite-type oxides based on $LaCrO_3$ had a tendency to react with $SrCe_{0.95}Yb_{0.05}O_{3-\alpha}$ ceramics to form a high resistance compound, and the cell performances were insufficient and unstable. Sn-doped In_2O_3 was also unsatisfactory as the cathode material because of its large polarization and relatively large contact resistance. Of the oxides examined, cobalt-containing perovskite-type oxides $La_{0.4}Ca_{0.6}CoO_{3-\alpha}$ and $La_{0.4}Sr_{0.6}CoO_{3-\alpha}$ exhibited comparatively good characteristics, although their polarization losses were not small compared with those of platinum cathode.

Then a fuel cell was constructed without using platinum for both electrodes. Figure 25 shows the performances of the fuel cell with Ni anode and $La_{0.4}Sr_{0.6}CoO_{3-\alpha}$ cathode.

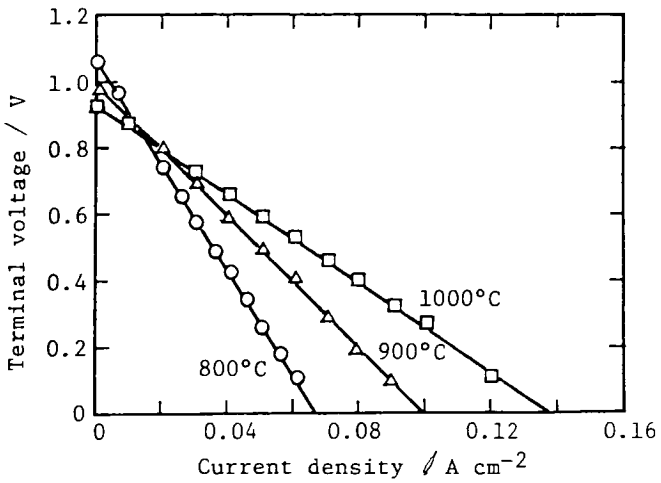

Fig. 25 Performance of the fuel cell ; H_2,Ni|$SrCe_{0.95}Yb_{0.05}O_{3-\alpha}$|$La_{0.4}Sr_{0.6}CoO_{3-\alpha}$,air

Their polarization curves are shown in Fig. 26. The cell could be operated stably and little deterioration in electrode chracteristics was recognized after 8 hours continuous discharge of 50 mA cm^{-2} at 900°C(Fig. 27) The internal resistance of this cell was higher than that of the cell with platinum electrodes probably because of high contact resistance due to unskillfulness in adhering the electrode materials to the specimen electrolyte.

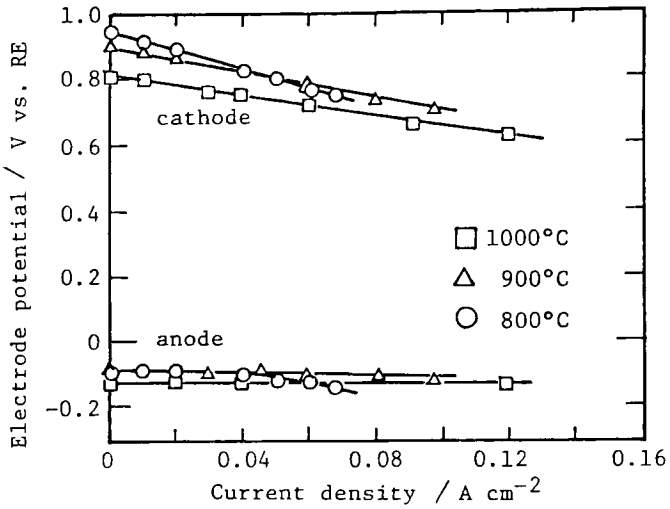

Fig. 26 Polarization of the electrodes in the fuel cell same as in Fig. 25

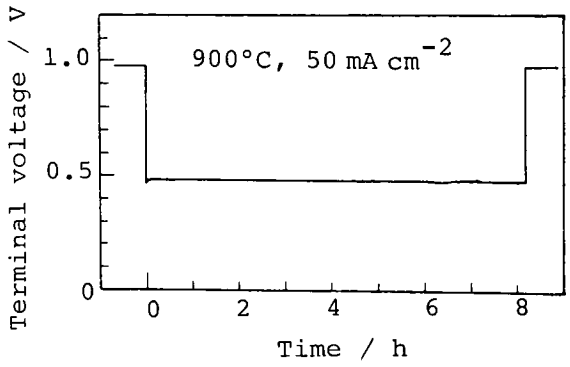

Fig. 27 Continuous discharge test of the fuel cell; H_2, Ni | $SrCe_{0.95}Yb_{0.05}O_{3-\alpha}$ | $La_{0.4}Sr_{0.6}CoO_{3-\alpha}$, O_2

3.3.3 Polarization characteristics of steam electrolyzer

Using $SrCe_{0.95}Yb_{0.05}O_{3-\alpha}$ electrolyte, the steam electrolysis was carried out as described in chapter 2. As well as $SrCe_{0.90}Sc_{0.10}O_{3-\alpha}$ electrolyte, this electrolyte exhibited good characteristics for the electrolysis and the current efficiency for hydrogen evolution was close to unity at 800°C.

Figure 28 shows the cyclic voltammograms of the anode and the cathode for the steam electrolysis. From Fig. 28, water vapor can be electrolyzed when the potential difference between both electrodes reaches to about 0.8 V at 800°C. For both electrodes, the hysterisis observed in the potential sweep toward up and down was small.

Figure 29 shows the steady-state galvanostatic polarization curves excluding ohmic losses at 900°C. It was found that the

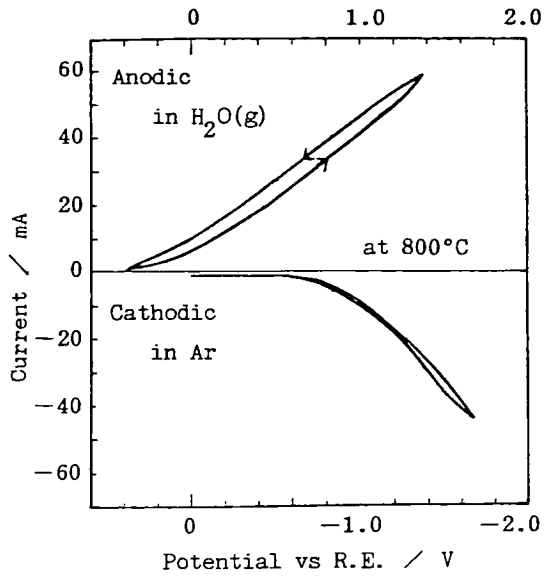

Fig. 28 Potential sweep curves of the electrodes for steam electrolyzer;
H_2O(1 atm), Pt $|SrCe_{0.95}Yb_{0.05}O_{3-\alpha}|$ Pt, Ar
sweep rate = 10 mV/s

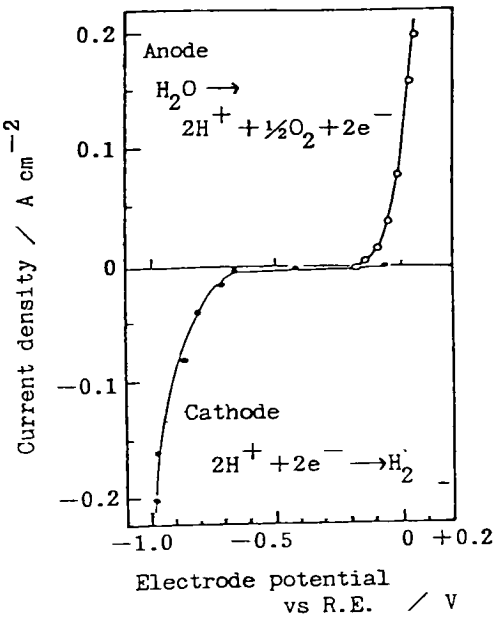

Fig. 29 Polarization curves in the same cell as in Fig. 28 at 900°C (iR free)

cathodic polarization was larger than the anodic one in this cell probably due to the concentration polarization at the cathode for evolved hydrogen.

3.4 Summary

The polarization behaviors of the gas electrodes on the high temperature-type proton conductive solid electrolyte based on $SrCeO_3$ are studied in the fuel cell and the steam electrolyzer. In the hydrogen fuel cell, the anodic polarization was negligibly small at 800 - 1000°C for the porous platinum electrode. From the dependence of the polarization resistance R_p for the cathodic reaction upon the P_{O_2} ($R_p \propto P_{O_2}^{-1/4}$), it was suggested that the rate-determining step for platinum cathode may be the surface diffusion of adsorbed oxygen atoms into the reaction zone, similar to the mechanism proposed for the platinum electrode in some oxide ion conductor cells.

For the fuel cells, nickel, as well as platinum, was one of promising materials for the anode, and some perovskite-type oxide electronic conductors for the cathode.

In the steam electrolyzer with platinum electrodes, the cathodic overpotential was larger than the anodic one. Although much more detailed study for the polarization characteristics of these cells will be necessary, the overpotential might be significant at the cathode where protons are discharged to evolve hydrogen(steam electrolysis) or water vapor(fuel cell) at present investigation stage.

CHAPTER 4 STEAM CONCENTRATION CELL USING HIGH TEMPERATURE-TYPE PROTON CONDUCTIVE SOLID ELECTROLYTE*

4.1 Introduction

In chapter 1, it was confirmed that some sintered oxides based on $SrCeO_3$ exhibited proton conduction under a hydrogen-containing atmosphere at high temperatures. A concept of a steam concentration cell using high temperature-type proton conductor was also proposed. When gases with different humidities were supplied to the electrode compartments of the gas cell with an electrolyte diaphragm based on $SrCeO_3$ ceramics, a distinct emf was observed, the electrode of higher water-vapor pressure being negative. A stable and steady current could be drawn from the cell. Although this is a kind of gas concentration cell, the concept of a steam concentration cell has not yet been reported, probably, due to lack of appropriate proton conductive solids.

In this chapter, the characteristics of the steam concentration cells are examined using a $SrCeO_3$ based proton conductor as the electrolyte and the cell reaction is investigated under various conditions. Proton transport numbers in this solid electrolyte are derived from the emf of the cell.

4.2 Experimental

The proton conductive solids used in this chapter were the sintered oxides $SrCe_{1-x}M_xO_{3-\alpha}$ (M= Yb, Mg; x = 0.05 or 0.10) The preparation of specimens were the same as in the previous

---

* J. Appl. Electrochem., 12, 645 (1982)
Solid State Ionics, 9/10, 1021 (1983)

chapter. The construction of the solid electrolyte gas cell

gas I, Pt / specimen disc / Pt, gas II

was the same as in Fig. 1(chapter 1). Both electrode compartments are separated by the solid electrolyte disc, both faces of which are covered with porous platinum to work an electrode material(projected electrode area : 0.5 cm^2). The cell temperature examined was 600-1000°C. Air, oxygen, nitrogen, helium or their mixtures at 1 atm was used as gas I or gas II.

The partial pressure of water vapor, P_{H_2O}, in the gases was controlled by saturating the water vapor at a given temperature within accuracy of $\pm$ 1 °C. Unless otherwise stated, the gas saturated with water vapor at room temperature was represented as simply wet gas(P_{H_2O} = 17-20 Torr). And dry gas was prepared by passing through silica gel and P_2O_5.

The partial pressure of oxygen, P_{O_2}, in the gas was measured with an oxygen meter which was an oxygen concentration cell using YSZ(yttria stabilized zirconia).

In order to test the discharge characteristics of the cell, a current pulse generator and a degital memory scope(Hitachi, Model VC-801-L) were employed.

The transitional resistance variation of the specimen disc was recorded as a voltage signal using an auto phase lock-in amplifier(N.F. Circuit Block Co., Model LI-574) with the frequency of 10 kHz. And the amplitude of the A.C. signal was less than 5 mV Figure 30 shows the block diagram of the measuring instruments.

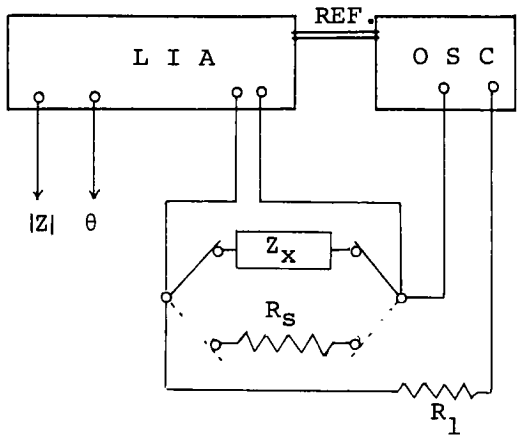

Fig. 30 Schematic diagram of the instruments for measuring the impedance by lock-in amplifier. LIA:lock-in amplifier, OSC:oscillator, REF:refrence signal, Z_x:sample, R_s:standard resistance, R_1:large resistance ($R_1 >> R_s$)

4.3 Results and discussion

4.3.1 Steam concentration cell

Typical examples of emf values for various gas cells are shown in Table 5. When dry air was introduced to both electrode compartments(cell 1 in Table 5), the emf observed was nearly zero, because of no difference in the P_{O_2} or P_{H_2O} expe-

Table 5 Emf of gas cells, gas I,Pt | specimen oxide | Pt,gas II

Cell no.	Cell type* gas I // gas II	emf / mV **			
		$SrCe_{0.95}Yb_{0.05}O_{3-\alpha}$		$SrCe_{0.90}Yb_{0.10}O_{3-\alpha}$	
		600 °C	800 °C	600 °C	800 °C
1	dry air//dry air	0.0	-0.5	0.0	0.0
2	wet air//dry air	59.0	30.0	76.0	40.0
3	dry air//dry O_2	0.5	1.0	0.0	0.0

* Dry gas - dried with silica gel and P_2O_5 ; wet gas - -saturated with H_2O at room temperature (21 - 22 °C)

** Negative sign shows that the electrode of gas II is negative

rienced by the electrode.

However, when wet air instead of dry air was introduced into one of the electrode compartments (cell 2 in Table 5), a build-up of the emf was observed as shown in Fig. 31. After a few minutes, the emf of the cell 2 reached a stable value. In this cell, the electrode with the higher humidity was negative. The emf of the cell responded to the water-vapor pressure difference between the two electrode gases as shown in Table 6. This can be regarded as a sort of steam concentration cell with a proton conductive solid electrolyte.

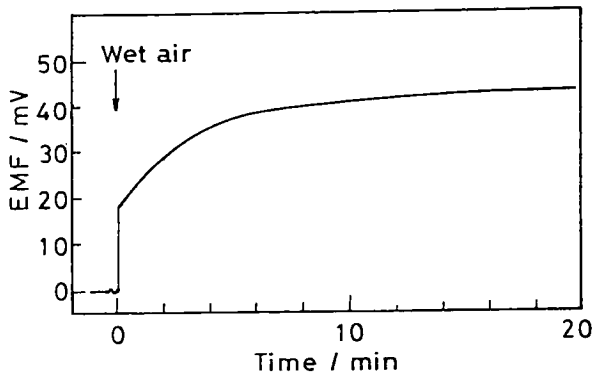

Fig. 31 Build-up of the emf on introducing wet air to one of the electrode compartments(cell 2) at 800°C.
Electrolyte : $SrCe_{0.95}Yb_{0.05}O_{3-\alpha}$

Table 6 Emf response of the cell ;
wet air (P_{H_2O} (I)) | $SrCe_{0.95}Yb_{0.05}O_{3-\alpha}$ | dry air (P_{H_2O} = 4.6 Torr)
to the change in P_{H_2O} (I).

P_{H_2O} (I) / Torr	emf / mV			
	600 °C		800 °C	
	E	E_0	E	E_0
4.6	0.0	0.0	0.0	0.0
12.8	17.8	38.4	11.0	47.3
23.8	39.5	61.8	26.0	76.0
42.2	52.5	83.4	31.4	102.5

E_0 : theoretical emf calculated from Eq.(4-3)

As described in the previous chapter, the cell did not act as an oxygen concentration cell(cell 3 in Table 5) when dry gases were used. The conduction in that case was electronic due to electron holes present in the oxides.

A steady and stable current could be drawn from the cell. During the discharge at a constant current density, the terminal voltage was very stable and no deterioration was observed even after 2 days of continuous discharge(Fig. 32). Response to the current pulse was rapid as shown in Fig. 33. Since the

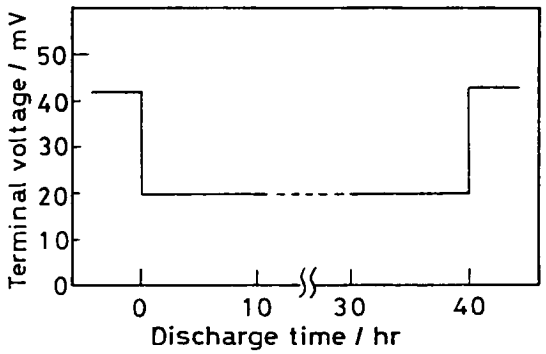

Fig. 32 Continuous discharge test of the cell : wet air//dry air, at constant current density of 2 mA cm^{-2} (800°C). Electrolyte : $SrCe_{0.95}Yb_{0.05}O_{3-\alpha}$

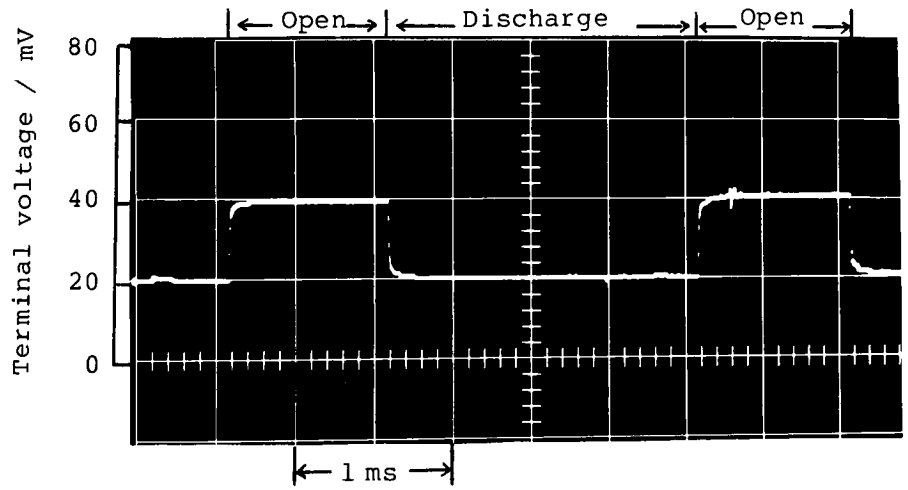

Fig. 33 Typical transient behavior on switching current on and off the cell: wet air/$SrCe_{0.95}Yb_{0.05}O_{3-\alpha}$/dry air, at 800°C, OCV=40 mV, i= 2 mA cm^{-2}

instantaneous voltage drop after current interruption is taken as the iR drop, it was suggested that the ohmic polarization was dominant in this cell. This agreed with the following experimental data obtained from the discharge curves shown in Fig. 34. The relationship between the terminal voltage and the current output are linear in this cell. From the slope of the discharge curve, D.C. resistances of the cells were calculated to be 21 Ω at 800°C and 6.5 Ω at 1000°C, respectively. On the other hand, the resistances of the cell measured by A.C. bridge at 10 kHz were 16.2 Ω at 800°C and 5.8 Ω at 1000°C, respectively. Although the D.C. resistance of the cell was somewhat higher than the A.C. value, tbe resistance of the specimen electrolyte was a major factor in the voltage drop for the cell and the electrode reactions can be considered to occur reversibly.

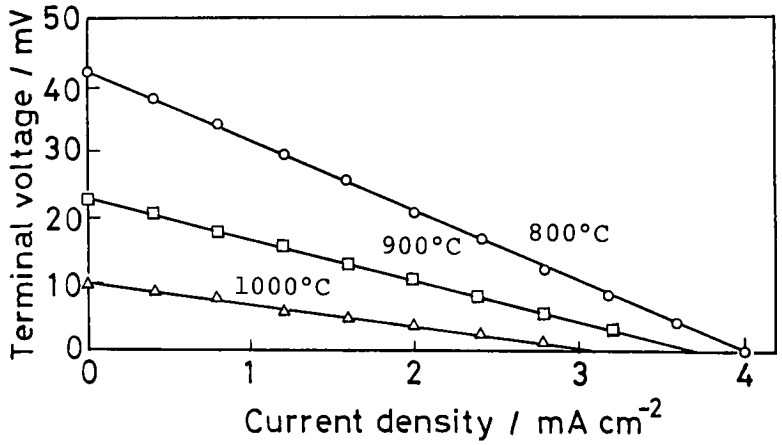

Fig. 34 Performances of the cell : wet air//dry air
Electrolyte : same as in Fig. 33

The cell behavior described above can be rationally explained by assuming that the specimen has proton conduction in the wet atmosphere. If the specimen diaphragm in cell 2 is a proton

conductor, the difference in the P_{H_2O} between the two electrodes can be a driving force of the following reactions;

Electrode reaction with higher P_{H_2O}

$$H_2O \longrightarrow 2\ H^+ + 1/2\ O_2 + 2\ e^- \qquad (4\text{-}1)$$

Electrode reaction with lower P_{H_2O}

$$2\ H^+ + 1/2\ O_2 + 2\ e^- \longrightarrow H_2O \qquad (4\text{-}2)$$

For this reason, this cell may give a stable emf, with the electrode at the lower P_{H_2O} being the cathode.

In order to verify the above reactions, the oxygen evolution or consumption at the electrode during discharge of the cell was checked as illustrated in Fig. 35(a). In this case, dry and wet helium gases were supplied to each electrode compartment at a regulated flow rate(60 ml min^{-1}). The electrolyte diaphragm used was $SrCe_{0.95}Yb_{0.05}O_{3-\alpha}$ The emf of the cell was 108 mV at 800°C. The partial pressure of oxygen in the wet gas was monitored at the outlet of the cell by using a YSZ oxygen meter kept at 800°C.

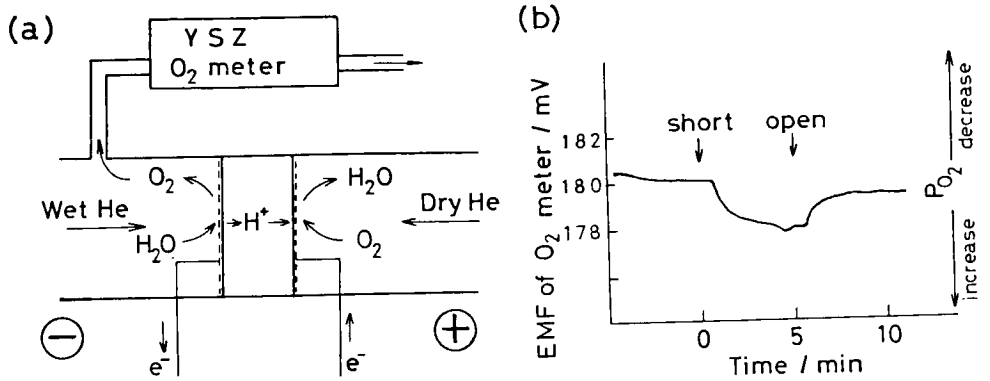

Fig. 35 Schematic illustration of the oxygen evolution at the anode of the steam concentration cell (a)Schematic illustration of the cell reaction. Concept and method for oxygen detection. (b)Change in the P_{O_2} in wet helium detected by the emf response of the YSZ oxygen meter.

When this cell was short-circuited, a current of 287 μA was observed and the increase in P_{O_2} in the wet helium at the outlet of the anode compartment was detected by the emf of the oxygen meter(Fig. 35(b)). On opening the circuit, the P_{O_2} returned to the original value rapidly. At the outlet of the cathode compartment, the inverse response(decrease in P_{O_2} in dry helium on short-circuiting) was observed. Thus, it could be confirmed that the electrode reactions are the oxygen evolution at the anode and consumption at the cathode while discharging the cell. These results support the validity of Eq.(4-1) and (4-2).

From thermodynamic, electrochemicel consideration on Eq.(4-1) and (4-2), the theoretical emf of the steam concentration cell can be derived. Generally, when gas I and gas II in the cell include oxygen and water vapor at different partial pressures, the emf, E, of the cell can be given as

$$E = \frac{RT}{2F} \ln \frac{P_{H_2O}(I)}{P_{H_2O}(II)} \left(\frac{P_{O_2}(II)}{P_{O_2}(I)} \right)^{1/2} \qquad (4\text{-}3).$$

Further experiments to measure the emf were carried out and the results are shown in Table 7. A stable emf was also observed when the two electrode gases had different P_{O_2} but equal P_{H_2O} like cell 4 in Table 7. This is reasonable since the emf of cell 4 can be written according to Eq.(4-3) by

$$E = \frac{RT}{4F} \ln \frac{P_{O_2}(II)}{P_{O_2}(I)} \quad \text{when } P_{H_2O}(I) = P_{H_2O}(II) \qquad (4\text{-}4).$$

This is a "wet" oxygen concentration cell(cf, cell 3 in Table 5). Cells 5 and 6 show that the electrodes with higher humidity are

Table 7 Emf of gas cells, gas I,Pt | specimen oxide | Pt,gas II

Cell no.	Cell type* gas I // gas II	emf / mV ** $SrCe_{0.95}Yb_{0.05}O_{3-\alpha}$ 600 °C	$SrCe_{0.95}Yb_{0.05}O_{3-\alpha}$ 800 °C	$SrCe_{0.95}Mg_{0.05}O_{3-\alpha}$ 600 °C	$SrCe_{0.95}Mg_{0.05}O_{3-\alpha}$ 800 °C
4	wet air//wet O_2	25.0	14.0	16.0	12.0
5	wet air//dry O_2	69.5	30.5	46.8	19.5
6	dry air//wet O_2	-43.5	-13.0	-25.0	-10.5

* Dry gas - dried with silica gel and P_2O_5 ; wet gas - -saturated with H_2O at room temperature (21 - 22 °C)

** Negative sign shows that the electrode of gas II is negative

also negative and that the absolute emf value at 600°C are higher than those of oxygen concentration cells(29.5 mv at 600°C). Similarly, the emf behavior of cell 5 and 6 can be explained qualitatively by Eq.(4-3).

4.3.2 Transitional variation of the electrode potential and the resistance of the electrolyte in the steam concentration cell

As shown in Fig. 31, when wet air instead of dry air was introduced into one of electrode compartments, a build-up of emf was observed. And the resistance of the electrolyte increased simultaneously(Fig. 6 in chapter 1), probably due to the decrease in the hole concentration in the specimen. In order to investigate the transient behavior of the proton conduction in this oxide, the transitional change in the electrode potential and the conductivity variation of the specimen electrolyte were

measured immediately after wet air had been introduced into one of the electrode compartments.

A rough sketch of the cell and the results are shown in Fig. 36. At first, dry air was supplied to both electrode compartments and the reference electrode on the lateral of the specimen disc was exposed to the atmosphere in the electric furnace. After that, wet air was introduced into one of the compartments (A in Fig. 36), and the variation of the potential and the resistance between electrodes were measured continuously.

As shown in Fig. 36, the change in the potential was remarkable at the anode(wet air electrode) whereas it was negligible

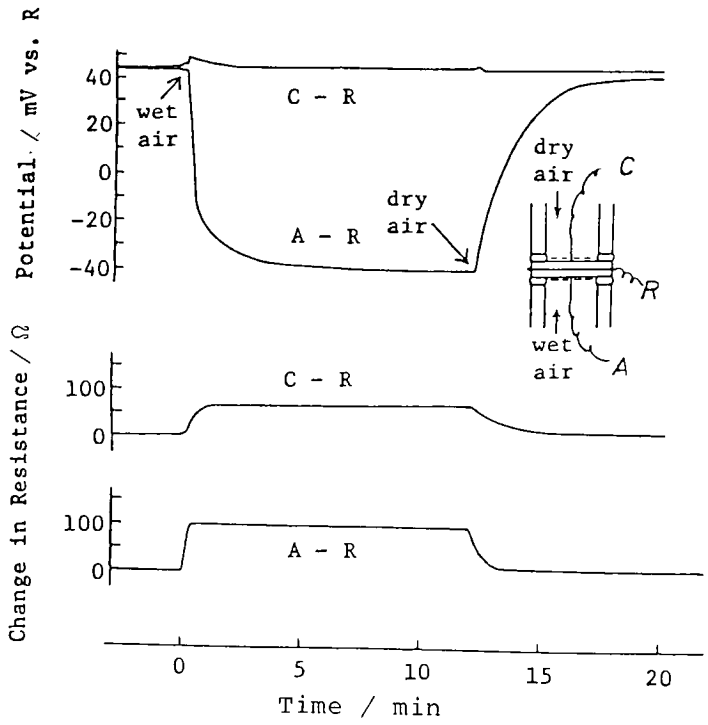

Fig. 36 Transitional variation of the potential and resistance between electrodes of steam concentration cell (800°C)

at the cathode, indicating that the increase in the P_{H_2O} at the anode does not influence to the potential at the cathode.

The change in the resistance, measured by an auto phase lock-in amplifier, was more remarkable at the anode than at the cathode, but the time required to reach a constant resistance was somewhat longer at the cathode than at the anode, suggesting that the protons injected at the anode had to migrate through the electrolyte toward the cathode. However, the short transitional time within a few minutes suggests that the rates of proton formation at the oxide surface and the proton diffusion into the bulk of the oxides are fairly fast.

4.3.3 Electroactive species at the anode

For the formation of protons at the anode, two distinguishable reaction models are possible.

Model 1 ;

$$H_2O(g) \rightarrow 2\,H^+(\text{electrolyte}) + 2\,e^-(\text{electrode}) + 1/2\;O_2(g) \qquad (4\text{-}5)$$

Model 2 ;

$$H_2O(g) \overset{K}{\rightleftarrows} H_2(g) + 1/2\;O_2(g) \qquad (4\text{-}6)$$

$$H_2(g) \rightarrow 2\,H^+(\text{electrolyte}) + 2\,e^-(\text{electrode}) \qquad (4\text{-}7)$$

In model 1, protons are extracted directly from water molecules at the anode. In model 2, hydrogen molecules, which are produced by the thermal dissociation equilibrium(Eq.(4-6)), are ionized at the anode. Which model is more valid?

As shown in Fig. 34, quite a high current density(4 mA cm^{-2}) could be drawn out stably from the steam concentration cell at 800°C. Considering the two electron reaction for the ionization of one

water molecule or one hydrogen molecule, the rate of consumption at the anode was 1.25×10^{16} molecules $sec^{-1}cm^{-2}$. Assuming that only the molecules which collide with the electrode plane(wall) could be ionized to protons, the number of molecules supplied to the electrode was estimated as follows.

The mean velocity of a molecule, $\bar{c}$, is given by

$$\bar{c} = \left(\frac{8RT}{\pi M}\right)^{1/2} \qquad [\ cm\ sec^{-1}\ ] \qquad (4\text{-}8),$$

where M, R and T are molecular weight, gas constant and absolute temperature, respectively. The rate of collision of the molecules with a wall per unit area, Z, is given by

$$Z = 1/4\ N\ \bar{c} \quad [\ molecules\ sec^{-1}cm^{-2}\ ] \qquad (4\text{-}9)$$

where N is the number of molecules per unit volume.

The equilibrium partial pressure of hydrogen, P_{H_2}, in the experimental condition calculated from the dissociation constant K[30] is $P_{H_2} = 4.49 \times 10^{-11}$ atm.
Using this value, $\bar{c}_{H_2}$ and Z_{H_2} are calculated as

$$\bar{c}_{H_2} = 3.37 \times 10^{5}\ cm\ sec^{-1}$$
$$Z_{H_2} = 2.59 \times 10^{13}\ molecules\ sec^{-1}cm^{-2}\ .$$

For water vapor($P_{H_2O} = 2.63 \times 10^{-2}$ atm), these values are

$$\bar{c}_{H_2O} = 1.12 \times 10^{5}\ cm\ sec^{-1}$$
$$Z_{H_2O} = 5.04 \times 10^{21}\ molecules\ sec^{-1}\ cm^{-2}\ .$$

The consumption rate by the discharge current is higher than the rate of supply of hydrogen to the electrode by a factor of 500. Although the gas flow rate(60 ml min^{-1}: 2 cm sec^{-1}) was com-

pletely neglected in these calculations, the values of Z might be somewhat higher in the actual cell. At 1000°C, the equilibrium constant K is about two orders of magnitude higher than at 800°C. However, even though the rate of supply of hydrogen became comparable to that of consumption, a considerable concentration polarization should occur on discharging the cell. Such polarization could not be observed as described above.

On the other hand, water molecules are sufficiently supplied to the electrode at the temperature examined(about 6 orders of magnitude over the consumption rate) so that the number of molecules consumed at the electrode can be neglected.

Therfore, the species ionized at the anode of this steam concentration cell must be water molecules(Eq.(4-5)) and not hydrogen molecules(Eq.(4-7)).

4.3.4 Proton transport number of $SrCe_{0.95}Yb_{0.05}O_{3-\alpha}$

As shown in Table 6, observed emfs of the steam concentration cells were generally lower than the value calculated from Eq.(4-3). This shows that the conductions in specimen ceramics are not purely ionic but partially electronic.

In order to determine the proton transport numbers, t_{H^+}, in the specimens, the emf values of the following steam concentration cells were measured. The P_{H_2O} added to each electrode gas were 23.8 Torr and 4.6 Torr, corresponding to the vapor pressures at 25°C and 0°C, respectively. And the P_{O_2} at both electrodes were kept at the same value.

When $P_{O_2}(I) = P_{O_2}(II)$, according to Eq.(4-3), the theoretical emf of the cell is given by

$$E_0 = \frac{RT}{2F} \ln \frac{P_{H_2O}(I)\ (=23.8\ \text{Torr})}{P_{H_2O}(II)\ (=\ 4.6\ \text{Torr})} \qquad (4\text{-}10)$$

And t_H^+ was determined to be E/E_0(E is the measured emf).

Figure 37 shows the proton transport number of $SrCe_{0.95}Yb_{0.05}O_{3-\alpha}$ at 600-1000°C. When nitrogen gas($P_{O_2} = 1.7 \times 10^{-3}$ atm) was used, the proton transport number was about unity at 600°C. However, with increase in P_{O_2}, the t_H^+ decreases. Such experimental facts could be rationally explained by the mechanism of proton conduction in this specimen proposed in the previous chapter. Decreases in t_H^+ with increases in P_{O_2} might be ascribed to the increases in hole concentration in the specimen oxide. Electron holes surviving in the oxides might make t_H^+ decrease.

Although the t_H^+ in the specimen under wet air decreased at higher temperatures, the t_H^+ was about 0.95 at 800°C for the case

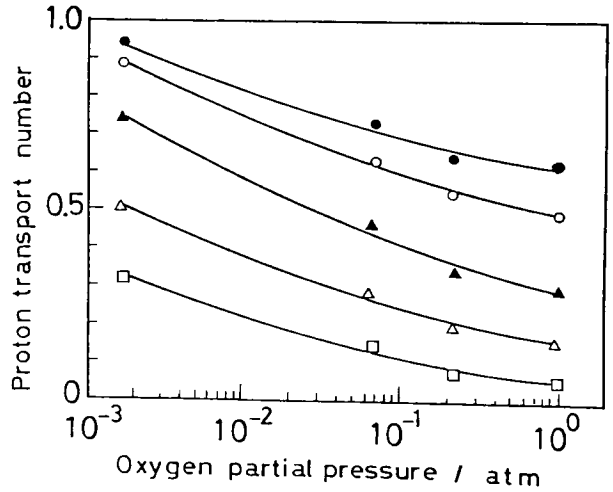

Fig. 37 Dependence of the proton transport number on the P_{O_2}. Specimen: $SrCe_{0.95}Yb_{0.05}O_{3-\alpha}$. ●:600°C, ○:700°C, ▲:800°C, △:900°C, □:1000°C

of hydrogen-air fuel cell. Furthermore, in the steam electrolyzer to produce hydrogen with $SrCeO_3$-based electrolytes, the current efficiencies were about 0.9 at 700-900°C. These facts suggests that the t_{H^+} may become much higher in the steam concentration cell if the gas with higher P_{H_2O}, which results in higher P_{H_2} and lower P_{O_2}, is used as the anode gas. Detailed studies of proton conduction in the oxides are presented in chapter 7.

4.4 Summary

A steam concentration cell could be constructed using the high temperature proton conductor based on $SrCeO_3$ at 600-1000°C. When gases with different humidities were supplied to the gas cells with these electrolytes, a distinct emf was observed, the electrode of higher P_{H_2O} being negative. The resistance of the specimen electrolyte was the major factor determining the voltage drop on discharging the cell and the electrode reactions occur reversibly.

The transient conduction behavior of this material suggested that the rates of proton formation at oxide surface and the proton diffusion into the bulk were fairly fast at high temperatures.

From the analysis of the change in P_{O_2} in the electrode gas on short-circuiting the cell, the electrode reactions were confirmed to be those of Eq.(4-1) and (4-2). It was also clarified that, at the anode, protons are extracted directly from water molecules, and that the contribution of hydrogen molecules produced by the thermal dissociation equilibrium is negligible as electroactive species at the anode.

Based on Eq.(4-1) and (4-2), the theoretical emf of the steam concentration cell was derived, and the emf behavior of this cell could be rationally explained by this equation. As the conduction in the ceramics were not purely ionic but partially electronic, the proton transport number, t_{H^+}, in the specimen was determined from the emf. The t_{H^+} increased with decreasing P_{O_2} and with decreasing temperature.

The steam concentration cell may be applied, in principle, to the high temperature-type humidity sensor and the recovery of electric energy from exhaust gas from large-scale burner in the industrial plants. In the former case, the P_{H_2O} can be known from the emf of the cell, if the P_{H_2O} at one electrode and the P_{O_2} at both electrodes are known. This type of sensor has the possibility of serving as a check and control device for water vapor.

CHAPTER 5 GALVANIC CELL-TYPE HUMIDITY SENSOR USING HIGH TEMPERATURE-TYPE PROTON CONDUCTIVE SOLID ELECTROLYTE*

5.1 Introduction

Using the $SrCeO_3$-based solid proton conductor as the electrolyte for the gas cell, a steam concentration cell has been constructed. One possible application of the steam concentration cell will be a galvanic cell-type humidity sensor which had not previously been reported.

There has been an increasing demand for humidity control. Various types of the humidity sensors have been studied by many workers[61-68]. Adsorption of water vapor changes the conductance or capacitance of solids(metal oxides, organic compounds or some electrolytes, etc.) In the conventional humidity sensors, changes in humidity can be converted into an electrical signal by applying A.C. or D.C. bias from the external power supply. However, since almost all of the chemisorbed water are eliminated from the surface at high temperatures(> 400 °C)[69], the working temperature of the conventional sensor is restricted to relatively low(below 160°C[67]) Although a high temperature-type sensor(up to 500°C) based on $LiMO_4$(M = Al and Ga) has been reported recently[68], the response speed to the humidity change seemed to be slow in this material.

In contrast to the conventional humidity sensors, the galvanic cell-type sensor proposed here may, in principle, have the following features; (a) the humidity is directly given by the emf

---

* J. Appl. Electrochem., 13, 365 (1983)

of galvanic cell, (b) the working temperature can be high because proton conduction in the ceramics appears at elevated temperature.

In this chapter, the galvanic humidity sensors were constructed using high temperature proton conductors based on $SrCeO_3$ and their performances were examined. These sensors exhibited a stable operation over a wide humidity range, a very short response time and relatively small response to impurity gases.

5.2 Working principles of the sensor

As illustrated in Fig. 38, a gas cell constructed with a proton conductive ceramics as the electrolyte exhibits an emf due to the concentration difference of water vapor, when air with different humidities are introduced to each electrode compartment.

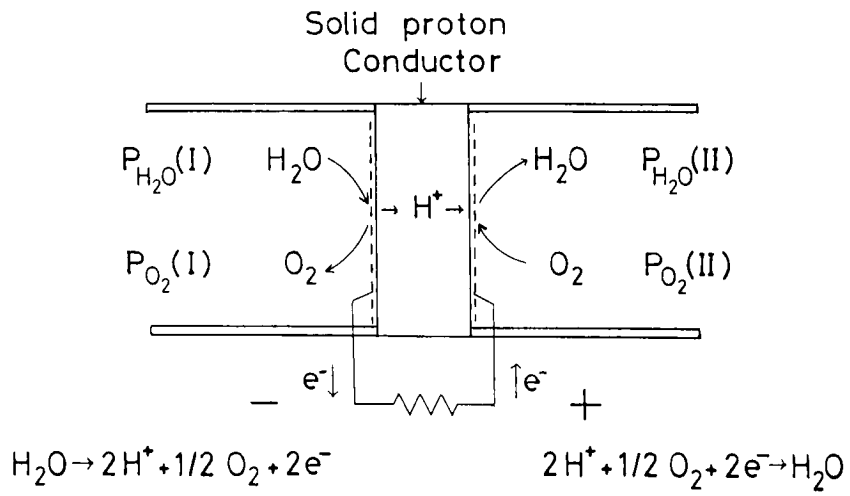

Fig. 38 The concept of a steam concentration cell using solid proton conductor. $P_{H_2O}(I) > P_{H_2O}(II)$

The theoretical emf E_0 can be written as

$$E_0 = \frac{RT}{2F} \ln \frac{P_{H_2O}(I)}{P_{H_2O}(II)} \left(\frac{P_{O_2}(II)}{P_{O_2}(I)} \right)^{1/2} \qquad (5\text{-}1)$$

When $P_{O_2}(I)$ is close to $P_{O_2}(II)$, as in ambient atmosphere with different humidities, E_0 can be written as

$$E_0 = \frac{RT}{2F} \ln \frac{P_{H_2O}(I)}{P_{H_2O}(II)} \qquad (5\text{-}2)$$

If $P_{H_2O}(II)$ is a known value and is constant, the humidity in the compartment I (or $P_{H_2O}(I)$) may be estimated from the measured emf of the cell.

When an electrolyte involves electronic conduction, emf is lowered to some extent

$$E \leqq t_H^+ \cdot E_0 \qquad (5\text{-}3)$$

where t_H^+ is the proton transport number in the solid electrolyte. Even in such a case, $P_{H_2O}(I)$ can be determined from the measured emf by using a calibration curve.

5.3 Experimental

The proton conductive ceramics used in this experiment was $SrCe_{0.95}Yb_{0.05}O_{3-\alpha}$. The dense sinters obtained were sliced into thin discs(thickness : about 0.5 mm, dia : 12 mm) to provide the electrolyte diaphragm for the gas cell.

The construction of the galvanic cell-type humidity sensor was illustrated in Fig. 39. Each face of solid electrolyte diaphragm was smeared with platinum paste and baked at 1000°C

to provide a porous electrode material. The specimen electrolyte thus obtained was attached to a ceramic tube by ceramic adhesives based on Al_2O_3(SUMICERAM®). Thus, two electrode compartments, inside and outside the tube, were separated by the specimen electrolyte. The electrolyte was heated by a nichrome wire heater wound around the outer tube of the sensor.

As is clear from Eq.(5-2), it is necessary to keep either $P_{H_2O}(I)$ or $P_{H_2O}(II)$ constant in order to obtain a steady emf response to a given humidity. Two types of sensors were examined. One is a gas flow type(A-type in Fig. 39) in which air saturated with water vapor at 0°C was passed through the inner electrode compartment(inside the tube - $P_{H_2O}(II)$ = 4.6 Torr). Another is a packing type(B-type in Fig. 39) in which a molecular sieve is packed in order to keep the P_{H_2O} inside the

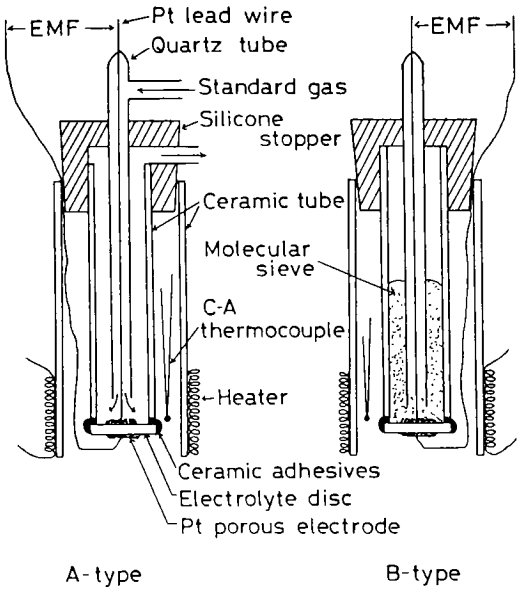

Fig. 39 Schematic illustration of the galvanic cell-type humidity sensors

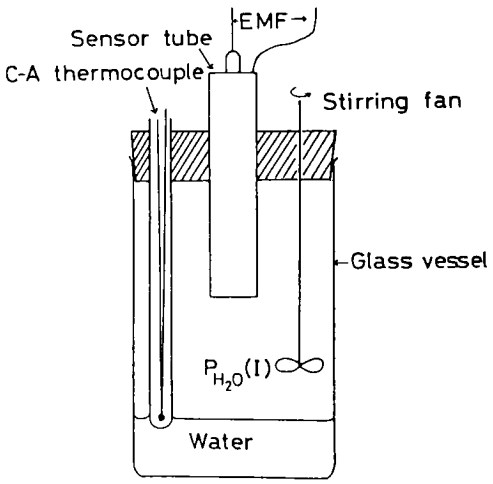

Fig. 40 Setting of the sensor tube in the test chamber

tube constant. As shown in Fig. 40, the sensor tube was set in a glass vessel(volume: about 1000 ml) settled in a thermostat. A small stirring fan was placed in the vessel.

The humidity in the vessel(outside the tube) was controlled by regulating the temperature of water at the bottom of the vessel. The temperature of water was controlled within $\pm$ 1°C accuracy. The humidity in the vessel was represented by the partial pressure of water (Torr), assuming that the gas in the vessel(normally, air) was completely saturated with water.

The emf of the sensor was measured by a conventional electrometer. Also, the emf and the temperature of water were recorded simultaneously by a recorder.

Prior to the initial measurement, the sensor was heated to 400°C for a overnight in order to eliminate the impurities from ceramic adhesives.

5.4 Results and discussion

5.4.1 Emf response to the humidity

Figure 41 shows the emf response of the A-type sensor to the logarithm of P_{H_2O}(I) at 400°C using $SrCe_{0.95}Yb_{0.05}O_{3-\alpha}$ as the electrolyte. The sensor exhibited a stable, good, linear response against the logarithm of P_{H_2O} and good agreement with the theoretical emf value calculated from Eq.(5-2) There was no change in the emf on stirring with the fan in the vessel, but the response time became somewhat shorter.

The response of the emf following an increase or a decrease in humidities were examined by changing the temperature of vessel

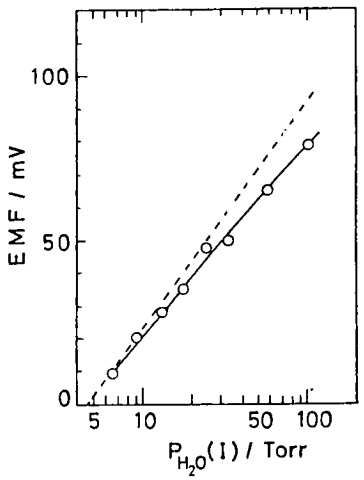

Fig. 41 EMF response of the A-type sensor to P_{H_2O}(I). Working temperature: 400°C (---:theoretical value calculated from Eq.(5-2))

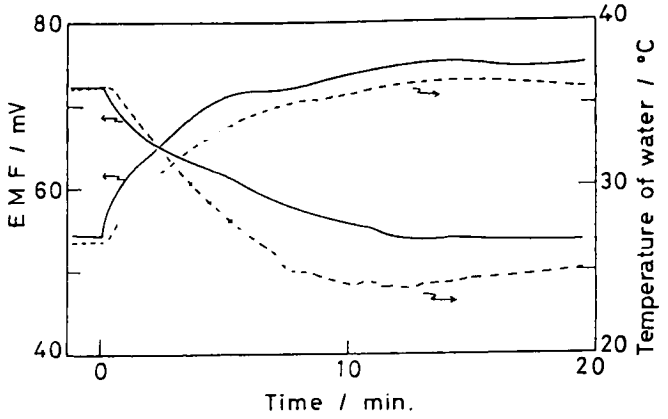

Fig. 42 Change in EMF response during increase or decrease in the P_{H_2O}(I). A-type sensor (working temperature: 400°C). ———:EMF response, ----: temperature of water

gradually. Figure 42 shows the results. The emf and the temperature of water change parallel against time during increasing humidity, and, during humidity decrease, the change in emf with time corresponds to the change in temperature of water with time.

To examine the rapid response characteristics, the humidity in the vessel was changed quickly by injecting hot water into the bottom of the vessel. The emf of the sensor increased rapidly corresponding to the rise of the temperature of the water as shown in Fig. 43. It took only a few seconds for the emf to establish a stable value after vapor pressure was changed rapidly from 12 Torr to 20 Torr.

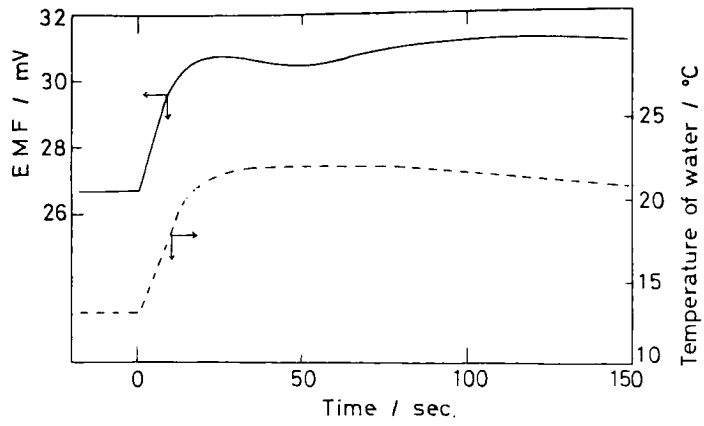

Fig. 43 EMF response of the A-type sensor on rapid increase in the P_{H_2O}(I) (working temperature:400°C)

5.4.2 Some improvement of the sensor

It may be unfavorable for a practical sensor to use a flow of standard humidity gas. So, the B-type sensor was examined as described in experimental section.

Figure 44 shows the emf response of this type of sensor at 300-400°C. This sensor exhibited a good linear response of emf aginst the logarithm of P_{H_2O}(I) The emf at 400°C was expressed as $E\,(mV) = -23.0 + 93.7 \log P_{H_2O}(Torr)$ with a standard deviation of 4.6 mv for P_{H_2O}= 10-100 Torr. Due to the lower vapor pressure inside the tube compared to the case of the A-type sensor, the emf of B-type sensor is higher than that of the A-type one. Since the equilibrium vapor pressure inside the tube becomes lower with decreasing temperature, it is reasonable that the emfs at lower temperatures are larger than those at higher temperatures. Similarly to the A-type sensor, the response of the B-type sensor was also rapid(within a few seconds)

The sensitivity of the sensor was determined from Fig. 44 and listed in Table 8. The B-type sensor had a larger sensi-

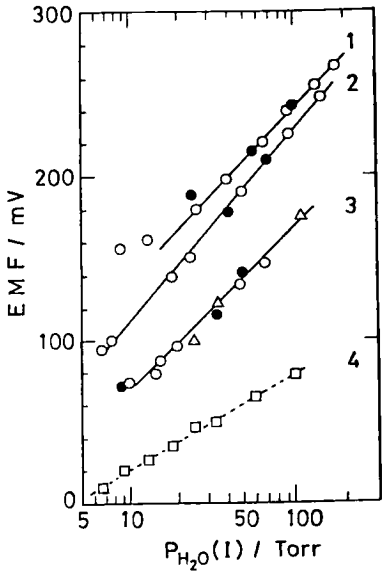

Fig.44 EMF response of the B-type sensor(line 1-3) and the A-type sensor(line 4) to P_{H_2O}(I). Working temperature; 1:300°C, 2:350°C, 3 and 4:400°C.
○:1 st increasing the P_{H_2O}(I),
●:1 st decreasing,
△:2 nd increasing.

Table 8 Sensitivity of the galvanic cell-type sensor at 400°C

	Sensitivity / mV decade^{-1}
A-type	58.0
B-type	93.7
Theoretical ($2.303 \frac{RT}{2F}$)	66.7

tivity than the A-type. However, the sensitivity of the B-type exceeded the theoretical value(= $2.303 \frac{RT}{2F}$)

This phenomenon can be explained by considering the proton transport number, t_H^+, in $SrCe_{0.95}Yb_{0.05}O_{3-\alpha}$ electrolyte. As described previously, the conduction in these ceramics is not purely ionic but partially electronic, and the t_H^+ at very low vapor pressure is small. In the case of A-type sensor, the

vapor pressure at the standard electrode inside the tube is not so low(4.6 Torr) so that the t_{H^+} of the electrolyte can be regarded as almost constant(about 0.9, from Fig. 41) irrespective of vapor pressure outside the tube ($P_{H_2O}(I)$).

On the other hand, in the case of the B-type sensor, the humidity inside the sensor tube has a much lower value than the case of the A-type. Also the t_{H^+} may decrease with decreasing vapor pressure in the outer atmosphere. As a result, the gradient of E aginst log $P_{H_2O}(I)$ is steep.

5.4.3 Response to the impurity gas

The effect of some gases on the emf response of the B-type sensor were tested as follows. Air(flow rate = 100 ml min^{-1}) in the laboratory room(60 %Rh, 17°C, P_{H_2O} = 8.7 Torr) was introduced to the glass vessel. When the sensor exhibited a constant emf response, an impurity gas of 100 µl was injected into the vessel with the flow of air. Hydrogen, butane and carbon dioxide were injected as the impurity gas.

The emf response and the maximum deviation from the usual humidity response are shown in Fig. 45 and Table 9, respectively. Hydrogen gas increased the emf. This is reasonable because the electrolyte of the sensor is a proton conductor. On the other hand, there was no change in the emf for the injection of carbon dioxide, even if a few ml of carbon dioxide was injected. Butane gas made tbe emf decrease somewhat, probably because of its adsorption to the electrode surface instead of water vapor. However, the emf change caused by the impurity gas injection was small compared with the emf response to the humidity, especially

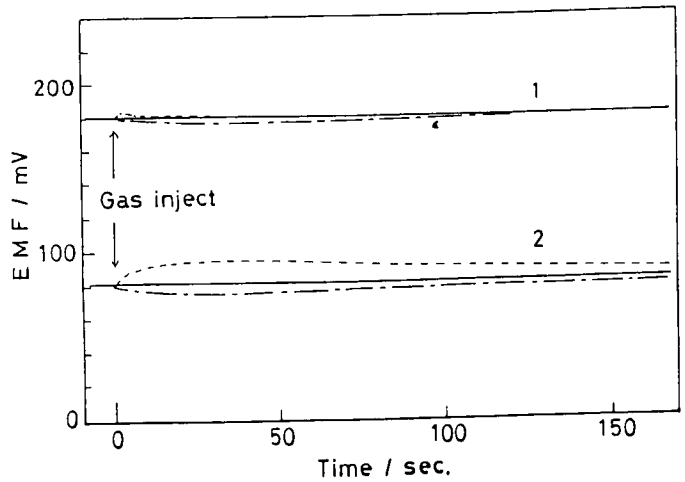

Fig. 45 Response of the B-type sensor to the impurity gas injection. impurity gas; ---:H_2, -·-:C_4H_{10}, ——:none and CO_2, Working temperature; 1:300°C, 2:400°C

Table 9 Deviation of the emf from the usual humidity response caused by the impurity gas injection

	Maximum deviation of the emf / %	
impurity gas	300 °C	400 °C
H_2	+ 0.78	+ 17
C_4H_{10}	- 1.7	- 6.3
CO_2	± 0.0	± 0.0

at 300°C(Table 9).

According to Eq.(5-1), this sensor responds to the pressure difference in oxygen between two electrode compartments. However, the vapor pressure can be determined by using calibration curve if the pressure difference in oxygen is constant.

Furthermore, even if oxygen pressures at both electrodes are variable, the emf due to oxygen partial pressure can be canceled by connecting a galvanic cell-type oxyge sensor electrically to this sensor in series.

5.5 Summary

Using high temperature-type proton conductive solid electrolyte, a galvanic cell-type humidity sensor, which is based on the steam concentration cell, could be constructed. This sensor exhibits fast response, good reproducibility, small response to impurity gases, and linear response against logarithm of vapor pressure over a wide humidities.

An important feature of this sensor lies on its high temperature working(up to 1000°C), which is unavailable for conventional humidity sensor. This sensor may be available for vapor pressure mesurements of high temperature gases in various industrial plants.

CHAPTER 6 STUDIES ON SOLID ELECTROLYTE GAS CELLS WITH HIGH TEMPERATURE-TYPE PROTON CONDUCTOR AND OXIDE ION CONDUCTOR*

6.1 Introduction

Using high temperature-type solid electrolytes, various galvanic gas cells can be constructed. Fuel cells and oxygen concentration cells have been intensively studied by many workers[38-60]. In these studies, oxide ion conductive solid electrolyte, like stabilized zirconias or doped cerias, were predominantly used.

If one can apply high temperature-type proton conductors to the solid electrolyte for the gas cell, much more informations can be obtained, e.g., for electrode reactions or thermal equilibrium in hydrogen-containing atmosphere. However, such solids had been scarcely known.

Using the $SrCeO_3$-based proton conductive ceramics as the solid electrolyte, the steam electrolyzers, the hydrogen fuel cells and the steam concentration cells could be constructed at high temperature.

In this chapter, various gas cells are characterized under hydrogen-water vapor or oxygen-water vapor atmosphere. The emf behavior of these cells is investigated using high temperature-type proton conductor based on $SrCeO_3$ and the oxide ion conductor, YSZ(yttria stabilized zirconia) Oxygen, steam and hydrogen concentration cells were examined at 600-1000°C. Some characteristics of these cells on discharging are also discussed.

---

* Solid State Ionics, 11, 109 (1983)

6.2 Concept of various gas cells

Although many kinds of gas cells can be constructed by using proton conductors or oxide ion conductors, the discussion in this chapter is restricted to atmospheres including hydrogen, oxygen and/or water vapor at elevated temperatures. When the electrode gas contains water vapor and oxygen or hydrogen, the chemical equilibrium can be established as

$$H_2(g) + 1/2\ O_2(g) \overset{K}{\rightleftarrows} H_2O(g) \qquad (6\text{-}1)$$

$$K = \frac{P_{H_2O}}{P_{H_2}\ P_{O_2}^{1/2}} \qquad (6\text{-}2)$$

where K is the equilibrium constant at the given temperature and P_{H_2}, P_{O_2} and P_{H_2O} are the equilibrated partial pressure of hydrogen, oxygen and water vapor, respectively.

Figure 46 illustrated the concept of various gas cells using a proton conductor and an oxide ion conductor as the electrolyte. Electrode reactions and the theoretical emfs of these cells are tabulated in Table 10.

As is well known, in the case of the oxide ion conductor cell, the difference in P_{O_2} between the two electrodes drives the following electrode reactions.

Electrode reaction with higher P_{O_2} : Cathode

$$O_2(g) + 4\ e^-(\text{electrode}) \longrightarrow 2\ O^=(\text{electrolyte}) \qquad (6\text{-}3)$$

Electrode reaction with lower P_{O_2} : Anode

$$2\ O^=(\text{electrolyte}) \longrightarrow O_2(g) + 4\ e^-(\text{electrode}) \qquad (6\text{-}4)$$

Therefore, the theoretical emf of the cell is given by

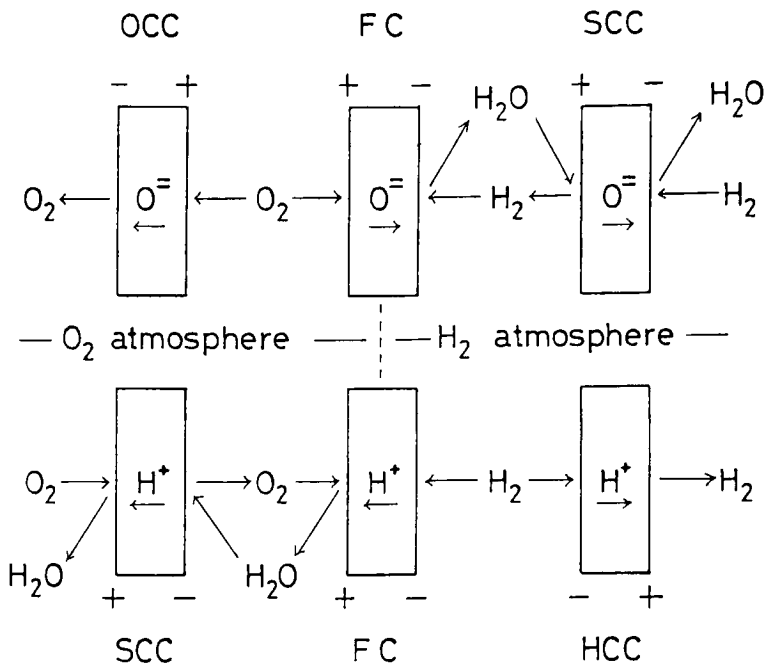

Fig. 46 Schematic illustration of solid electrolyte gas cells constructed with oxide ion conductor and proton conductor.
OCC : oxygen concentration cell, FC : fuel cell, SCC : steam concentration cell, HCC : hydrogen concentration cell

$$E_o = \frac{RT}{4F} \ln \frac{P_{O_2}(c)}{P_{O_2}(a)} \qquad (6\text{-}5)$$

The oxygen concentration cell(OCC) can be constructed by using an oxide ion conductive solid electrolyte. The hydrogen-oxygen fuel cell(FC) can be regarded as a sort of oxygen concentration cell, in which the P_{O_2} at the anode is extremely low. The emf of the fuel cell is derived from Eq.(6-2) and (6-5) as

$$E^{FC} = \frac{RT}{2F} \ln \frac{K P_{H_2} P_{O_2}^{1/2}}{P_{H_2O}} \qquad (6\text{-}6).$$

The oxygen concentration cell and the fuel cell have been studied by many investigators using stabilized zirconias[6-10,38,40-42, 44,47,48,52,55,57,58], doped cerias[49-51,53,54,57,58] and some perovskite-type oxides[43] as the electrolytes.

Table 10 Electrode reactions and theoretical emfs of various gas cells

Cell-type	H^+ conductor cell	$O^=$ conductor cell
O C C	can not be constructed without H_2O	$O_2 + 4e^- \rightleftarrows 2O^=$ $E_O = \frac{RT}{4F} \ln \frac{P_{O_2}(c)}{P_{O_2}(a)}$
H C C	$H_2 \rightleftarrows 2H^+ + 2e^-$ $E_H = \frac{RT}{2F} \ln \frac{P_{H_2}(a)}{P_{H_2}(c)}$	can not be constructed without H_2O
F C	anode; $H_2 \rightarrow 2H^+ + 2e^-$ cathode; $2H^+ + 1/2\,O_2 + 2e^- \rightarrow H_2O$ $E_H^{FC} = \frac{RT}{2F} \ln \frac{K P_{H_2} P_{O_2}^{1/2}}{P_{H_2O}(c)}$	anode; $H_2 + O^= \rightarrow H_2O + 2e^-$ cathode; $1/2\,O_2 + 2e^- \rightarrow O^=$ $E_O^{FC} = \ln \frac{K P_{H_2} P_{O_2}^{1/2}}{P_{H_2O}(a)}$
S C C	$H_2O \rightleftarrows 2H^+ + 1/2\,O_2 + 2e^-$ $E_H^S = \frac{RT}{2F} \ln \frac{P_{H_2O}(a)}{P_{H_2O}(c)} \left(\frac{P_{O_2}(c)}{P_{O_2}(a)} \right)^{1/2}$	$H_2O + 2e^- \rightleftarrows H_2 + O^=$ $E_O^S = \frac{RT}{2F} \ln \frac{P_{H_2O}(c)}{P_{H_2O}(a)} \frac{P_{H_2}(a)}{P_{H_2}(c)}$

* OCC ; oxygen concentration cell, HCC ; hydrogen concentration cell, FC ; H_2-O_2 fuel cell, SCC ; steam concentration cell

** P_{H_2}, P_{O_2} and P_{H_2O} are the partial pressure of hydrogen, oxygen and water vapor, respectively. (a) and (c) denote the anode and cathode compartment

On the other hand, in the case of the proton conductor cell, the difference in P_{H_2} between two electrodes drives the folowing electrode reactions.

Electrode reaction with higher P_{H_2} : Anode

$$H_2(g) \longrightarrow 2\ H^+(\text{electrolyte}) + 2\ e^-(\text{electrode}) \qquad (6\text{-}7)$$

Electrode reaction with lower P_{H_2} : Cathode

$$2\ H^+(\text{electrolyte}) + 2\ e^-(\text{electrode}) \longrightarrow H_2(g) \qquad (6\text{-}8)$$

The theoretical emf of the cell is given by

$$E_H = \frac{RT}{2F} \ln \frac{P_{H_2}(a)}{P_{H_2}(c)} \qquad (6\text{-}9).$$

Hydrogen concentration cells(HCC) and also hydrogen fuel cells (FC) may be constructed by using proton conductive solid electrolytes. As to hydrogen fuel cell, however, it should be noted that the meaning of P_{H_2O} in Eq.(6-6) is different from the case of oxide ion conductor cell; as is seen in Fig. 46, P_{H_2O} is important in the cathode compartment in the case of proton conductor(E_H^{FC}), and the anode compartment in the case of oxide ion conductor(E_O^{FC}) Although several investigators have examined HCC and FC at room temperatures using some proton conductors like $H_3Mo_{12}PO_{40}\cdot 29\,H_2O$[21,71,72], Nafion[73], $Zr(HPO_4)_2\cdot n\,H_2O$[74], $HUO_2PO_4\cdot 4\,H_2O$[75], KH_2PO_4[76], etc., such cells had been scarcely constructed at high temperature because of lack of good proton conductors. However, high temperature-type fuel cell could be constructed using the $SrCeO_3$-based proton conductor(in chapter 1-3)

The steam concentration cell(SCC) was also described previously by using $SrCeO_3$-based electrolytes. When gases with different

humidities were introduced to each electrode compartment of the gas cell with these oxides as the solid electrolyte, a steady and stable emf was observed in response to the humidity difference. The electrode reactions and theoretical emf for the steam concentration cell, shown in Table 10, were experimentally verified in chapter 4.

The steam concentration cell may also be constructed using an oxide ion conductor as the electrolyte. In this case, the use of hydrogen gas is inevitable. When hydrogen gases with different P_{H_2O} are used as the electrode gas, the difference in P_{H_2O} may become a driving force for the electrode reaction of Eq.(6-3) and (6-4) because P_{O_2} in equilibrium with H_2-H_2O is different at each electrode (Eq.(6-2)). Although this is a sort of oxygen concentration cell, it may also be regarded as a steam concentration cell since the overall electrode reactions can be written as follows.

Electrode reaction with higher P_{H_2O} : Cathode

$$H_2O(g) + 2\ e^-(\text{electrode}) \longrightarrow H_2(g) + O^=(\text{electrolyte}) \qquad (6\text{-}10)$$

Electrode reaction with lower P_{H_2O} : Anode

$$H_2(g) + O^=(\text{electrolyte}) \longrightarrow H_2O(g) + 2\ e^-(\text{electrode}) \qquad (6\text{-}11)$$

The theoretical emf of this cell can be derived from Eq.(6-2) and (6-5).

$$E_o^s = \frac{RT}{2F} \ln \frac{P_{H_2O}(c)\ P_{H_2}(a)}{P_{H_2O}(a)\ P_{H_2}(c)} \qquad (6\text{-}12)$$

If the hydrogen concentration cell with proton conductor and the steam concentration cell with oxide ion conductor can be constructed, all cells shown in Fig. 46 can be characterized, which connects oxygen and hydrogen by solid state ionics.

6.3 Experimental

Proton conductive solid used was $SrCe_{0.95}Yb_{0.05}O_{3-\alpha}$ (thickness: about 0.5 mm, dia: 12 mm). Oxide ion conductive solid examined here was 10 m/o YSZ, $(ZrO_2)_{0.90}(Y_2O_3)_{0.10}$, (thickness: 1.8 mm, dia: 12 mm).

The construction of the solid electrolyte gas cell

gas I, Pt/ specimen disc /Pt, gas II

was the same as that described previously. The cell temperature examined was 600-1000°C.

Air, oxygen, nitrogen, helium, hydrogen, argon or their mixtures at 1 atm were used as gas I or gas II with various P_{H_2O}. Unless otherwise stated, the gas saturated with water vapor at room temperature is represented as simply "wet" gas(P_{H_2O} = 17-20 Torr) and the gas prepared by saturating water vapor at 0°C(P_{H_2O} = 4.58 Torr) as "dry" gas.

6.4 Results and discussion

6.4.1 Emfs of various gas concentration cells

The typical examples of emfs of various gas concentration cells are shown in Table 11. If an electrolyte involves electronic conduction, the emf is lowered from its theoretical value E_0 to some extent, and the ionic transport number expressed as

$$t = E / E_0 \qquad (6\text{-}13)$$

is smaller than unity.

When dry air was introduced to both electrode compartments (cell 1 in Table 11), the emf observed was nearly zero for both the proton conductor cell and the oxide ion conductor cell,

Table 11 Emfs of various gas cells at 800°C

Cell no.	Cell type[a) gas I//gas II	EMF / mV[b) Electrolyte: Oxide ion conductor 10 m/o YSZ	Electrolyte: Proton conductor $SrCe_{0.95}Yb_{0.05}O_{3-\alpha}$
1	dry air//dry air	~0.6	0.0
2	wet air//dry air	~0.6	26.0(t_{H^+} = 0.34)
3	wet N_2//dry N_2[c)	~0.9	58.0(t_{H^+} = 0.74)
4	dry H_2//dry H_2	6.5	0.0
5	wet H_2//dry H_2	-56.5($t_{O^=}$ = 0.93)	0.0
6	dry air//dry O_2	36.2($t_{O^=}$ = 1.00)	2.0
7	wet air//wet O_2	36.4	14.0(t_{H^+} = 0.39)
8	wet air//dry* O_2	36.4	30.5

a) wet gas ; saturated with H_2O at room temperature
(P_{H_2O} = 19.8 Torr for cell 5, 23.8 Torr for cell 2 and 3)
dry gas ; saturated with H_2O at 0 °C (P_{H_2O} = 4.58 Torr)

b) negative sign shows that the electrode of gas II is negative

c) Partial pressure of oxygen in N_2 gas is 3×10^{-4} atm

because of no difference in the partial pressure of oxygen or water vapor between two electrodes.

6.4.1.1 Gas concentration cell under oxygen atmosphere---
steam concentration cell and oxygen concentration cell

When wet air was introduced to one of the electrode compartments(cell 2), a distinct emf was observed for the proton conductor cell, the electrode with higher P_{H_2O} being the negative. This is a sort of steam concentration cell with proton conductor. Since P_{O_2}(a) is nearly equal to P_{O_2}(c) in this cell, the theoretical emf given by E_H^S in Table 10 is simplified to

$$E_H^S = \frac{RT}{2F} \ln \frac{P_{H_2O}(a)}{P_{H_2O}(c)} \qquad (6\text{-}14).$$

As described previously, the conduction in $SrCe_{0.95}Yb_{0.05}O_{3-\alpha}$ was not purely ionic but partially electronic(p-type) at high P_{O_2}. The emf of cell 2 is not so high as the theoretical value, and a decrease in P_{O_2} increases the emf(cell 3), since p-type conductivity decreases with decreasing P_{O_2}.

Whereas the oxygen concentration cell with YSZ exhibited a stable and theoretical emf, the proton conductor cell did not act as an oxygen concentration cell when dry gases were used(cell 6). However, a "wet" oxygen concentration cell could be constructed when both electrode gases contained the same P_{H_2O}(E_H^S in Table 10).

The steam concentration cell could not be constructed by using oxide ion conductor(YSZ) under an oxygen atmosphere(cell 2 and 3). This can be explained as follows. In cell 2 and 3, the P_{O_2} at each electrode is almost same value. Even though the P_{O_2} difference might be caused by the P_{H_2O} difference(4.58 Torr and 23.8 Torr), the emf calculated from Eq.(6-5) is less than 1 mV. Therefore, the emf is negligibly small in the steam concentration cell with YSZ under oxygen atmosphere.

6.4.1.2 Gas concentration cell under hydrogen atmosphere---
steam concentration cell and hydrogen concentration cell

When hydrogen gases with different P_{H_2O} were introduced to YSZ cell, a distinct emf was observed, the electrode with higher P_{H_2O} being the positive(cell 5, c.f. cell 2). As explained in the previous section, this is a sort of steam concentration cell constructed with YSZ. The theoretical emf of this cell is given by Eq.(6-12). However, since the P_{H_2} at both electrodes were almost the same in this experiment, the emf equation can be written a

similar form to Eq.(6-14) except the sign of the emf being inverse in the YSZ cell. The emf of cell 5 using YSZ was somewhat smaller than its calculated value(t was about 0.93, taking into account of the emf of cell 4 as zero point). The equilibrated P_{O_2} in cell 5 was determined from Eq.(6-2) and the equilibrium constant K[30] as

$$P_{O_2}(c) = 4.37 \times 10^{-22} \text{ atm}$$
$$P_{O_2}(a) = 2.25 \times 10^{-23} \text{ atm}$$

at 800°C. According to Weppner[70], the electronic conductivity of YSZ is very low in this condition. Therefore the somewhat smaller emf observed in cell 5 should be ascribed to experimental error but not to electronic conduction.

No emf was observed in cell 5 with proton conductor. As described above, for the proton conductor cell, the difference in the equilibrated P_{H_2} is essential to exhibit the emf. In cell 5, since the P_{H_2} at both electrodes are nearly 1 atm, an addition of water vapor in small amount does not affect the equilibrated P_{H_2}. This situation is analogous to cell 2 or 3 with YSZ.

A hydrogen concentration cell(HCC) could be constructed by using $SrCe_{0.95}Yb_{0.05}O_{3-\alpha}$ electrolyte. Pure hydrogen gas at 1 atm and the mixture of hydrogen and helium gas were used as the electrode gases. Figure 47 shows the emf response of the cell to various P_{H_2}. A stable emf was observed, the electrode with higher P_{H_2} being the negative. As predicted from Eq.(6-9), the relation between the emf and the logarithm of $P_{H_2}(c)$ was linear. Due to an electronic conduction, the slope of the line was somewhat smaller than the theoretical one(= $2.303 \frac{RT}{2F}$).

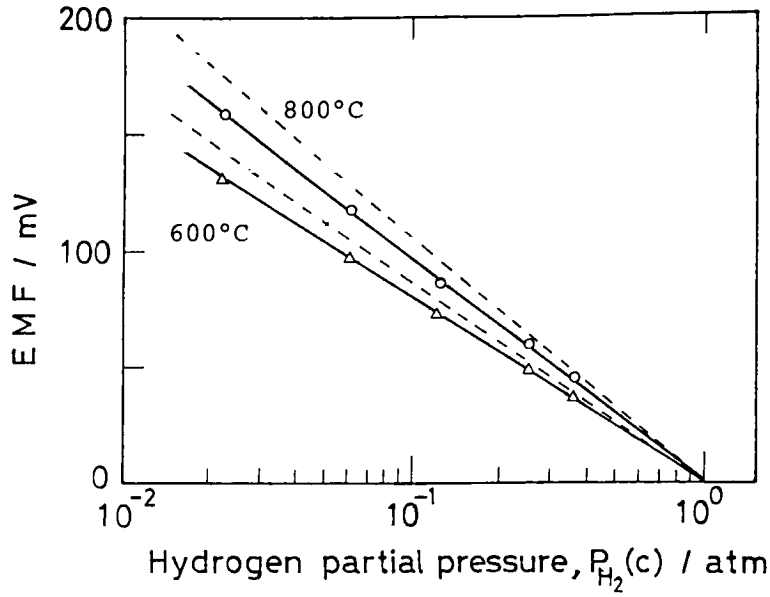

Fig. 47 Emf response of the hydrogen concentration cell to P_{H_2}(c); H_2(1 atm),Pt | $SrCe_{0.95}Yb_{0.05}O_{3-\alpha}$ | Pt, H_2 (P_{H_2}(c))
(broken line shows the theoretical emf)

The t_{H^+} of the specimen electrolyte was 0.95-0.98 at 600°C, 0.92-0.94 at 800°C in this cell. This cell may be applied to a high temperature-type hydrogen sensor.

6.4.2 Cell characteristics

6.4.2.1 Steam concentration cell using oxide ion conductor

As described in chapter 4, a steady and stable current could be drawn from the steam concentration cell with proton conductive electrolyte based on $SrCeO_3$. The resistance of the specimen electrolyte was major factor in the voltage drop on discharging the cell and the electrode reactions occured reversibly.

However, in the steam concentration cell with YSZ electrolyte (cell 5), the output current was very small as shown in Fig. 48,

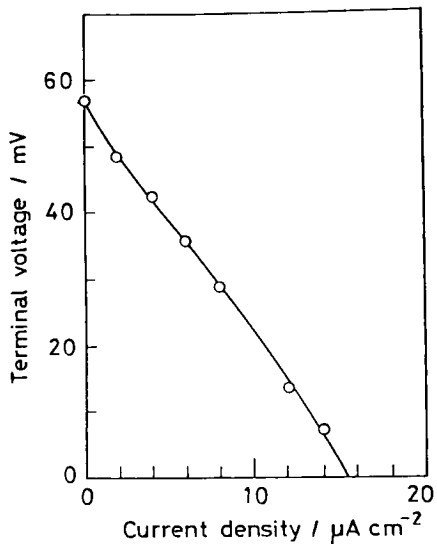

Fig. 48 Discharge curve of the steam concentration cell with YSZ at 800°C.
wet H_2, Pt / YSZ / Pt, dry H_2
(P_{H_2O}=19.8 Torr) (P_{H_2O}=4.58 Torr)
projected electrode area: 0.5 cm^2
thickness of electrolyte: 1.8 mm

compared with the proton conductor cell(Fig. 34 in chapter 3) Since the resistance of the cell measured by A.C. bridge at 10 kHz was only 37 Ω, a considerable polarization may occur on discharging this cell. The electrode polarizations have been studied by many workers using some oxide ion conductive solid electrolytes[38-58]. According to their results, appreciable cathodic polarizations were observed at platinum electrodes in doped ceria or zirconia cells under the low P_{O_2} atmosphere($\sim 10^{-4}$ atm) In cell 5 at 800°C, the P_{O_2} can be estimated to be $P_{O_2} = 4.38 \times 10^{-22}$ atm at the cathode($P_{H_2O} = 2.61 \times 10^{-2}$ atm). Therefore, a considerable polarization observed in cell 5 with YSZ may be due to such low P_{O_2} condition.

For the steam concentration cell with $SrCe_{0.95}Yb_{0.05}O_{3-\alpha}$ electrolyte, it was clarified that, at the anode, protons are extracted directly from water molecules, and that the contribution of hydrogen molecules produced by the thermal dissociation equilib-

rium(Eq.(6-1)) is negligible as electroactive species at the anode.

In the steam concentration cell with YSZ, two distinguishable reaction models are possible for the formation of oxide ion at the cathode.

Model 1

$$H_2O(g) + 2\,e^-(\text{electrode}) \rightarrow H_2(g) + O^=(\text{electrolyte}) \qquad (6\text{-}15)$$

Model 2

$$H_2O(g) \rightleftarrows H_2(g) + 1/2\ O_2(g) \qquad (6\text{-}16)$$

$$1/2\ O_2(g) + 2\,e^-(\text{electrode}) \longrightarrow O^=(\text{electrolyte}) \qquad (6\text{-}17)$$

In model 1, oxide ions are extracted directly from water molecules at the cathode. In model 2, thermally formed oxygen molecules are ionized to oxide ions at the cathode. Which model should be more valid?

As shown in Fig. 48, a short-circuit current observed was about 15 $\mu A\,cm^{-2}$ at 800°C, which corresponds to a consumption rate of 4.68×10^{13} molecules $sec^{-1}cm^{-2}$ as water molecules, or 2.34×10^{13} molecules $sec^{-1}cm^{-2}$ as oxygen molecules at the cathode. From the kinetic theory of gases, the number of molecules that collide with the electrode plane, Z, was calculated as

$$Z_{O_2} = 63.1 \text{ molecules } sec^{-1}cm^{-2}$$

and

$$Z_{H_2O} = 4.98 \times 10^{21} \text{ molecules } sec^{-1}cm^{-2}.$$

Assuming that only the molecules that collide with the electrode plane(wall) could be ionized to oxide ions, the consumption rate by the current is much higher than the supplying rate of oxygen to the electrode. As water molecules are sufficiently supplied to the electrode(about 8 orders of magnitude over the

consumption rate), they would not be depleted even on short-circuiting the cell. Consequently, the species ionized at the cathode of the steam concentration cell with YSZ electrolyte must be water molecules(Eq.(6-15)), and not oxygen molecules.

6.4.2.2 Hydrogen concentration cell using proton conductor

From the hydrogen concentration cell with the $SrCe_{0.95}Yb_{0.05}O_{3-\alpha}$ electrolyte, a steady and stable current could be drawn as shown in Fig. 49. Similar to the steam concentration cell with this electrolyte, the relation between the terminal voltage and the current output is linear in this cell. From the slope of the discharge curve, the D.C. resistance of the cells were calculated to be 43.5 Ω at 800°C, and 16.1 Ω at 1000°C, respectively. On the other hand, the resistance of the cells measured by A.C. bridge at 10 kHz were 38 Ω at 800°C, and 15.1 Ω at 1000°C, respectively. Although the D.C. resistance of the cell was somewhat higher than that the A.C. value, the ohmic polarization was pre-

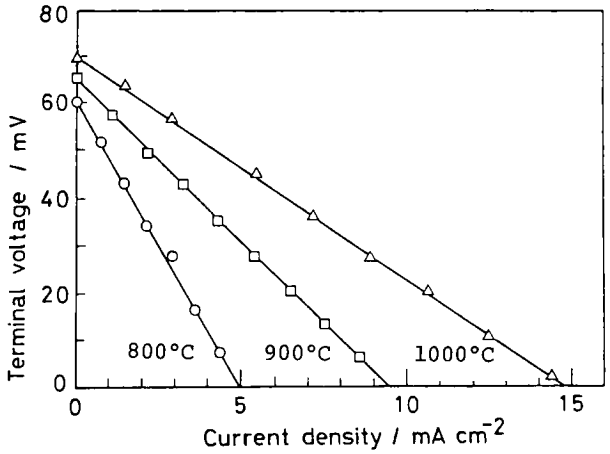

Fig. 49 Performances of the hydrogen concentration cell: H_2(1 atm), Pt|$SrCe_{0.95}Yb_{0.05}O_{3-\alpha}$|Pt, H_2(0.25 atm) projected electrode area:0.28 cm^2, thickness of the electrolyte:0.5 mm

dominant for this cell, suggesting that the electrode reactions may occur reversibly in the hydrogen concentration cell with the $SrCe_{0.95}Yb_{0.05}O_{3-\alpha}$ electrolyte.

Furthermore, the proton transport number of $SrCe_{0.95}Yb_{0.05}O_{3-\alpha}$ in this cell was close to unity. Therefore, hydrogen atmosphere is desirable condition for this electrolyte. This may be an excellent character for applying this ceramics to a solid electrolyte cell device such as hydrogen fuel cell, steam electrolyzer to produce hydrogen, etc.

6.4.2.3 Hydrogen extraction in hydrogen concentration cell

An attempt was made to extract hydrogen gas from the anode compartment into the cathode compartment. The mixture of hydrogen and argon(P_{H_2} = 0.1 atm) was supplied to the both electrode compartments at a regulated flow rate. The increase or decrease in P_{H_2} was measured by a gas chromatograph as a fuction of the current density passed through the cell.

Figure 50 shows the plot of the hydrogen evolution rate at the cathode against the current density passed throuth the cell

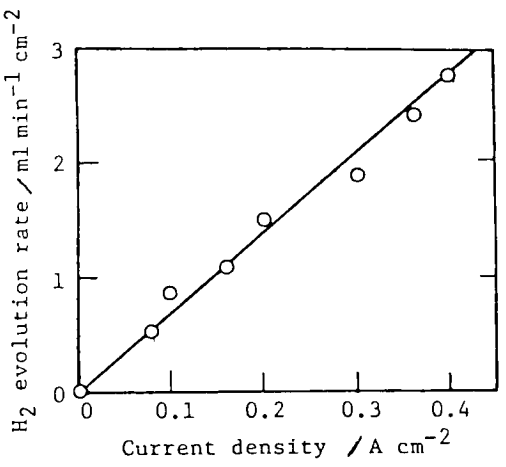

Fig. 50 Hydrogen evolution rate at the cathode at 800°C in HCC: H_2(0.1atm)//H_2(0.1atm) (—— :theoretical rate)

at 800°C. The evolution rate agreed with the theoretical rate calculated from Faraday's law. Similarly, the consumption rate of hydrogen at the anode agreed with the theoretical value. This cell device may be applied to the hydrogen extracter(electrochemical hydrogen pump) and to the hydrogen sensor, as well as the oxygen sensor and the oxygen pump using a solid oxide electrolyte like stabilized zirconias.

6.5 Summary

Using high temperature-type proton conductor and oxide ion conductor as the solid electrolyte, various gas cells were characterized under hydrogen-water vapor or oxygen-water vapor atmosphere. Under oxygen-water vapor atmosphere, a steam concentration cell could be constructed using $SrCeO_3$-based proton conductive solid electrolyte and the cell reactions occur reversibly. In hydrogen atmosphere, a steam concentration cell could also be constructed using an oxide ion conductor YSZ and relatively large overpotential was observed in this cell.

Using the $SrCe_{0.95}Yb_{0.05}O_{3-\alpha}$ electrolyte, high temperature-type hydrogen concentration cell was operated stably and the electrode reactions occured reversibly. By applying this cell, hydrogen gas could be extracted electrochemically with high current efficiency close to unity.

CHAPTER 7 RELATION BETWEEN PROTON AND HOLE CONDUCTION IN $SrCeO_3$-BASED SOLID ELECTROLYTE UNDER WATER-CONTAINING ATMOSPHERES AT HIGH TEMPERATURES*

7.1 Introduction

As previously described, it was confirmed that sintered oxides based on $SrCeO_3$ exhibit appreciable proton conduction in hydrogen-containing atmospheres at elevated temperature. However, the mechanism of proton conduction in these sintered oxides is not clear yet. Knowledges on the electrical properties of these materials got in previous chapters are summarized as follows:

(1) These sintered oxides have only p-type conduction(hole conduction) in an atmosphere free from hydrogen or water vapor.

(2) When water vapor or hydrogen is introduced to the atmosphere, electronic conductivity decreases and proton conduction appears in a short time. It seems that the proton conduction arises in the oxides at the expense of holes initially present in the crystal.

(3) A steam concentration cell using sintered specimen as an electrolyte diaphragm shows a stable electromotive force and that a steady current can be drawn from the cell.

(4) Hydrogen concentration cell constructed with the same electrolyte also has stable characteristics.

(5) Pure $SrCeO_3$ has low electronic conductivity in an oxygen atmosphere and does not behave as a proton conductor in a

---

* Solid State Ionics, 11, 117 (1983)

hydrogen containing atmosphere.

(6) Partial substitution by aliovalent cations such as Yb^{3+}, Sc^{3+}, Y^{3+}, etc., for Ce^{4+} site in the perovskite-type crystal $SrCeO_3$ seems to play an important role in the appearance of proton conduction.

In this chapter, the conduction in sintered specimens were precisely investigated in order to find a clue to clarify the mechanism of proton conduction. For that purpose, the total (proton + electron) conductivity was measured as a function of the partial pressure of oxygen and water vapor in the gas surrounding the specimen. The hole conductivity was also measured as a function of dopant concentration. Furthermore, the proton transport number was measured in a steam concentration cell in order to separate the proton conductivity from the total one and to investigate the effect of vapor pressure on the proton conductivity.

7.2 Experimental

The specimen oxides examined in this chapter were sintered solid solutions composed of $SrCe_{1-x}Yb_xO_{3-\alpha}$ (x = 0 - 0.10). The preparation of specimen was the same as in the previous chapter.

The proton conduction in the specimen was investigated by measuring the electrical conductivity and the proton transport number under various conditions. Similar to the previous chapter, the conductivity was measured by an A.C. impedance bridge and the frequency mainly used was 10 kHz. The conductivities measured at 10 kHz could be regarded as the bulk con-

ductivities of the oxide and not that of Pt electrode/specimen interface.

In order to measure the proton transport number, the following steam concentration cell same as in chapter 4 was constructed using specimen disc (thickness: 0.5 mm, dia: 12 mm) as a solid electrolyte.

gas I, Pt / specimen disc / Pt, gas II

($P_{H_2O}(I)$) ($P_{H_2O}(II)$)

The partial pressure of oxygen P_{O_2} at both electrodes were kept at the same value. P_{O_2} in the gas was measured with an oxygen meter using YSZ electrolyte.

The theoretical emf E_0 of this cell is given by

$$E_0 = \frac{RT}{2F} \ln \frac{P_{H_2O}(I)}{P_{H_2O}(II)} \qquad (7\text{-}1)$$

When the specimen electrolyte has some electronic conduction, the measured emf E is lowered from E_0 to some extent. Generally. transport number of the ion t_i is determined by

$$t_i = E / E_0 \qquad (7\text{-}2),$$

if the electrode reactions take place reversibly. As described previously, the electrode reactions proceed reversibly in the steam concentration cell. Therefore, the proton transport number, $t_{H^\cdot}$**, was determined as a ratio of measured emf to the theoretical emf. The proton conductivity was calculated as a product of proton transport number and total conductivity of the specimen measured with the A.C. bridge. Here, conductance (S) was used instead of conductivity(S cm^{-1}) since size factor

** $H^\cdot$; protons in the oxides; Kröger-Vink notation is used in this chapter for convenience.

for calculating the conductivity was indefinite in the specimen disc in the experimental cell.

7.3 Results

7.3.1 Hole conductivity vs. dopant concentration

Figure 51 shows Arrhenius plots of conductivity of $SrCe_{1-x}Yb_xO_{3-\alpha}$ for various x values measured in air dried with

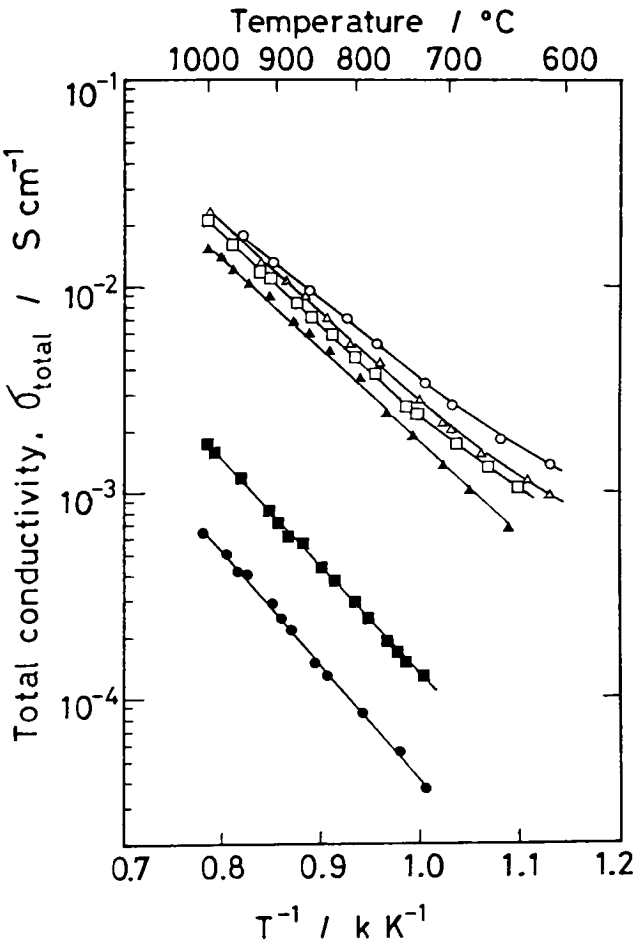

Fig. 51 Total conductivities of $SrCe_{1-x}Yb_xO_{3-\alpha}$ in air dried with P_2O_5. x; ●:0(nominally pure), ■:0.02, ▲:0.03, □:0.05, △:0.07, ○:0.10

phosphorus pentoxide. Conduction under dry air is electronic due to electron holes (p-type). Conductivities of doped specimens were remarkably high compared to nominally "pure" $SrCeO_3$. Effect of Yb doping on conductivity was most marked at low concentration of dopant, and the conductivity levels off at about x = 0.05. Essentially, "pure" $SrCeO_3$ should have lower conductivity than the value shown in Fig. 51. However, nominally "pure" $SrCeO_3$ might contain considerable amounts of inevitable impurities, and, as a result, the conductivity is probably high compared to that of ideally pure material.

7.3.2 Total conductivity vs. partial pressure of water vapor or oxygen

The conductivities of $SrCe_{0.95}Yb_{0.05}O_{3-\alpha}$ were measured as a function of the pressure of water vapor or of oxygen at various temperatures. Typical results are shown in Fig. 52 and Fig. 53.

As shown in Fig. 52, the conductivitiy decreased with increasing partial pressure of water vapor when partial pressure of oxygen is constant. This tendency was somewhat more marked as the temperature was increased. At constant partial pressure of water vapor, however, the conductivity increased with increasing partial pressure of oxygen as shown in Fig. 53. This tendency was also marked as the temperature was increased.

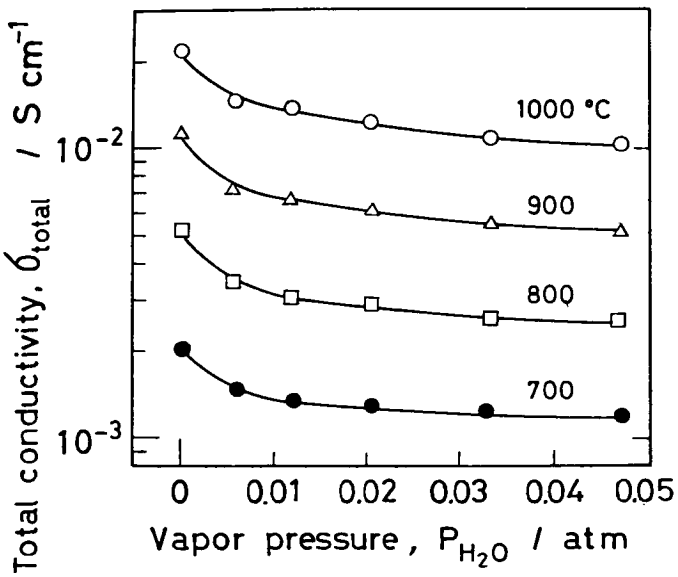

Fig. 52 Dependence of total conductivity on partial pressure of water vapor.
specimen : $SrCe_{0.95}Yb_{0.05}O_{3-\alpha}$
P_{O_2} = 0.21 atm

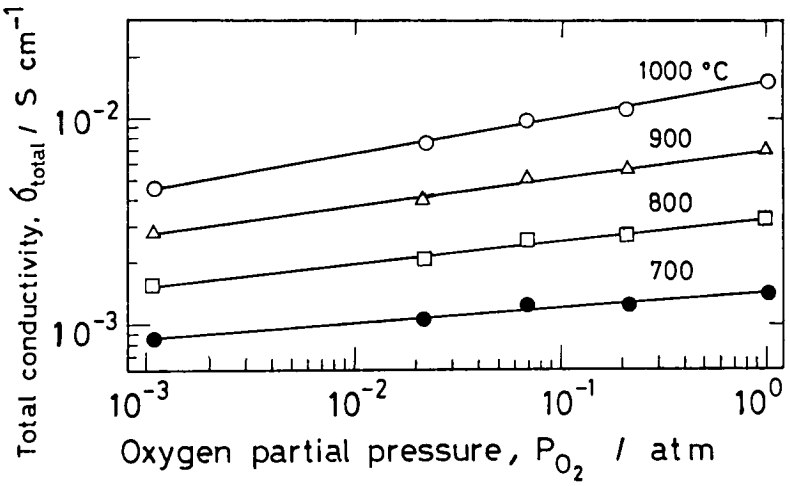

Fig. 53 Dependence of total conductivity on oxygen partial pressure. specimen : $SrCe_{0.95}Yb_{0.05}O_{3-\alpha}$
P_{H_2O} = 3.32 x 10^{-2} atm

7.3.3 Separation of proton and electronic conductivity from total conductivity

The proton transport number, $t_{H^{\cdot}}$, in $SrCe_{0.95}Yb_{0.05}O_{3-\alpha}$ was measured in a steam concentration cell under various partial pressure of oxygen and at different temperatures. Results are represented in Fig. 54. The proton transport number increased as the temperature decreased or as P_{O_2} decreased.

The conductance G of the electrolyte specimen in the steam concentration cell was measured so as to calculate the proton conductance $G_{H^{\cdot}}$ from total conductance G_{total}

$$G_{H^{\cdot}} = t_{H^{\cdot}} \quad G_{total} \qquad (7\text{-}3)$$

Proton conductances thus obtained were plotted against the P_{H_2O} and against P_{O_2}, respectively. As shown in Fig. 55, the proton conductance increased with increasing the mean vapor pressure P_{H_2O}*, whereas it did not depend on partial pressure of oxygen(Fig. 56)

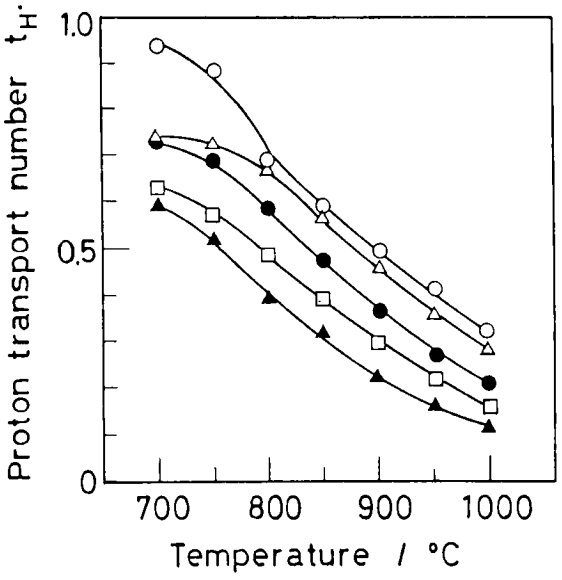

Fig. 54 Proton transport numbers in $SrCe_{0.95}Yb_{0.05}O_{3-\alpha}$ in the steam concentration cell;
wet gas,Pt/specimen/Pt, dry gas
P_{H_2O}(I) P_{H_2O}(II)
(2.1×10^{-2} atm) (6.03×10^{-3} atm)
P_{O_2} (atm) ; ○:4.49×10^{-4}, △:1.07×10^{-3}, ●:3.02×10^{-3} □:1.6×10^{-2}, ▲:6.25×10^{-2}

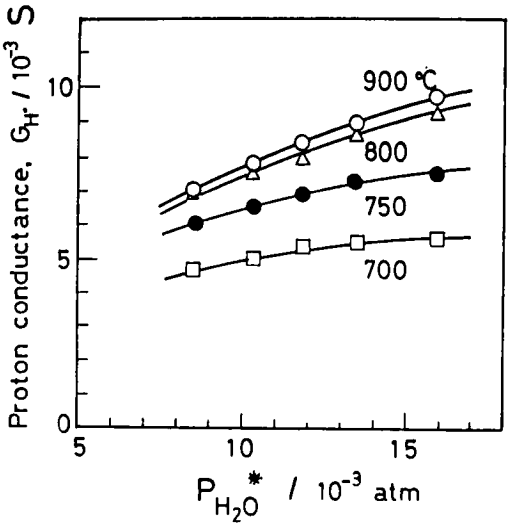

Fig. 55 Dependence of proton conductance on mean vapor pressure $P^*_{H_2O}$ in the steam concentration cell; wet air, Pt|$SrCe_{0.95}Yb_{0.05}O_{3-\alpha}$|Pt, dry air ($P_{H_2O}$(I)) ($P_{H_2O}$(II)=6.03 x 10^{-3} atm)

$P^*_{H_2O} = (P_{H_2O}(I)\ P_{H_2O}(II))^{1/2}$

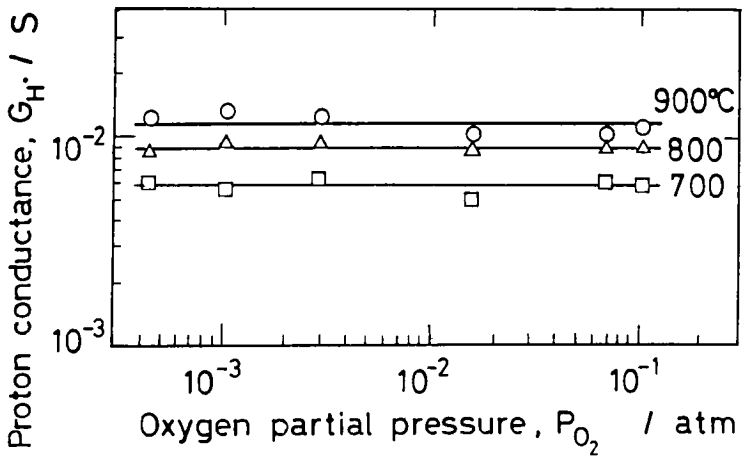

Fig. 56 Plots of proton conductance G_H. against P_{O_2} in the same cell as in Fig. 54

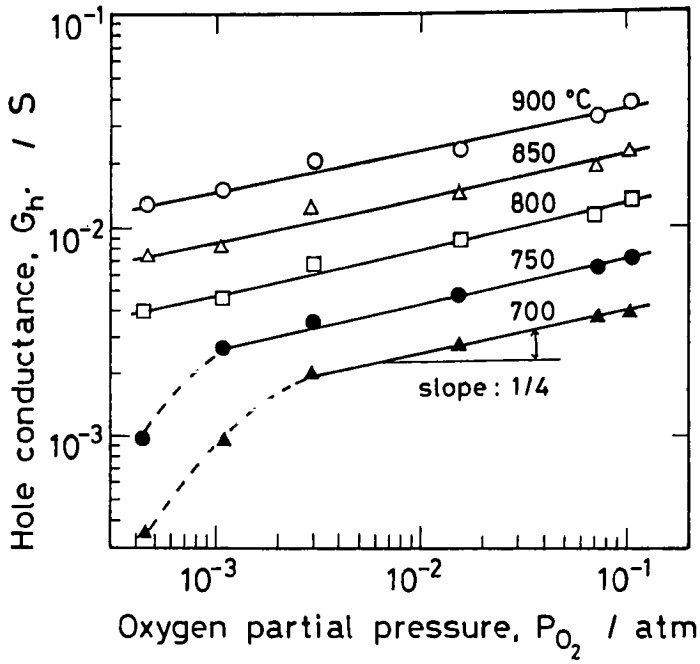

Fig. 57 Dependence of hole conductance on P_{O_2} in the steam concentration cell as in Fig. 54.

The hole conductance G_h , defined by

$$G_{h\cdot} = G_{total} - G_{H\cdot} \qquad (7\text{-}4) \ ,$$

is plotted in Fig. 57 as a function of the P_{O_2} It increased as the P_{O_2} increased over the whole temperature range examined.

7.4 Discussion

7.4.1 Effect of doping

Figure 51 suggests that the concentration of charge carrier would be increased by doping aliovalent cation. In this case, substitution of Yb^{3+} for Ce^{4+} (Yb_{Ce}') in $SrCeO_3$ will provide oxygen vacancies $V_O^{\cdot\cdot}$ as a result of charge compensation,

$$Yb^{3+} \longrightarrow Yb_{Ce}' + 1/2\ V_O^{\cdot\cdot} \qquad (7\text{-}5)$$

and electron holes may arise under equilibrium between oxygen vacancies and oxygen gas

$$V_O^{\cdot\cdot} + 1/2\ O_2 \overset{K_1}{\rightleftharpoons} O_O + 2\ h^{\cdot} \qquad (7\text{-}6),$$

where $h^{\cdot}$ represents an electron hole, O_O an oxide ion on a normal lattice site. Figure 53 supports hole conduction in the specimen since the conductivity increases with increasing P_{O_2}. As described previously, an undoped specimen shows no protonic conduction in wet air and hole generated by doping seems to play an important role in the formation of protons in the oxides.

7.4.2 Possible explanation of change in conductivity with atmosphere

As shown in Fig. 52, the total conductivity falls as the P_{H_2O} increases. Appearance of proton conduction could be confirmed in this wet condition. This phenomenon suggests that the protons in the oxide may be produced from H_2O at the expense of the electron holes[12,13], since the decrease in the hole concentration should make the total conductivity decrease.

One possible model for proton formation is

$$H_2O(g) + 2\ h^{\cdot} \overset{K_2}{\rightleftharpoons} 2\ H^{\cdot} + 1/2\ O_2(g) \qquad (7\text{-}7)$$

where $H^{\cdot}$ is the protons in the oxide.

In order to explain the conductivity behavior as a function of atmosphere, two equilibriums(Eq.(7-6) and (7-7)) were considered between the specimen oxide and the atmosphere. From Eq.(7-6) and (7-7), the equilibrium constants K_1 and K_2 are given by

$$K_1 = \frac{[O_o]\ [h^\cdot]^2}{[V_o^{\cdot\cdot}]\ P_{O_2}^{1/2}} \qquad (7\text{-}8)$$

$$K_2 = \frac{[H^\cdot]^2\ P_{O_2}^{1/2}}{[h^\cdot]^2\ P_{H_2O}} \qquad (7\text{-}9)$$

where branckets denote the concentration of the species. Using these equations, the concentrations of holes and protons at constant temperature are given as a function of P_{O_2} and P_{H_2O} respectively by

$$[h^\cdot] = K'\ P_{O_2}^{1/4} \qquad (7\text{-}10)$$

$$[H^\cdot] = K''\ P_{H_2O}^{1/2} \qquad (7\text{-}11)$$

where

$$K' = (\ [V_o^{\cdot\cdot}]\ K_1 / [O_o]\ )^{1/2} \qquad (7\text{-}12)$$

$$K'' = K'\ K_2^{1/2} \qquad (7\text{-}13).$$

From the electrical neutrality condition, the concentration of the doped Yb^{3+} at Ce^{4+} site, $[Yb_{Ce}']$, is expressed as

$$[Yb_{Ce}'] = [h^\cdot] + 2[V_o^{\cdot\cdot}] + [H^\cdot] \qquad (7\text{-}14).$$

And $[Yb_{Ce}']$ can be regarded as a constant value for a given specimen oxide.

The electrical conductivity σ_i of a charged species i is given by

$$\sigma_i = c_i\ q_i\ \mu_i \qquad (7\text{-}15)$$

where c_i, q_i and μ_i are carrier concentration, charge and the mobility of species i, respectively. As the charge carriers in this oxide are protons and holes, total conductivity σ_{total} is expressed as the sum of the proton $\sigma_{H^\cdot}$ and hole $\sigma_{h^\cdot}$ con-

ductivities.

$$\sigma_{total} = \sigma_{H^{\cdot}} + \sigma_{h^{\cdot}} \qquad (7\text{-}16)$$

If one applys Eq.(7-10),(7-11),(7-14) and (7-15) to Eq.(7-16), the following representations for the total conductivity at a fixed temperature can be derived ;

at a fixed given P_{O_2}

$$\sigma_{total} = e\left\{(\mu_{H^{\cdot}} - \mu_{h^{\cdot}})[H^{\cdot}] + \mu_{h^{\cdot}}([Yb_{Ce}{}'] - 2[V_O^{\cdot\cdot}])\right\}$$
$$= e\left\{(\mu_{H^{\cdot}} - \mu_{h^{\cdot}})K''\, P_{H_2O}{}^{1/2} + \mu_{h^{\cdot}}([Yb_{Ce}{}'] - 2[V_O^{\cdot\cdot}])\right\} \qquad (7\text{-}17)$$

at a fixed given P_{H_2O}

$$\sigma_{total} = e\left\{(\mu_{h^{\cdot}} - \mu_{H^{\cdot}})[h^{\cdot}] + \mu_{H^{\cdot}}([Yb_{Ce}{}'] - 2[V_O^{\cdot\cdot}])\right\}$$
$$= e\left\{(\mu_{h^{\cdot}} - \mu_{H^{\cdot}})K'\, P_{O_2}{}^{1/4} + \mu_{H^{\cdot}}([Yb_{Ce}{}'] - 2[V_O^{\cdot\cdot}])\right\} \qquad (7\text{-}18)$$

where e is the elementary charge.

Equation(7-17) indicates that the total conductivity is a linear function of $P_{H_2O}{}^{1/2}$ at constant P_{O_2} if the mobilities and the concentration of $V_O^{\cdot\cdot}$ are constant irrespective of P_{H_2O}. Also, Eq.(7-18) indicates that the total conductivity is a linear function of $P_{O_2}{}^{1/4}$ at constant P_{H_2O} if the mobilities and the concentration of $V_O^{\cdot\cdot}$ are constant irrespective of P_{O_2}

Replotting the data shown in Fig. 52 as a function of $P_{H_2O}{}^{1/2}$ gives, in fact, straight lines as represented in Fig. 58, and Fig. 59. This supports the validity of the assumptions made in deriving Eq.(7-17), and informs the followings;

(i) in accordance with Eq.(7-17), the slope($e(\mu_{H^{\cdot}} - \mu_{h^{\cdot}})K''$) is independent of P_{O_2} at fixed temperature and depends on temperature at constant P_{O_2}, since μ and K are functions of temperature.

(ii) negative slopes of the line show that the mobility of the hole is higher than that of the proton($\mu_{h^{\cdot}} > \mu_{H^{\cdot}}$, in Eq.(7-17)).

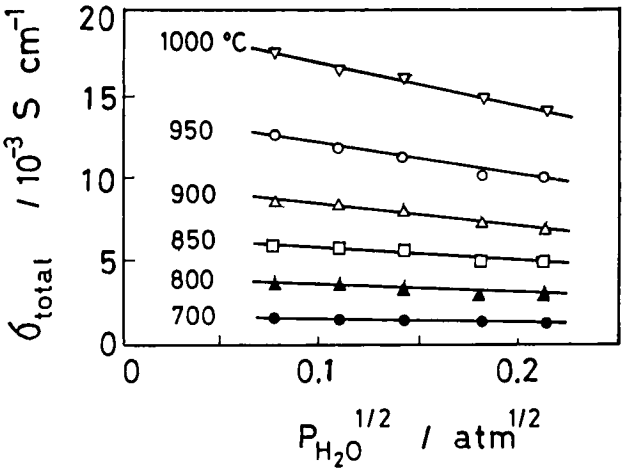

Fig. 58 Plots of total conductivity of $SrCe_{0.95}Yb_{0.05}O_{3-\alpha}$ against $P_{H_2O}^{1/2}$. P_{O_2} = 1.0 atm

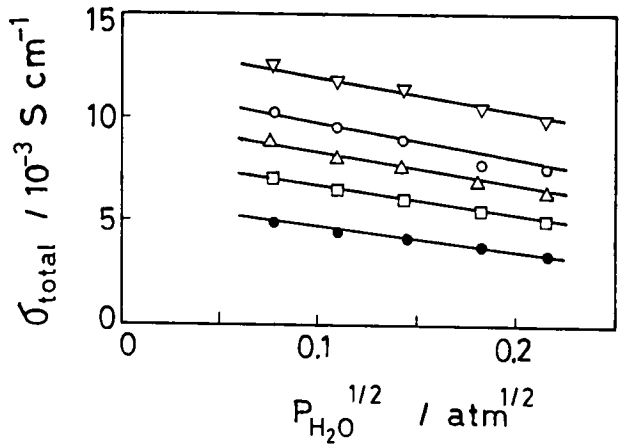

Fig. 59 Plots of total conductivity against $P_{H_2O}^{1/2}$ at 950°C. P_{O_2}(atm) ; ▽:1.0, ○:0.21, △:0.0673, □:0.0218, ●:1.07×10^{-3}

(iii) the proton concentration [H$^{\bullet}$] is proportional to $P_{H_2O}^{1/2}$, because Eq.(7-11) is adopted on deriving Eq.(7-17).

Similarly, replotting the data shown in Fig. 53 as a function of $P_{O_2}^{1/4}$ gives straight line as shown in Fig. 60 and Fig. 61. In this case, the slope of the line($e(\mu_h \cdot - \mu_H \cdot)K'$) is positive, being consistent with the above result that the hole mobility is higher than the proton mobility. The slope is also independent of P_{H_2O} at a given temperature and is temperature-dependent at constant P_{O_2}. These results support the validity of Eq.(7-18).

Consequently. it can be considered that protons are provided from water vapor at the expense of the electron holes as expressed by Eq.(7-7), and that the mobility of the protons is lower than that of the holes in the oxide.

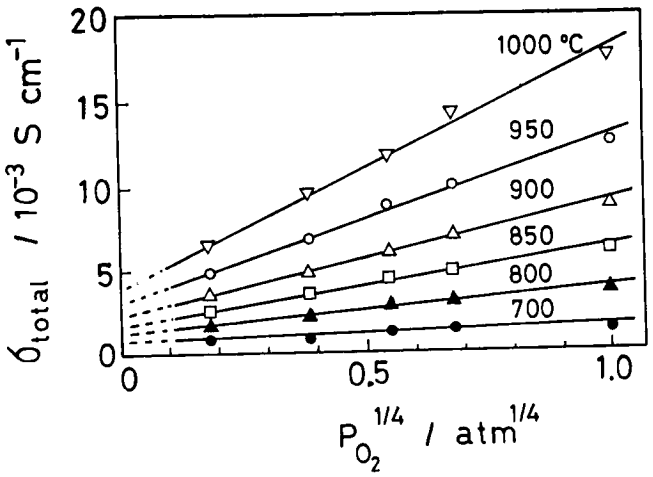

Fig. 60 Plots of total conductivity of $SrCe_{0.95}Yb_{0.05}O_{3-\alpha}$ aginst $P_{O_2}^{1/4}$. P_{H_2O}= 6.03 x 10^{-3} atm

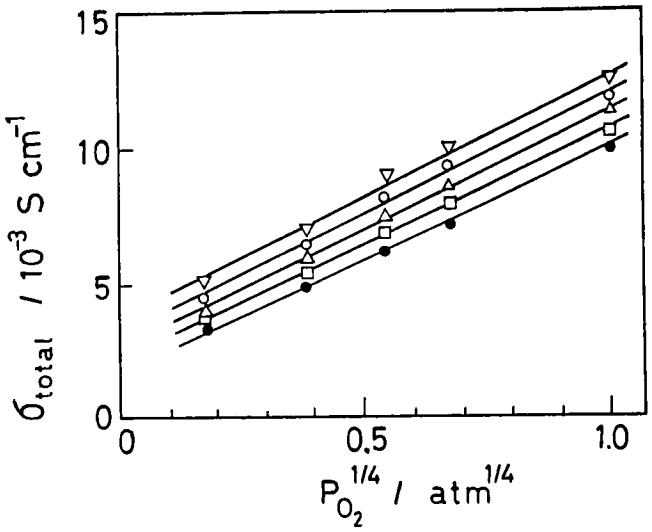

Fig. 61 Plots of total conductivity against $P_{O_2}^{1/4}$ at 950°C.
P_{H_2O}(atm) ; ▽:6.03×10^{-3}, ○:1.21×10^{-2}, △:2.04×10^{-2},
□:3.32×10^{-2}, ●:4.70×10^{-2}

7.4.3 Dependence of separate conductivities on atmospheres

The above described result suggests also the validity of Eq.(7-10) and (7-11). If so, the proton conductivity is a linear function of $P_{H_2O}^{1/2}$ and independent of P_{O_2}, whereas the hole conductivity is proportional to $P_{O_2}^{1/4}$, i.e.

$$\sigma_{H\cdot} \propto P_{H_2O}^{1/2} \qquad (7\text{-}19)$$

$$\sigma_{h\cdot} \propto P_{O_2}^{1/4} \qquad (7\text{-}20).$$

These are obvious from the experimental results shown in Fig. 56, Fig. 57 and Fig. 62 in which the proton conductance shown in Fig. 55 is rewritten as a function of $P_{H_2O}^{*\,1/2}$

As a summary, a three dimensional representation of the total conductivity and the proton conductivity is drawn schematically as a function of P_{O_2} and P_{H_2O} in Fig. 63.

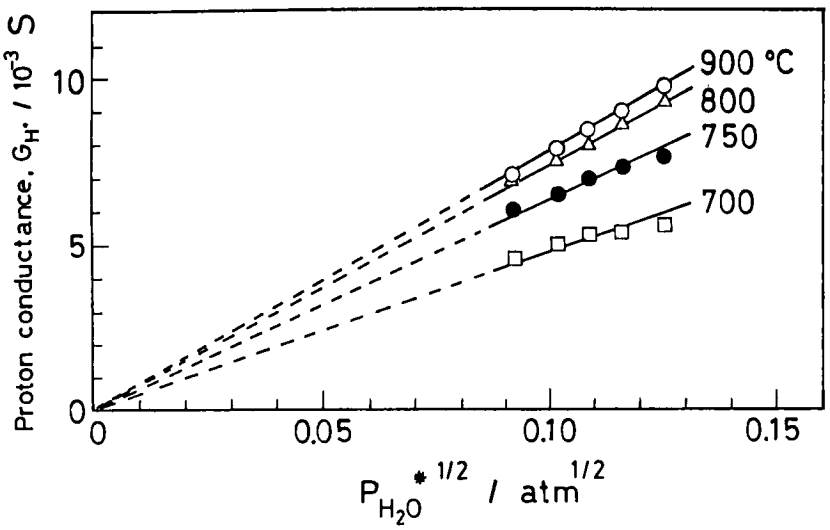

Fig. 62 Plots of proton conductance $G_{H^\cdot}$ against $P_{H_2O}{}^{*1/2}$ in the same cell as in Fig. 55.

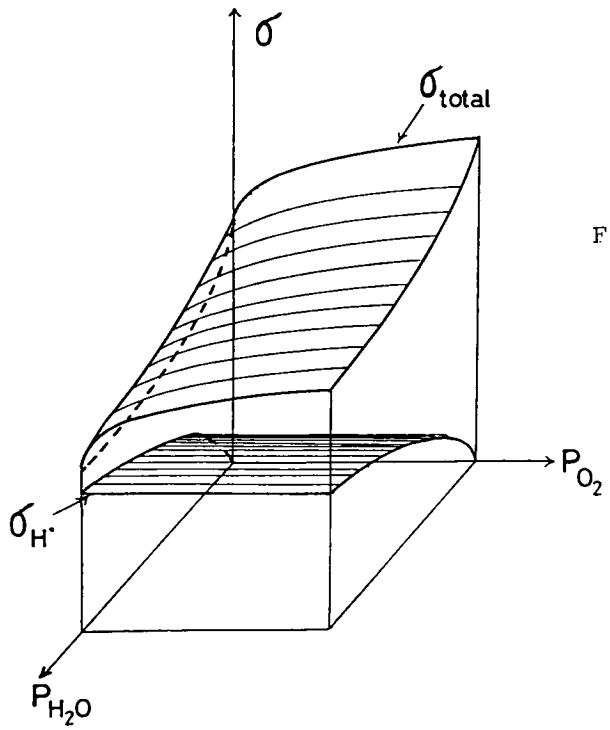

Fig. 63 Schematic illustration of three dimensional representation of total conductivity and proton conductivity as a function of P_{O_2} and P_{H_2O}. (P_{O_2} represented here is restricted to the region where Eq.(7-17) and (7-19) are available. i.e. electronic conduction is exclusively due to holes)

7.4.4 Consideration on the situation of the protons in the oxides

It has been reported that the adsorption of water vapor enhances the surface conductivities of silica gels and some oxides[62,66,77.78]. Proton conduction models at the surface have also been reported. Hydroxyl groups and the adsorbed water play an important role in these models.

However, it has been reported that almost all the chemisorbed water can be desorbed from the surface above 400°C[69]. The $SrCeO_3$-based sinters exhibit an appreciable proton conduction even at 1000°C. Furthermore, the appearance of the proton conduction is closely related with the disappearance of the electron holes in the bulk of the oxides. Therefore, a bulk-type proton conduction model may be more acceptable than the surface conduction model at the present stage of investigation.

As to bulk-type proton conduction in oxides, Stotz and Wagner [12] have proposed two possibilities whereby hydrogen can dissolve into oxides which have oxygen vacancies as the predominant defect. Shores and Rapp [13] have also applied similar models to doped ThO_2. These involve either interstitial protons($H_i^{\bullet}$) or hydride ions(H^-) located on oxygen lattice sites($H_O^{\bullet}$). Such defects have a net electrical charge of +1 relative to the host crystal.

If negatively charged hydride ions are located on oxygen lattice sites, the equilibrium between water vapor and oxide crystal are given by

$$H_2O(g) \rightleftarrows H_2(g) + 1/2\ O_2(g) \qquad (7\text{-}21)$$

$$2\ H_2(g) + V_O^{\bullet\bullet} + O_O \rightleftarrows 2\ H_O^{\bullet} + H_2O(g) \qquad (7\text{-}22)$$

Assuming dilute solutions of defects , the partial conductivity

of the hydride ion is given by

$$\sigma_{H_O^\cdot} \propto [V_O^{\cdot\cdot}]^{1/2} P_{H_2O}^{1/2} P_{O_2}^{-1/2} \qquad (7\text{-}23).$$

On the other hand, for the case of interstitial protons, since the equilibrium are similarly given by Eq.(7-6) and (7-7), the proton conductivity is derived as

$$\sigma_{H_i^\cdot} \propto [V_O^{\cdot\cdot}]^{1/2} P_{H_2O}^{1/2} \qquad (7\text{-}24).$$

In this study, the proton conductivity was proportional to $P_{H_2O}^{1/2}$ and was independent of P_{O_2} at constant P_{H_2O}(Fig. 56) in accordance with Eq.(7-24). Therefore it is probable that the proton present in the $SrCeO_3$-based sinters must be of the interstitial-type, and not hydride ions.

7.4.5 Proton conductivity of $SrCe_{0.95}Yb_{0.05}O_{3-\alpha}$

In above sections, various electrochemical behaviors of the solid electrolytes based on $SrCeO_3$ were discussed. However, the absolute values of the proton conductivity have not yet been described. Then the proton conductivity $\sigma_{H^\cdot}$ of $SrCe_{0.95}Yb_{0.05}O_{3-\alpha}$ is estimated by various methods and results are shown in Fig. 64.

The $\sigma_{H^\cdot}$ could be estimated from the resistance and the $t_{H^\cdot}$ of the hydrogen-air fuel cell and the hydrogen concentration cell. As mentioned previously, the $t_{H^\cdot}$ of the specimen electrolyte was close to unity in both cells at 600-1000°C. Although the size factor for calculating the conductivity was not so definite in the specimen disc used in the experimental cell, the $\sigma_{H^\cdot}$ values estimated from both cells are in good agreement with the total conductivity measured in hydrogen gas.

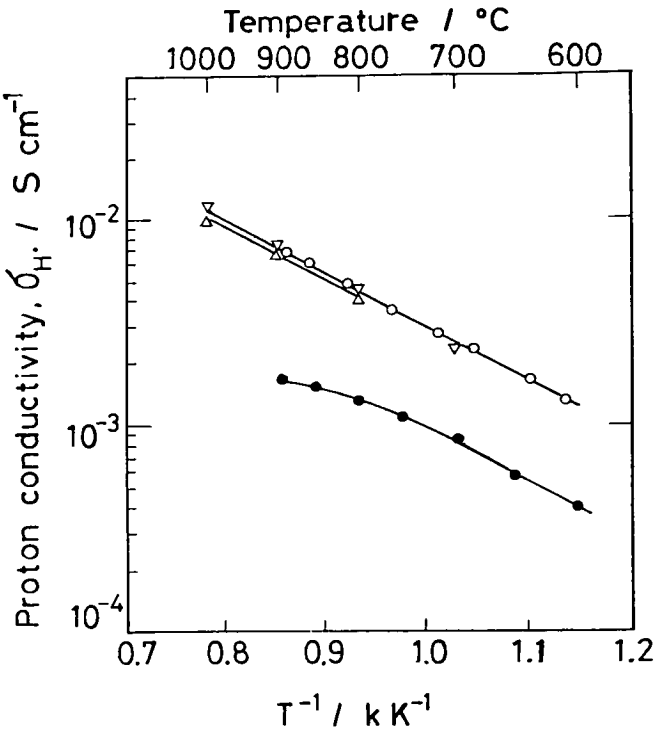

Fig. 64 Proton conductivity of $SrCe_{0.95}Yb_{0.05}O_{3-\alpha}$

- ○ : Total conductivity in H_2
- △ : Estimated from t_H. and resistance of H_2-air fuel cell
- ▽ : Estimated from t_H. and resistance of hydrogen concentration cell, H_2(1 atm)//H_2(0.25 atm)
- ● : Estimated from t_H. and resistance of steam concentration cell, P_{H_2O}(I)=2.1 x 10^{-2} atm, P_{H_2O}(II)= 6.05 x 10^{-3} atm, P_{O_2}= 3.02 x 10^{-3} atm

On the other hand, the σ_H. estimated from the resistance and the t_H. of the steam concentration cell is rather lower value than that obtained above. Although a stable and steady current could be drawn from the steam concentration cell as well as the hydrogen concentration cell, the proton conductivity itself may

be low in the steam concentartion cell. It may be due to insufficient P_{H_2O} condition. Since the σ_H. was found to increase in proportion to $P_{H_2O}^{1/2}$, higher P_{H_2O} may provide higher σ_H. even in the steam concentration cell.

Thus, the solid electrolyte $SrCe_{0.95}Yb_{0.05}O_{3-\alpha}$ exhibits the highest proton conductivity in hydrogen atmosphere like in the hydrogen fuel cell or the hydrogen concentration cell. The activation energies of $SrCe_{0.95}Yb_{0.05}O_{3-\alpha}$ calculated from Arrhenius plot were 0.53 eV for the proton conduction(in hydrogen gas) and 0.89 eV for the hole conduction(in dry air). The σ_H. values are 4×10^{-3} S cm^{-1} at 800°C and 1×10^{-2} S cm^{-1} at 1000°C, respectively. Such conductivities are not sufficiently high for practical use which requires large current, however, the high temperature-type proton conductive solid electrolytes based on $SrCeO_3$ may be a promising material for various electrochemical cell devices if used in thin films to reduce ohmic losses.

7.5 Summary

The total conductivities of $SrCeO_3$-based sinters were studied systematically as a function of dopant concentration and partial pressure of water vapor or oxygen. Proton and hole conductances were also measured separately using the steam concentration cell method. It was found that the proton conductivity increased in proportion to $P_{H_2O}^{1/2}$ and was independent of P_{O_2}, suggesting that interstitial-type protons, but not hydride ion, were provided from water vapor. The hole conductivity followed $P_{O_2}^{1/4}$ in the P_{O_2} region examined.

The total conductivity decreased with increasing P_{H_2O} and

increased with increasing P_{O_2} at a given temperature. Such experimental facts could be explained if the protons were provided from water vapor at the expense of the electron holes.

These sinters exhibited the highest proton conductivity under hydrogen atmosphere. The proton conductivities in $SrCe_{0.95}Yb_{0.05}O_{3-\alpha}$ were 4×10^{-3} S cm^{-1} at 800°C and 1×10^{-2} S cm^{-1} at 1000°C, respectively.

CONCLUSION

The aim of the present research is to study the conduction and the electrochemical application of $SrCeO_3$-based proton conductors.

The main conclusions drawn from this work are as follows.

In chapter 1, the sintered oxides $SrCe_{1-x}M_xO_{3-\alpha}$ exhibit appreciable proton conduction under hydrogen- or water-containing atmospheres at high temperature. Partial substitution by aliovalent cation M such as Yb^{3+}, Sc^{3+}, Y^{3+}, Mg^{2+}, In^{3+},etc., for Ce^{4+} site in the perovskite-type crystal $SrCeO_3$ with $x = 0.05$-0.10 is effective in the appearance of the proton conduction. These oxides have only p-type conduction(hole conduction) in an atmosphere free from hydrogen or water vapor. When water vapor or hydrogen is introduced to the atmosphere, the electronic conductivity decreases and the proton conduction appears in a short time.

In chapter 2, high temperature steam electrolyzers and fuel cells can be constructed by using these oxides as the electrolytes. Both devices are operated stably at 800-1000°C. In the steam electrolyzer, hydrogen can be generated at the cathode with high current efficiency close to unity. This is a direct demonstration of the proton conduction in the specimen oxides that protons migrate across the electrolyte from the steam electrode to the cathode. Furthermore, on discharging the fuel cell, it is confirmed that water molecules are produced at the air electrode(cathode).

The major limitation of the cell system is the resistance of the

specimen electrolyte.

In chapter 3, the polarization behavior of the gas electrodes on the $SrCeO_3$-based solid electrolytes is stucied in the fuel cells and the steam electrolyzers. In the hydrogen fuel cell, the anodic polarization is negligibly small at 800-1000°C for the porous platinum electrode. The polarization resistance R_p for the cathodic reaction decreases in proportion to $P_{O_2}^{1/4}$ ($R_p \propto P_{O_2}^{-1/4}$), suggesting that the rate-determining step for the platinum cathode may be the surface diffusion of adsorbed oxygen atoms into the reaction zone. In the steam electrolyzer with platinum electrodes, the cathodic overpotential is larger than the anodic one. From these results, the overpotential may be significant at the cathode where protons are discharged to evolve hydrogen or water vapor.

In chapter 4, a steam concentration cell can be constructed using the $SrCeO_3$-based electrolytes at high temperature. When gases with different humidities are supplied to the electrode compartments of the gas cell with these electrolytes, a distinct and stable emf is observed, the electrode of higher P_{H_2O} being negative. The resistance of the specimen electrolyte is the major factor determining the voltage drop on discharging the cell and the electrode reactions occur reversibly. At the anode, protons are extracted directly from water molecules to evolve oxygen($H_2O \longrightarrow 2H^+ + 1/2\ O_2 + 2e^-$).

In chapter 5, galvanic cell-type humidity sensors are constructed by applying the steam concentration cell. These sensors can be operated stably at elevated temperatures(>300°C). They exhibit a linear emf response against logarithm of P_{H_2O}

over a wide range, a good reproducibility, a very fast response and small response to impurity gases.

In chapter 6, various gas cells are characterized under hydrogen-water vapor or oxygen water vapor atmosphere using high temperature-type proton conductor and oxide ion conductor as the solid electrolyte. Under oxygen-water vapor atmosphere, a steam concentration cell can be constructed using $SrCeO_3$-based proton conductive solid electrolyte. In hydrogen atmosphere, a steam concentration cell can also be constructed using an oxide ion conductor YSZ and relatively large overpotential is observed in this cell. The hydrogen concentration cell constructed with $SrCe_{0.95}Yb_{0.05}O_{3-\alpha}$ electrolyte has stable characteristics at 600-1000°C. Passing a direct current through the cell, hydrogen can be extracted from the anode compartment into the cathode compartment with the current efficiency close to unity.

In chapter 7, the conductivities of $SrCeO_3$-based sinters are studied systematically as a function of dopant concentration and P_{H_2O} or P_{O_2}. It is found that the proton conductivity increases in proportion to $P_{H_2O}^{1/2}$ and is independent of P_{O_2}, suggesting that interstitial-type protons, but not hydride ions, are provided from water under water vapor-oxygen atmospheres ($\sigma_{H\cdot} \propto P_{H_2O}^{1/2}$). The hole conductivity follows $P_{O_2}^{1/4}$ role in the P_{O_2} region examined ($\sigma_{h\cdot} \propto P_{O_2}^{1/4}$).
The total conductivity decreases with increasing P_{H_2O} and increases with increasing P_{O_2} at a given temperature. Such facts can be explained by the proton formation model that the protons are provided from water at the expense of the holes

($H_2O(g)$ + 2 $h^{\cdot}$(oxides) $\rightleftarrows$ 2 $H^{\bullet}$(oxides) + 1/2 $O_2(g)$).

These sinters exhibit the highest proton conductivity under hydrogen atmosphere. The proton conductivities in $SrCe_{0.95}Yb_{0.05}O_{3-\alpha}$ are 4 x 10^{-3} S cm^{-1} at 800°C and 1 x 10^{-2} S cm^{-1} at 1000°C, respectively. These values are not sufficiently high for the practical use which requires large current, however, the high temperature-type proton conductive solid electrolyte based on $SrCeO_3$ may be a prospective material for various electrochemical cell devices if used in thin films to reduce ohmic losses.

LIST OF SYMBOLS

α	number of oxygen deficiencies per perovskite-type oxide unit cell
P_{H_2O}	partial pressure of water vapor
P_{O_2}	oxygen partial pressure
P_{H_2}	hydrogen partial pressure
R	gas constant
T	absolute temperature
F	Faraday's constant
E or emf	electromotive force
E°	emf under standard conditions($P_{H_2}=P_{O_2}=P_{H_2O}=1$)
$\Delta G°$	change of free energy under standard conditions
H^+ or $H^\cdot$	protons in the oxides
h^+ or $h^\cdot$	electron holes in the oxides
e^-	electrons
$O^=$	oxide ions
YSZ	yttria stabilized zirconia; typical oxide ion conductor
V	hydrogen evolution rate(ml $min^{-1}cm^{-2}$)
V_{theo}	theoretical value of V
R_p	polarization resistance
O(ad)	adsorbed oxygen atoms
$\bar{c}$	mean velocity of a molecule(cm sec^{-1})
M	molecular weight
Z	rate of collision of molecules with a wall (molecules $sec^{-1}cm^{-2}$)

N	number of molecules per unit volume (molecules cm^{-3})
E_0	theoretical emf
t_{H^+} or $t_{H^\cdot}$	proton transport number
OCC	oxygen concentration cell
E_o	emf of OCC
HCC	hydrogen concentration cell
E_H	emf of HCC
FC	fuel cell(hydrogen-fuel cell)
E_H^{FC}, E_o^{FC}	emf of FC with proton and oxide ion conductor, respectively
SCC	steam concentration cell
E_H^S, E_o^S	emf of SCC with proton and oxide ion conductor, respectively
σ_{total}	total conductivity
$\sigma_{H^\cdot}$, $\sigma_{h^\cdot}$	proton and hole conductivity, respectively
G_{total}	total conductance
$G_{H^\cdot}$, $G_{h^\cdot}$	proton and hole conductance, respectively
$P_{H_2O}^*$	mean vapor pressure, $P_{H_2O}^* = [P_{H_2O}(I) P_{H_2O}(II)]^{1/2}$
Yb_{Ce}'	Yb^{3+} on Ce^{4+} site
$V_o^{\cdot\cdot}$	oxygen vacancy
O_o	oxide ion on a normal lattice site
$[H^\cdot]$, $[h^\cdot]$	concentration of protons and holes, respectively
$[V_o^{\cdot\cdot}]$, $[O_o]$	concentration of oxygen vacancies and oxide ions on normal lattice sites, respectively
e	elementary charge
$\mu_{H^\cdot}$, μ_h	mobilities of protons and holes, respectively
H^- or $H_o^\cdot$	hydride ions on oxygen lattice site
$H_i^\cdot$	interstitial protons

REFERENCES

[1] H.S.Spacil and C.S.Tedmon,Jr., J. Electrochem. Soc., 116, 1618 (1969)

[2] S.P.S.Badwal, D.J.M.Bevan and J.O'M.Bockris, Electrochim. Acta, 25, 1115 (1980)

[3] W.Doenitz, R.Schmidberger, E.Steinheil and R.Streincher, Int. J. Hydrogen Energy, 5, 55 (1980)

[4] R.Accorsi and E.Bergmann, J. Electrochem. Soc., 127, 804 (1980)

[5] M.Takemori and I.Abe, Denki Kagaku, 47, 204 (1979)

[6] F.J.Rohr, "Applications of Solid Electrolytes" (Edited by T.Takahashi and A.Kozawa), JEC Press, Cleveland, OH, p-196 (1980)

[7] A.O.Isenberg, Solid State Ionics, 3/4, 431 (1981)

[8] F.J.Rohr, Proceedings of The Workshop on High Temperature Solid Oxide Fuel Cells, May 5-6, 1977, p-122

[9] Y.Ohno, S.Nagata and H.Sato, Solid State Ionics, 3/4,439 (1981)

[10] A.Negishi, K.Kozaki and T.Ozawa, ibid, 3/4, 443 (1981)

[11] L.Glasser, Chem. Rev., 75, 21 (1975)

[12] S.Stotz and C.Wagner, Ber. Bunsenges. Physik. Chem., 70, 781 (1966)

[13] D.A.Shores and R.A.Rapp, J. Electrochem. Soc., 119, 300 (1972)

[14] P.J.Jorgensen and F.J.Norton, Phys. Chem. Glasses, 10, 23 (1969)

[15] S.White, Nature, 225, 375 (1970)

[16] F.Forrat, R.Jansen and P. Trévoux , Compt. Rend. Acad. Sci.

(Paris), 257, 1271 (1963)

[17] F.Forrat, G.Dauge, P.Trévoux, G.Danner and M.Christen, Copt. Rend. Acadi. Sci. (Paris), 259, 2813 (1964)

[18] T.Takahashi and H.Iwahara, Rev. Chim. Minérale, 17, 243 (1980)

[19] T.Takahashi, S.Tanase and O.Yamamoto, Electrochim. Acta, 23, 369 (1978)

[20] W.Weppner, Solid State Ionics, 5, 3 (1981)

[21] O.Nakamura, T.Kodama, I.Ogino and Y.Miyake, Chem. Lett., 1979, 17 (1979)

[22] M.G.Shilton and A.T.Howe, Conference on Fast Ion Conductors, (Lake Geneve, U.S.A., May. 1979)

[23] M.G.Shilton and A.T.Howe, Mat. Res. Bull., 12, 701 (1977)

[24] A.T.Howe and M.G.Schilton, J. Solid State Chem., 28, 345 (1979)

[25] S.H.Sheffield and A.T.Howe, Mat. Res. Bull., 14, 929 (1979)

[26] G.C.Farrington and J.L.Briant, ibid, 13, 763 (1978)

[27] G.C.Farrington, J.L.Briant, H.S.Story and W.C.Bailey, Electrochim. Acta, 24, 769 (1979)

[28] F.S.Galasso, "Property, Structure and Preparation of Perovskite-Type Compounds", Pergamon Press, N.Y., p-19 and p-145 (1969)

[29] D.Mastromonaco, I.Barbariol and A.Cocco, Ann. Chim.(Rome), 59, 465 (1969)

[30] C.J.West, "International Critical Tables", McGraw-Hill, N.Y., Vol. VII, p-231 (1930)

[31] H.S.Spacil and C.S.Tedmon,Jr., J. Electrochem. Soc., 116, 1627 (1969)

[51] Da Yu Wang and A.S.Nowick, J. Electrochem. Soc., 127, 113 (1980)

[52] T.M.Gür, I.D.Raistrick and R.A.Huggins, ibid, 127, 2620 (1980)

[53] Da Yu Wang and A.S.Nowick, ibid, 128, 55 (1981)

[54] D.Braushtein, D.S.Tannhauser and I.Riess, ibid, 128, 82 (1981)

[55] J.Sasaki, J.Mizusaki, S.Yamauchi and K.Fueki, Bull. Chem. Soc. Jpn., 54, 1688 (1981)

[56] S.P.S.Badwal and H.J.de Bruin, J. Electrochem. Soc., 129, 1921 (1982)

[57] M.J.Verkerk, M.W.J.Hammink and A.J.Burggraaf, ibid, 130, 70 (1983)

[58] M.Okamoto, G.Kawamura and T.Kudo, Electrochim. Acta, 28, 379 (1983)

[59] R.Lewis and R.Gomer, Surf. Sci., 18, 157 (1968)

[60] M.Kertesz, I.Riess, D.S.Tannhauser, R.Langpape and F.J.Rohr, J.Solid State Chem., 42, 125 (1982)

[61] T.Nitta and S.Hayakawa, Denshi Gijutsu, 21, 8 (1979)

[62] H.Arai, Denki Kagaku, 50, 38 (1982)

[63] K.Kanoh and K.Kawasaki, Jpn. J. Electron., 1966, 2172 (1966)

[64] T.Kawasaki, Z.Minowa and T.Inamatsu, Oyo Butsuri, 35, 355 (1966)

[65] N.Ichinose, Y.Yokomizo and M.Katsura, Denshi Zairyo, 1977, 69 (1977)

[66] T.Nitta, Z.Terada and S.Hayakawa, J. Amer Ceram. Soc., 63, 295 (1980)

[67] I.G.Young, ISA Trans., 11, 65 (1972)

[68] R.T.Johnson,Jr., and R.M.Biefeld, Mat. Res. Bull., 14, 537 (1979)

[69] T.Morimoto, N.Nagao and F.Tokuda, J. Phys. Chem., 73, 243 (1969)

[70] W.Weppner, J Solid State Chem., 20, 305 (1977)

[71] O.Nakamura, I.Ogino, R.N.Casteellano and J.B.Goodenough, Solid State Ionics, 6, 337 (1982)

[72] N.Miura, Y.Ozawa, N.Yamazoe and T.Seiyama, Chem. Lett., 1980, 1275 (1980)

[73] N.Miura, H.Kato, N.Yamazoe and T.Seiyama, Denki Kagaku, 50, 858 (1982)

[74] Y.Ozawa, N.Miura, N.Yamazoe and T.Seiyama, ibid, 51, 350 (1983)

[75] J.S.Lundsgaard, J.Malling and M.L.S.Birchall, Solid State Ionics, 7, 53 (1982)

[76] F.Croce and G.Cigna, ibid, 6, 201 (1982)

[77] J.H.Anderson and G.A.Parks, J. Phys. Chem., 72, 3662 (1968)

[78] J.J.Fripiat, Catalysis Review, 5, 269 (1971)